UNIVERSITÀ DEGLI STUDI DI NAPOLI "FEDERICO II"

Dipartimento di Ingegneria Chimica, dei Materiali

e della Produzione Industriale

Dottorato di ricerca in Ingegneria Chimica

XXVII CICLO

Microfluidics of Multiphase Flows

Thesis Advisor: **Candidate**

Prof. Stefano Guido Ing. Antonio Perazzo

Scientific Committee

Prof. Luigi Paduano

Ing. Vincenzo Guida

Ing. Sergio Caserta

Ing. Valentina Preziosi

a.a. 2014/2015

Summary

Abstract

In this thesis, three kind of multiphase flow have been investigated with microfluidics methods, confocal microscopy and rheology: i) phase inversion emulsification, ii) emulsion interfacial tensiometry and iii) arylamine synthesis (based on a solid-liquid multiphase system).

Multiphase systems are ubiquitous in industrial application, being emulsion one of the most relevant multiphase system. Emulsion microfluidics has been exploited as a mean to investigate emulsion morphology and flow behavior along with other well established technique such as optical microscopy and rheology. Phase inversion emulsification (the phenomenon by which the dispersed phase is switched into the continuous one) is one of the most popular route to obtain nano-sized droplet or capsules with tailored features and sometimes could also represent an inconvenient related with process operations, being the crude oil pipeline transportation one of the main example. Experimental techniques such as, rheology, confocal microscopy and microfluidics were used in order to obtain deep insight on such emulsification process.

Microfluidic techniques have been applied also to characterize emulsion interfacial properties. Some limitations, e.g., droplet with surfactant covered interface, are related with the latter. Pendant drop tensiometry and capillary pressure tensiometry were used in order to elucidate and develop such droplet based microfluidic methodologies.

A microreactor for the handling of a multiphase reactive flows for the synthesis of a pharmaceutical valuable arylamine via Buchwald-Hartwig reaction (one of the most exploited reaction pathway in pharmaceutical industries) has been developed obtaining better performance with respect to the classical batch operations.

The phase inversion emulsification, especially from the flow behavior point of view, has been investigated. The emulsion morphology has been characterized in detail by direct observation in confocal microscopy within microfluidic channels. Long term stable nanoemulsions (average drople size equals to 170 nm) with great energy saving have been obtained. Higher emulsions stability is associated with both small droplet size and low polydispersity of the droplet size distribution. Confocal microscopy can be exploited to follow the time evolution of the phase inversion process. Confocal imaging clearly shows bicontinuous structure formation in emulsification, that signs the two phases point of inversion. Rheological test showed an increased viscoelastic behavior in the proximity of the inversion. Cylindrical microchannel coupled with laser scanning confocal microscopy gave the opportunity to investigate tiny detail of multiphase system morphology.

In the second part of the thesis, a method to measure interfacial tension in microfluidic divergent flow of emulsion was shown. Lowering of the interfacial tension due to droplet confinement has been noted and taken into account by scaling droplet deformation parameter. Results are comparable with literature data only in the case of pure droplet interface, while in

the case of interface covered or partially covered with surfactants, microfluidic technique is not able as pendant drop to evaluate properly interfacial tension, maybe due to the effects of interfacial Marangoni flow and wetting effect in confined droplet flow as well as the effect of droplet interface elasticity that are not taken into account in the microfluidic model.

In the final part we developed a microfluidic apparatus capable to deal with multiphasic reactive flow for the synthesis of a valuable pharmaceutical arylamine. Continuous flow microreactors exhibit a large number of advantages compared to traditional batch and macroscale flow reactors, such as the significant enhancement of transport phenomena, the safety of operation, the precise control of residence time, the possibility of automation and the ease of scale-up by operating several devices in parallel. Thus, the choice of a microfluidic approach for chemical synthesis meets sustainable and green chemistry requirements in terms of productivity, process handling, economic savings and operational safety. The microreactor, coupled with a highly active Palladium-N-heterocyclic carbene (NHC) catalyst, enabled the full conversion of the reagents within twenty minutes, even at very low catalyst concentrations. The influence of the microreactor operating parameters on the synthetic performance has been investigated showing that a slight increase in temperature allows faster conversion even at low catalyst loadings.

1. Introduction

1.1 Emulsion

Multiphase systems are for sure emulsions, i.e., mixtures of two immiscible liquids in which one is usually present as droplets (dispersed phase) immersed into the other one (continuous phase). Emulsion are ubiquitous in many industrial applications, e.g., in the food and biomedical sectors. Typically, one phase is organic(the oil phase),and the other is an aqueous solution. In some cases, the two phases are continuously interpenetrated into each other, thus making it impossible to distinguish between the dispersed and the continuous phase. These emulsions are referred to as co-continous or bicontinuous. Due to oil/water immiscibility, emulsions tend to be phase separated at thermodynamic equilibrium, hence emulsion stability is one of the main problems in several industrial applications. Many phenomena drive phase separation, e.g., creaming and sedimentation due to density difference of the phases, coalescence when two droplet merge into one [1, 2], flocculation when droplets tend to aggregate in clusters, Ostwald ripening when the smaller droplets diffuse into the bigger ones through the continuous phase [1-4]. As shown by Stoke’s sedimentation law,

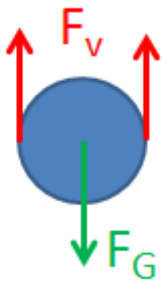

Fig.1: forces acting on sedimentating droplet

$$v = \frac{-2r^2(\rho_d - \rho_c)g}{9\mu_c} \qquad (1)$$

where: v is the sedimentation velocity, r is the droplet radius, ρ_c is the continuous phase density, ρ_d is the dispersed phase density, g is the standard gravity, μ_c is the continuous phase viscosity. By equation (1) it's clear what are the methods of retarding gravitational phase separation:

i) reducing the density difference between the phases

ii) lowering droplets radius

iii) increasing continuous phase viscosity

are all factors acting to hinder phase separation, making the emulsion meta-stable, i.e., the separation process "is slow enough" [5]. Such kinetic stability can also be achieved by exploiting surfactants, which are amphiphilic molecules stabilizing droplets by lowering interfacial tension and eliciting Marangoni stresses [6]. The role of surfactants and amphiphiles in general in lowering interfacial tension [7-11], their adsorption behavior as well as the interface behavior both in static and dynamic conditions [12-25] have been widely studied. Emulsions having fine droplet size are more stable against phase separation and widely exploited in application also due to their capability to incorporate hydrophilic or hydrophobic species. Such small-sized emulsions are mainly divided in two broad categories: nanoemulsions and microemulsions. Nanoemulsions have a size range between 20 nm – 200nm [26], can be almost transparent or rather turbid and are kinetically stable. Microemulsions are thermodynamically stable (interfacial tension nearby zero [27]) and transparent with droplet size ranging from 10 to 100 nm. Although this terminology is rather confusing and not always agreed upon in the literature [28], it can be stated that microemulsions exhibit smaller droplet size respect to nanoemulsion and are thermodynamically stable, while nanoemulsions are kinetically stable.

1.2 Emulsion phase inversion (EPI)

Several methods are used to obtain emulsions with stability levels suitable to industrial applications. Phase inversion emulsification is a popular technique characterized by low energy requirements. In this process, an inversion between the continuous and the dispersed phase is achieved by either changing temperature or composition, thus obtaining finely dispersed emulsions in a more sustainable way with respect to the classical high energy mixing emulsification routes.

The phase inversion pathways have been described as catastrophic or transitional. The former is a term introduced by Salager [29] to describe emulsion inversion reached by changing the water/oil ratio (this is also referred to as phase inversion composition or PIC, and emulsion inversion point or EIP) [30]. The term catastrophic comes from Dickinson [30-33], following the hypothesis that catastrophe theory might be useful to describe emulsion phase inversion. Despite all the efforts, catastrophe theory can only predict qualitative features of catastrophic phase inversion, but it cannot be used as a predictive model [30, 34]. This is due to the lack of a kinetics coupled thermodynamic approach as opposed to a mere thermodynamic one [34]. In transitional phase inversion the inversion is considered to be brought about by changing the surfactant affinity for the two phases [30, 35], e.g., non-ionic surfactants becoming more lipophilic when heated (phase inversion temperature or PIT). The latter assumption was stated clearly by Shinoda in 1968 [36].

However, in spite of the widespread use and the extensive investigation of phase inversion (dating from the pioneering work of Shinoda, who in turn refers to earlier work of Langmuir), its governing mechanisms are still debated. As stated by Nienow [37] and Orr [38], notwithstanding all the efforts made in order to model the catastrophic phase inversion, and phase inversion in general, satisfactory models are not available. One of the key issues is the high number of variables, such as concentration of surfactant(s), oil and water, temperature, agitation rate, flow type, vessel geometry, surface wetting, electrostatic charge [33]. The main approaches to model phase inversion in the literature can be related to three main areas: phase behavior, interfacial properties and flow-induced morphological changes, such as droplet breakup and coalescence. Most studies focus on one of these areas at a time and their interplay is still to be fully elucidated.

1.2.1 Nanoemulsions by EPI (for delivery systems)

In the last few decades an increasing interest in the formation of nanoemulsions (NEs) [26-28, 39-42] has been developing within the food [43, 44], biomedical [45, 46] and cosmetic [47-49] industries due to the advantages of NEs compared to conventional emulsions, like the small droplet size, high kinetic stability and optical transparency. Nanoemulsions are non-equilibrium dispersions with mean droplet radius between 20 and 200 nm; the droplets are so small that they

only scatter light waves weakly and then they tend to be transparent and can be incorporated into optically transparent products.

A comprehension of nanoemulsion formation methods [50], like phase inversion emulsification, is especially relevant for nanoparticles [51] generation for drug delivery systems [52-54]. In fact, the formation of nanoparticles (spheres or capsules) containing bioactive compounds, like vitamins, proteins, and drugs such as insulin, is deeply affected by the nano-emulsification method. Depending upon the method of preparation, nanoparticles can be divided into two main families: nanospheres [55-58], which have a homogeneous structure, and nanocapsules, which exhibit a typical core-shell structure. A main challenge in the formulation of nanoparticles is adapting their structure to drug delivery ability. The drug can be dissolved, entrapped, encapsulated or attached to nanoparticle matrix. Phase inversion emulsification is particularly suitable for the formation of nanocapsules, in which the drug is confined to a cavity surrounded by a membrane made of polymers [59] or lipids [60], because it allows to prevent the potential degradation of encapsulated molecules during processing or during oral delivery, where the harsh conditions of gastrointestinal tract play against. It has been widely demonstrated that these structures are useful for delivering a multitude of biocompatible agents [61, 62]. Moreover they can increase the bioavailability of poorly water soluble ingredients encapsulated within them [52, 63-65]. A common way to produce nanocapsules is the phase inversion nanoencapsulation (PIN). PIN nanocapsules are fabricated in a one-step process by preparing a mixed solution of polymer (e.g., PLGA) and drug (e.g., Zn-insulin) in a solvent such as methylene chloride and dispersing the so-obtained solution into a non-solvent (usually petroleum ether) present in larger quantity. Hence, the continuous phase is switched from solvent continuous to non-solvent continuous. Nanospheres with drug inside are spontaneously formed and then collected by vacuum filtration, frozen and lyophilized to remove excess solvent and water [192]. Further examples have been provided by McClements [66], who used phase inversion method [64] to produce food-grade nanoemulsions enriched with vitamin E acetate [67-69], that is an esterified form of the oil soluble Vitamin E (tocopherol) widely used in pharmaceutical, food and cosmetic products.

The use of nanoemulsions for encapsulation of medicines and their controlled delivery into the human body has been the focus of many researchers on this topic [70-75]. It has been underlined that the penetration rate of drugs using NEs is much higher than when using conventional macroemulsions and other carriers [70]. Recently, NEs have also been used in bacteriophage therapy [76], that is a an important alternative to antibiotics in the current era of multidrug resistant pathogens. In particular it has been demonstrated the *in vitro* antimicrobial efficacy of Bacteriophage K when stabilized in an oil-in-water nanoemulsion compared to simple delivery as an aqueous dispersion [77].

1.2.2 EPI in cosmetics

Nanoemulsions formed by phase inversion method are by far one of the most advanced nanoparticle systems for cosmetic industry [78, 79]. Unlike macroemulsions, they are much more stable systems and then suitable for skin care products like water-like fluids, easily adsorbed by the skin, or gel-like fluids, obtained by increasing the oil content or by adding thickening agents (usually polymers) [49]. Recently, phase inversion method has been used for the formation of nano-gels systems, used in sun care products and in anti-aging creams, and emulsion-based wet wipes used for makeup removal and for baby care [48]

1.2.3 EPI of particle-stabilized system

The use of solid particles as stabilizers in emulsions has been dated since the pioneering work of Pickering [80], who noted that emulsions (for this reason called Pickering emulsions) could also be stabilized by particles at the interface (Fig. 2) [81]. Recently there has been an upsurge of interest in using solid particles in the emulsification process [81-86], especially in food industry to stabilize products, like ice crystals in ice cream and fat particles in whipping cream [87]. Colloidal particles (micro and nano) behave in many ways like traditional surfactant molecules [88]: they can spontaneously accumulate at the interface between two immiscible fluids (liquid–gas or liquid–liquid) and therefore they are surface-active, but they offer distinct advantages compared to surfactants. For example, at variance with surfactants that adsorb and desorb on a relatively fast timescale, particles adsorb irreversibly to interfaces [89] due to their wettability. The latter can be quantified by the contact angle ϕ with the interface [90]. If particles are hydrophilic the angle ϕ, which is measured through the water phase, is normally $< 90°$ and a larger fraction of the particle surface resides in water, giving rise to O/W emulsion. On the other hand, for hydrophobic particles ($\phi > 90°$), W/O emulsions tend to be stabilized.

Particles stabilize emulsions according to two main mechanisms: i) particles form a dense film (monolayer or multilayer) around the dispersed drops impeding coalescence, ii) additional stabilization arises when the particle-particle interactions form a 3-D network of particles in the *continuous* phase surrounding the drops. It is clear that nanoparticles affect the emulsification process in a different way from surfactants [88, 91] .

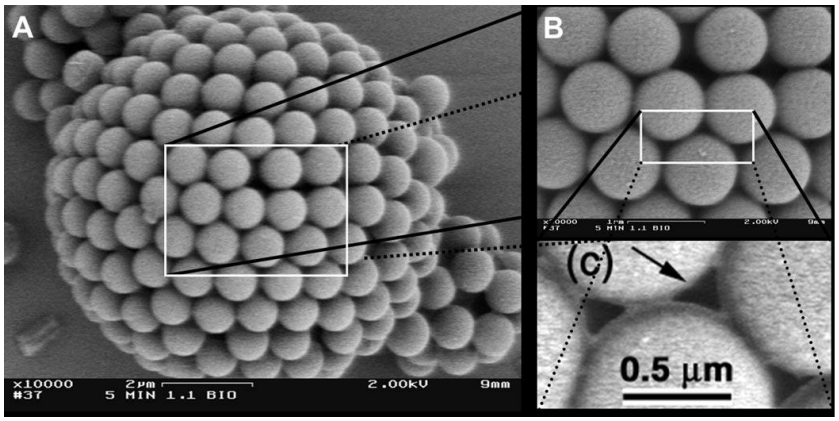

Fig. 2: Picture of particles at fluid-fluid interface; B and C images are close-ups of figure A and B respectively, where void spaces size among particles can be observed. (image taken from reference [81, 91])

The phase inversion method is widely used to produce particle-stabilized emulsions from oil in water to water in oil and viceversa [82, 92, 93]. Unlike emulsions stabilized by a single surfactant type, those made with small particles can be inverted by varying particle hydrophobicity or simply by increasing the volume fraction of the dispersed phase, as shown by Binks and Lumsdon [82]. They showed that emulsions stabilized by hydrophobic silica can be inverted from w/o to o/w upon increasing ϕ_w, and emulsions stabilized by hydrophilic silica can be inverted from o/w to w/o upon increasing the volume fraction of oil, ϕ_o.

They also studied, for their system, the effect of oil type on emulsion formation and showed that unlike emulsions stabilized by surfactants, where there is a chemical interaction between oil and surfactant structure, in systems stabilized by hydrophobic particles (w/o) the oil type does not affect the final product.

However, when particles have very low or very high ϕ, they are not very surface active, then surface modifications are required. A way is to use the so-called Janus particles, which are peculiar nanoparticles showing, similar to surfactants, hydrophilic and hydrophobic faces. Another way, much easier and less expensive than the previous one, is to modify the wettability of particles by interaction in aqueous media with amphiphilic compounds, as shown by Binks [94, 95], who demonstrated that the wettability modifications of the nanoparticles via interaction with amphiphilic species depend on both the particle surface properties and the structure of the surfactant.

Recently, phase inversion emulsification has been used to produce new particle-stabilized materials in which air or water become encapsulated and the adsorbed particle layer provides a means to control the release of gaseous or liquid components [92].

1.2.4 Waterborne dispersion of polymer resins

Phase inversion emulsification method has been found to be an highly effective technique for the formation of waterborne dispersions of polymer resins [96-100]. Such epoxy resins are widely used in various applications, like in biomedical field [101] and in microelectronics [102]. Starting from a mixture of an epoxy resin with an emulsifier, the addition of water drives the phase inversion until the formation of a dispersion where water phase, made of small droplets, becomes the continuous phase. Size and morphology of the emulsified waterborne particles could be controlled by the type and concentration of emulsifiers and by emulsification temperature. A physical model of phase inversion has been proposed to predict the effects of these parameters on the process. In particular, phase inversion process is completely accomplished when the temperature is relatively low and the emulsifier concentration relatively high and in this case all water droplets coalesce and become the continuous phase at the phase

inversion point (fig. 3). In comparison, when both the emulsification temperature and the emulsifier concentration are high, there is an irreversible coalescence of water droplets before the phase inversion point and not all water droplets are inverted into the continuous phase, thus inducing the formation of a complex W/O/W structure (fig.9).

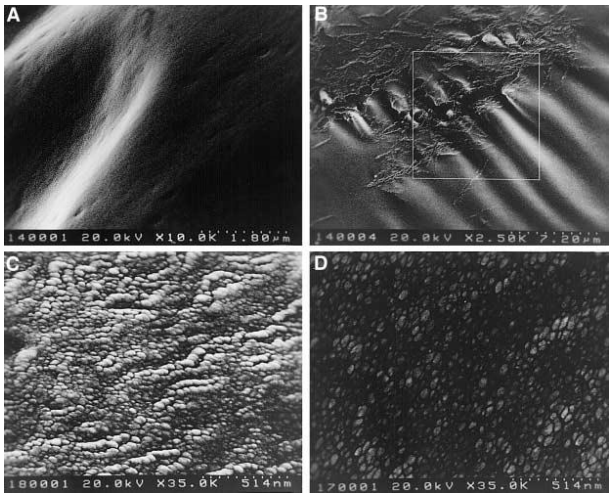

Fig. 3: Morphological evolution during complete phase inversion (image taken from reference [97])

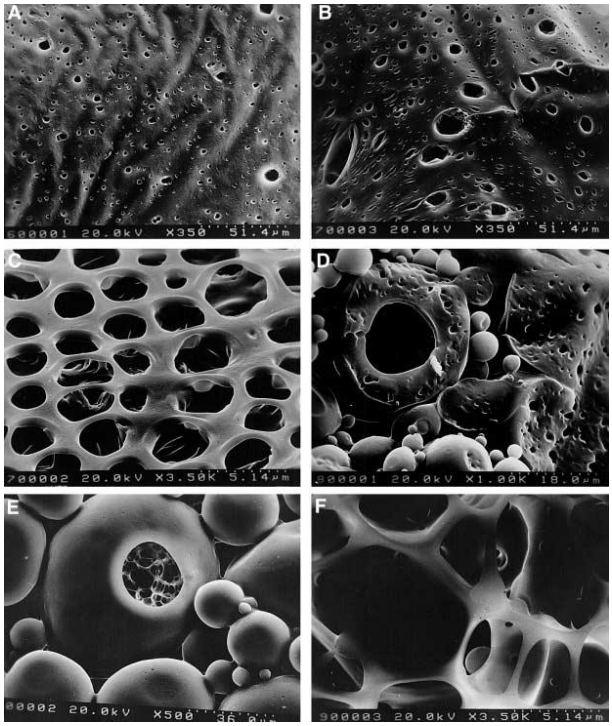

Fig. 3: Morphological evolution during incomplete phase inversion (image taken from reference [97])

By following the studies based on this model, a new method to encapsulate nanoparticles (fig.3) with polymers to prepare waterborne nanocomposite dispersion has been investigated [100].

1.3 Multiphase flow in porous medium – a relevant issue for petroleum industry

The water present within oil reservoir, as well as the water (or other liquid phases) injected into the oil reservoir with the aim to squeeze out oil from the well, makes emulsions ubiquitous in upstream operations. Emulsions are liquid-liquid metastable systems composed at least of two immiscible phases. Surface active molecules like low molecular weight fatty acids, naphtenic acids and asphaltenes are usually present within crude oil, thus changing rheological and chemical behavior [103]. Even if the emulsion phases are newtonian, emulsion flowing through porous media show non-newtonian behavior like shear thinning (i.e, viscosity lowering with increasing shear rate), due to the presence of the interfaces between dispersed and continuous phase. Obviously, if one of the phases is intrinsically non-newtonian, the non-newtonian emulsion behavior is enhanced [104]. Emulsions transport in porous media is often studied by adopting a multiphase generalization of Darcy's law [105, 106] :

$$\mathbf{v}_\alpha = -\frac{k_{r\alpha}}{\eta_\alpha} K(\nabla P_\alpha - \rho_\alpha \mathbf{g}) \qquad (2)$$

where v_α represents the flux of a fluid phase, k_r is the relative permeability and the subscript α denotes each phase. The local pressure difference at the fluid-fluid interface can be relevant because interfaces are highly curved due to small size of pores within porous medium [107]. When emulsion interfacial tension is pretty high and droplets size is comparable with pore size, the flow is unable to displace droplets from pores, making the droplets entrapped, even if the continuous phase can partially flow, thus leading to enormous difference in the volume flow rate of the two phases. Also wettability plays a key role in droplets entrapment: Torok et al. [108] studied the spontaneous segregation in the absence of external viscous forces and at low-tension conditions of polydispersed oil-in-water emulsion in porous media, monitoring the change in the separated oil volume. A vertical experimental porous medium was exploited founding the appearance and rise of three pseudo-phases. The first, with the relevant fraction of oil in the system, rising with high steady state velocity. The second, made of the remaining part of emulsion and characterized by an unsteady and decreasing velocity, the third with the segregation of the mobile oil particles in the phase microstructures. According to the mechanism proposed by Torok et al., the decreased probability of coalescence in pores and dispersion within pores connections are responsible for the displacement of mobile phases at low-conditions. The pore network, the size distributions of oil droplets, their density and the lengths of paths play a strong role in this case. When droplets size is similar to pores size, droplets are usually defined "confined". Confined droplets differ from plugs because the presence of a continuous phase layer near the solid wall, that is lacking in the case of slug formations. Confined droplets flow has been widely studied in the literature [109-116]. The main effects of confinement respect to the unconfined case of the same droplets are the

enhanced droplets deformability, as shown in Figure 4, an hindered breakup and a more homogeneous droplet size distributions after breakup [109, 111, 112].

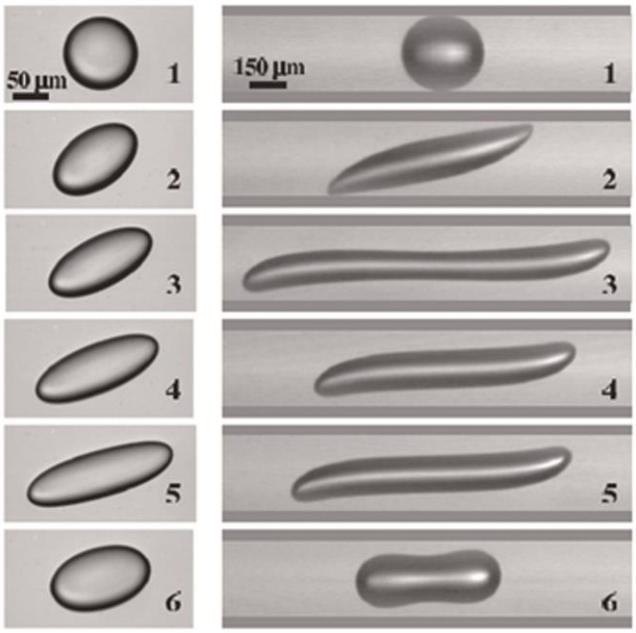

Fig. 4: Transient drop deformation at Ca= 0.4 and a/h=0.07 (left sequence) and 0.5 (right sequence) as observed along the vorticity direction in a parallel flow apparatus. A droplet of the same material is much higher deformed in the confined case (right sequence) respect to the unconfined one (left sequence). Image from [109].

By numerical simulation it has been shown (Figure 5A) how a droplet is squeezed through narrow pores having size comparable to the droplet, i.e., another case of confinement. The droplet is squeezed if Ca number is adequately high, while is entrapped if Ca number is too low. In Figure 5B the same consideration were applied for multiple droplets through a narrow pore simulated by a bed of solid spheres [114, 115]. Emulsion flow through porous media can be highly affected by the changes in the droplet size distribution caused by breakup and coalescence phenomena. The droplet entrapment mechanism can also cause permeability reductions in sandpacks medium, as reported in the case of diluted oil-in-water emulsion by filtration model-based numerical simulations [117].

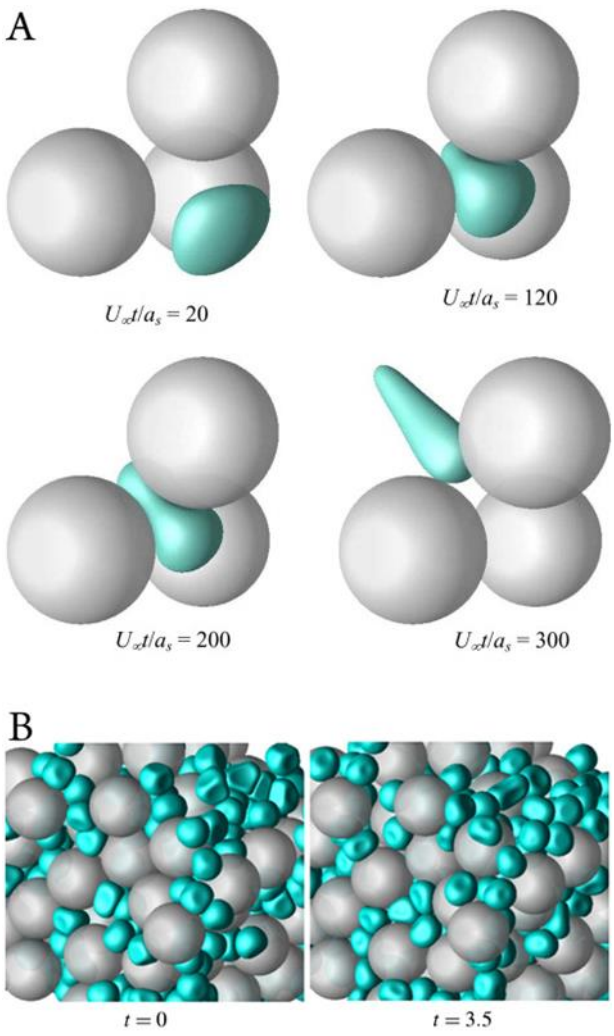

Fig. 5.A: Single Droplet motion squeezing between three non-touching spheres for Ca = 1.5, where U∞ t/as is a time scaled according to the velocity of the external flow and the sphere radius. **B**.Many droplets squeezing through a Random Loose Packing Algorithm of solid spheres at Ca = 0.006, where t is a time scaled according to the Carman–Kozeny velocity and the sphere radius. Image from [114] and [115].

However, filtration model seems to be not good enough to predict pore-scale permeability fluctuations and the reduction of absolute permeability that are not seldom phenomena during emulsion transport in porous media [118]. To overcome this matter, Cortis and Ghezzehei [118] introduced a continuous time random walk based approach that gives good fitting between predictions and experimental data. Romero et al. [119] also pointed out the limitation of filtration model. In their work on oil-in-water emulsion through porous media they developed a network model that takes into account droplet confinement, permeability effect and dispersed phase droplet size. The model well describe the oil-in-water emulsion flow of their experiments. Hysteresis and fluid entrapment in emulsion displacement through porous media was approached by Hilfer [120] by introducing the concept of a percolating and a non-percolating phase. Doster and Hilfer [121] studied in an analitically tractable hyperbolic limit this theory. NMR (nuclear magnetic resonance) is also suitable to studye mulsion in porous media.

Godefroy and Callaghan [122] reported how nuclear magnetic distance is useful to characterize water and oil dynamics and microemulsion systems. In this work is outlined how the exchange spectra of the phases can be exploited to get insights on coalescence phenomena. The residual oil distribution during waterflooding of the wellbore can also be studied by NMR [122]. Bryan et al. [123] reported how low field NMR is suitable for emulsion in porous medium monitoring, in particular, to verify how emulsion production is related with flow and injection pressure.

1.3.1 Oil Recovery

In the last few decades research on petroleum recovery has been widely intensified due to the increased global demand. Improved methods for enhancing oil recovery (EOR) by injecting appropriate agents not normally present in the reservoir, such as chemicals, solvents, oxidizers and heat carriers in order to induce new mechanisms for displacing oil, as defined by Bavière in 1991[124], have been thoroughly studied [125-127]. EOR methods can be divided in three categories, based on chemical, thermal and miscible methods. One of the three methods, based on chemical interactions between the injected fluid and the reservoir fluid, can be applied by using as injecting fluid surfactant solutions used to reduce interfacial tension between oil and water. However, this method can fail due to the low viscosity of surfactant solutions, then microemulsions, nano-emulsions [128] or high concentrated surfactant solutions can be a valid alternative inducing a very low interfacial tension [127, 129], which provide the proper conditions to ensure the trapped oil displacement in the porous reservoir and a successful final recovery [130]. Recently, some experiments to investigate the efficiency of nanoemulsions in EOR in terms of particle size distribution of dispersed oil droplets in water and experiments by using nanoemulsion as displacing fluid for EOR were performed [126]. Finally, within the field of oil recovery, phase inversion can be exploited to obtain reversible emulsion drilling fluids [131].

1.3.2 Drilling and fracturing

Another application of emulsion can be found in the wellbore drilling process, that is the first step to spill oil from underground. This is performed by rotary drilling using a drilling fluid [132]], forming a low film on the freshly created wellbore surface [132] and the right physicochemical characteristics to avoid chemo-mechanical breakage of clay-rocks, swelling shales [132]. Water based mud often containing smectite clay colloids, such as the most utilized bentonite and montmorillonite [132]. In order to maximize wellbore productivity Haudybert-Ayet and Dalmazzone [133] realized a water based mud containing a surfactant molecule engineered to pass through a drill-in fluid with the following characteristics: i) prevent the irreversible adsorption of the fluid polymers on the reservoir surface area, ii) increase flow area, iii) promote compatibility between the brine filtrate with formation crude, and iv) reduce the adhesion properties between filter cake particles to enhance the ease of wellbore clean up during

displacement and natural cake "lift-off" during the onset of production. Oil based mud emulsion [132], due to the reduced permeation of oil respect to water towards wellbore walls, have demonstrated their utility in drilling operation.

Within underground reservoir, oil and/or gas are entrapped between rocks. Hydraulic fracturing is the typical route to release oil and gas from the rocks [132]. Mainly, fracturing fluids are made of natural polymers, such as guar, cross-linked by borate or transition metal (Zr, Ti) complexes to form viscoelastic gels [132] [134] [135]. Fluids have the role to transmit hydraulic pressure towards rocks to create fractures. Sand and other ceramic particles ('proppant') are present within the gel to give a complex porous medium which keeps the fractures open after the removal of the imposed fluid pressure [132]. A limitation of these fluids is the low level of hydraulic conductivity once the complex pack inside fracture is formed. The problem has been solved by using wormlike micellar solution. A wormlike micelle is an elongated, cylindrical surfactant micelle [136-144]. Wormlike phases are able to give a proper gel-like behavior [136, 137] but, what makes them valuable is that once this elongated micelles come into contact with the oil, they become spherical micelles or microemulsions [132] (whit a consistent elasticity loss), thus permitting a good hydraulic pressure conductivity. Chu et al. [139] have recently reviewed wormlike micelles applications in oil production reporting that wormlike micelles can be used in drilling, gravel packing, oil well stimulation, tertiary oil recovery. Maybe, the best known surfactant able to give wormlike micelles with a lot of co-surfactant is the cetyl-trimethylammonium bromide (CTAB) [141-146]. Indeed, its use during hydraulic fracturing is well established [132].

1.3.3 Enhanced Oil recovery (EOR) by liquid phases

Aqueous alkali-surfactant solutions are injected into the oil reservoir to lower interfacial tension and increase oil recovery respect to the simple water flooding [123, 147-149]. Macroemulsion injection have also been used for oil recovery. Engelke et al. [150] modeled macro-emulsion flow injection by the changes of relative permeability curves with and without oil droplets dispersed in the aqueous phase. Low salinity water injection and surfactant flooding are two important tools to enhance oil recovery. Johannessen and Spildo [151] coupled these two techniques founding that low salinity surfactant flooding process at moderately low interfacial tensions it is better than an injection of an optimal salinity surfactant solution at ultralow interfacial tensions. A review on the ultralow interfacial tension surfactant solutions for injection can be found in the work of Salager et al. [152]. Chu et al. [139] reported that wormlike micellar solutions led to an optimized oil and gas asset performance along with an improved oil recovery in many wells spacing from South America, North America, North Sea, Caspian Sea, Middle East Sea to China. Furthermore, micro-emulsion injection [153, 154] into oil reservoir were exploited with the same purpose.

The study of surfactant adsorption behavior [7, 8, 11, 14, 15, 18, 155-162] behavior is a key-step in the oil recovery process, allowing the optimization of the injection of surfactant mixture. Bera et al. [163] studied the adsorption of some surfactants commercially available, such as SDS (Sodium dodecylsulphate, anionic surfactant), CTAB (cethyltrimethylammonium bromide, cationic surfactant) and Tergitol 15-S-7 (an ethoxylated C11-15 secondary alcohol, non-ionic surfactant) onto reservoir sand surface. Langmuir, Freundlich, Redlich and Sips adsorption isotherms were exploited to best fit experimental results. Also salt and pH effect has been take into account. In the same study, the interaction between sand particles and surfactants has been characterized by Fourier transform infrared spectroscopy (FTIR). Bera et al. [163] also reported the experimental evidence of a high level adsorption of cationic surfactant onto sand surface, low level of anionic surfactant adsorption onto the same sand, non-ionic surfactants having intermediate behavior. It is clear that this particular injected solutions affect physico-chemical properties of the emulsion already present within porous media, mainly because they are rich of surfactants.

1.3.4 Emulsion phase inversion in porous medium

Other important phenomena that occur during the flow of emulsions in a porous medium are dynamic blocking and phase inversion. The former happens when the emulsion flow is stopped despite a constant pressure gradient. Khasanov et al. [164] developed a two phase filtration model that takes into account microdroplets deformation and microdroplets friction in order to predict the dynamic blocking. The intriguing aspect here is that also when droplet are order of magnitude less than pore size, dynamic blocking could occur. Maybe, the key role is played by microdroplets deformation. Regarding saturation (relative volume fraction of a fluid phase) in porous medium, Boersma et al. [165] studied capillary behavior of multi-phase systems (experimentally and numerically) founding that saturation distribution depends on the oil type and on the presence of surface active molecules. One of the main risk of emulsion flow through porous medium is emulsion phase inversion thus leading to porous medium plugging [152].

1.3.5 Transportation of heavy crude oil

Nowadays over 65% of the world overall energy resources come from hydrocarbons. With the increasing global demand and progressive decrease of light crude oil reserves, the interest in heavy and extra-heavy oil has been growing [166, 167]. In the past, these fluids were not much exploited because of their high viscosity that can cause problems in pipeline transportation. Thus, in order to facilitate mobility of such oils, several methods to reduce their viscosity have been investigated. One method consists in diluting the system with lighter oils or in producing emulsions of heavy oil in water [166]. The first method is quite used even if it requires light oils that are not always available close to production plants and then dilution change oil composition which can be difficult to be separated at the end of the process. An alternative method that

consists in transporting these fluids as emulsions in the form of crude oil droplets by using water as continuous phase, have been successfully used [168, 169]. In this case easier pumping due to a less viscous final system and the lack of contact between the crude oil and the pipe walls which results in less erosion and precipitation in pipes has been found. However, a further understanding of the mechanisms for the formation of emulsions is then critical to avoid blockage of the system, that can occur when increasing the oil content resulting in a phase inversion of the system leading to fine water droplets which are afterwards very difficult to separate [170].

1.4 Microfluidics

1.4.1 Emulsion Microfluidics

Microfluidics is the science and technology that gives the opportunity to study and develop the fluid physics, chemistry and biology at the micro-scale [171, 172] [173]. Microfluidics and microconfined flow are well established methods to study soft matter properties, e.g, red blood cells [174], vesicles [175, 176], capsules and droplets deformation and flow dynamics [177, 178] [179].

Emulsion microfluidics is gaining growing interest due to compatibility with many chemical and biological reagents, the capability to carry out automated experiments, precise control of droplet, manipulation of individual droplets such as coalescing droplets, mixing of their contents, and sorting in combination with fast analysis tools [177, 179, 180]. Droplet-based microfluidics is a key topic in multiphase systems microfluidics. Seemann et al. [179] reviewed a wide range of application, e.g.: device fabrications, droplet formation, biology and biophysics in droplets.

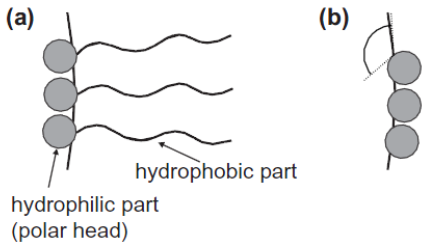

Fig. 6: Schematic of the stabilizing function of a molecular surfactant (a) having a polar head and a hydrophobic tail andinterface stabilization by solid particles (b), where the position at the fluid/fluid interface is given by the contact angle θ of one of the fluid phases. Image from [179]

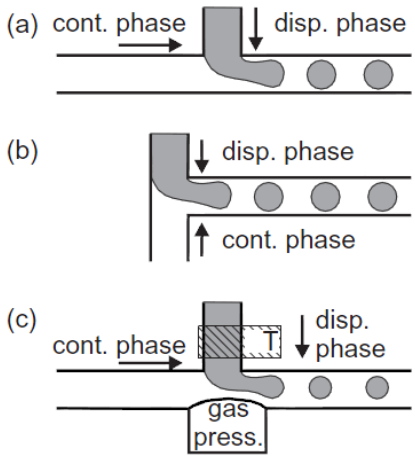

Fig. 7: Schematic of various T-junction geometries. (a) 'regular T-junction' geometry where the dispersed phase is injected perpendicular into a stream of continuous fluid. (b) 'Head on' geometry where the dispersed and the continuous phases are injected from opposite sides. (c) 'Active T-junction' allowing variations of the geometry by air pressure and temperature control of the dispersed phase. Image from [179]

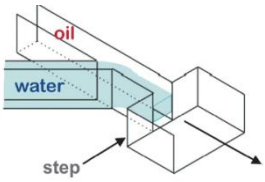

Fig. 8: A step-emulsification device. In the narrow duct behind the oil/water channel junction, a quasi-two-dimensional aqueous jet has formed within the oil as the carrier phase. At the 'step' the channel widens, forcing the aqueous filament into an effectively three-dimensional setting. Decay into droplets is the immediate effect. Image from [179]

A key issue in droplet based microfluidics is flow topology inside droplets moving in a microchannel:

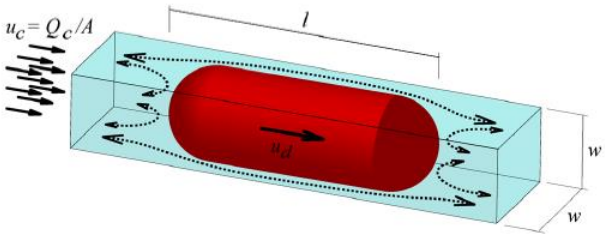

Fig. 9: Droplet of length l in a microchannel of width w. Neither the speed of the droplet, nor the topology of the streamlines are a priori known (dashed lines mark the unknown streamlines outside the droplet). Qc is the flow rate, A is section. The continuous liquid can bypass the droplet (β=ud=uc< 1) or the droplet can outrun the average speed of the continuous phase (β>1). Image from [181]

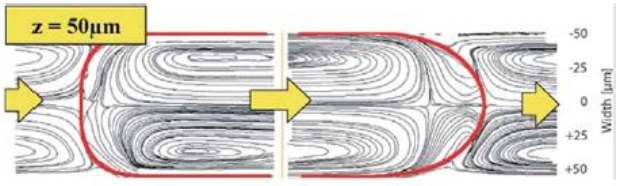

Fig. 10: Flow profile in a droplet flowing in a microfluidic channel as measured by PIV. The channel height (z =50μm) is half the channel width. Image from [182]

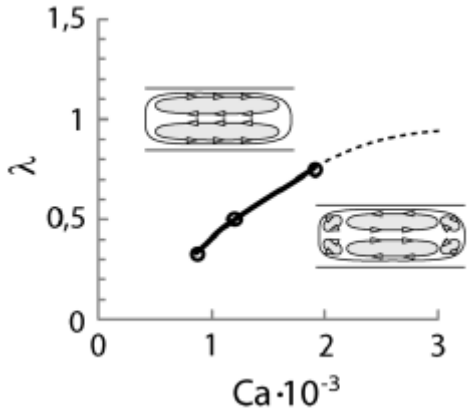

Fig. 11: A diagram illustrating the transition from the simple to more complicated pattern of flow in droplets in square capillaries, λ is the viscosity ratio, Ca is the capillary number. Image from [181]

1.4.2 Microfluidics to study oil recovery issue

Microfluidic models are a valuable tool that helps to improve the understanding of flow and transport phenomena at both microscale and macroscale. Examples can be found in the manipulation of instabilities in fluid-fluid systems in a Hele-Shaw cell [183-186] and in the diffusion process by using nano- and micro- fibrous media [187].

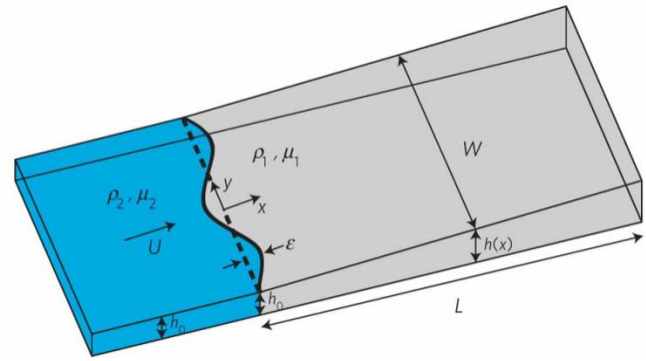

Fig. 12: A schematic of the experimental set-up of a non-uniform Hele–Shaw cell with a constant depth gradient, to study viscous fingering. The depth of the cell h(x), with h(x)<<W and h(x)<<L,varies linearly in the direction of fluid motion; dh/dx=α. Image from [183]

Nilsson et al. [188] exploited microfluidic devices (made of polydimethylsiloxane, PDMS) to outline how fluids shear thinning, shear thickening and viscoelastic behavior in general, affects oil recovery. They implemented a microfluidic device containing a sandstone media, testing water, a surfactant solution (CTAB the surfactant), a shear thinning fluid thickener (Flopaam) and a shear thickening solution containing nanoparticles as injected fluid. They reported that water is the worst fluid for this kind of operation and showed a high level of oil recovery by

using shear thickening solution. For all the performed experiments they imposed a shear rate of 10 s^{-1}, because they considered this number the typical shear rate value within sandstone media during oil recovery processes. The authors also pointed out that, for any injected viscoelastic solution, a two stages process is the best way to increase oil production, being the water injection the first stage and the viscoelastic solution injection the second one. Eventually, Nilsson et al. demonstrated how amicrofluidic device can be exploited to study EOR issues, the small scale giving a cheap and fast route to study multiphase fluid through porous media in many conditions.

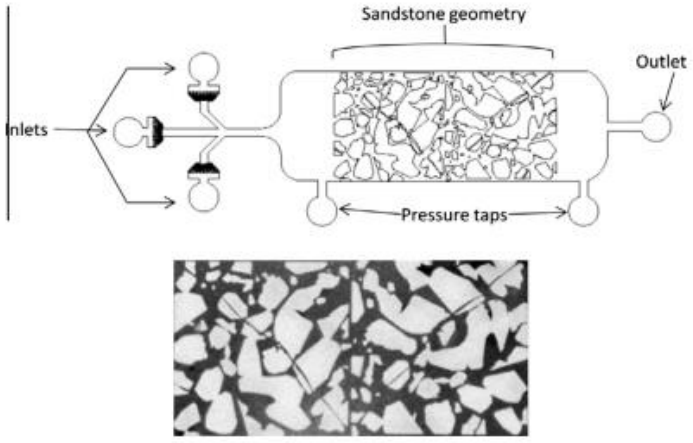

Fig. 13: Schematic diagram of the small sandstone device used in these experiments. The inlet is any of the three ports on the left, and flow goes from left to right. The two ports aside the main chamber are available for pressure drop measurements, and the port to the right is the outlet port. The lower image is what the sandstone portion looks like when filled with the Miglyol oil dyed with sudan blue. Image from [188].

1.5 Microfluidics of multiphase reactive flows

It is known that the two kind of approach for synthesis of chemicals are continuous flow operations and batch one, the latter often coupled with segmented unit operations [189]. Pharmaceutical industry has been historically based on batch processes for the productions of chemicals but nowadays both at a research and industry level an upsurge of interest has been devoting to continuous flow operations [189-194]. Such processes have been identified as indispensable in order to match the goals required by green chemistry [189, 190, 195], ensuring increased level of productivity, process handling, economics savings and operations safety. Recent improvements in sustainable production, flow chemistry and green chemistry have been provided by microfluidics [196]. This technology is continuously gaining ground in a broad range of applications such as biotechnology [174, 197], fluid mechanics [171-173] and chemical processes, where paved the way to make use of devices able to miniaturize reactive flows [180, 198]. Apparently, some cons are related with reactive flow confinement. E.g., in classical

macro-scale operations mixing and heat-transfer are governed by turbulence and diffusivity with the former playing a key role (Re >> 1000), whereas in microfluidics turbulence is hampered and mixing is mainly diffusive (Re < 200). Nevertheless, the loss of turbulence is compensated by a higher surface over volume ratio and the possibility to manipulate small amount of fluid thus giving more controlled and harnessed reaction pathways, a mandatory requirement in the experimentation of new drugs where high-throughput and small samples are needed [180, 191]. At a glance, there are many microreactors related enabling technologies in organic synthesis e.g., solid phase arrested synthesis, new heating techniques, accessibility of exothermic and runaway reactions, new solvent systems (including supercritical fluids and solvent free one), less waste due to high selectivity, reactions in droplets [199, 200] and the ease of scale-up just running several devices in parallel. Many examples of the microreactors superior performance in terms of safety, yield, selectivity and reaction rates with respect to traditional batch operations have been reported in photochemistry, electrochemistry, for the Haswell's Aldol Reaction, Wittig reaction, some additions, reductions, oxidations, halogenations, metalations, heterocycle formation and cross-coupling reactions [201-204]. Most of the performance improvements are due to a rapid heat transfer and mixing and a precise temperature control [201]. Regarding cross-coupling, Pommella et al. [202], recently demonstrated the overwhelming capability of a microreactor respect to a batch one in getting a simple arylamine via Buchwald-Hartwig synthesis, i.e., a cross-coupling reaction. The term coupling refers to a reaction where two hydrocarbons fragments are coupled exploiting a metal catalyst. They are named homo-coupling when the two coupled fragments are identical, e.g., C-C, whereas cross-coupling involves two different fragments such as C-N. The most exploited catalyst for cross coupling is Palladium and many reactive pathways have been identified and developed exploiting it to produce organic and organometallic compounds. Starting from the seminal works of Heck, Stille, Suzuki-Miyaura, Sonogashira, Kumada, Negishi, Hiyama and Buchwald-Hartwig provided deep insight and developments on such synthesis. Buchwald-Hartwig amination reaction involves the coupling of an aryl halide and an amine in the presence of base and a Pd-based catalyst creating a new C–N bond, i.e., an aromatic amine is synthesized. What makes B-H amination ubiquitous, is the key-role of aromatic amines in many fields such as pharmaceuticals, agrochemicals, photography, pigments and electronic materials [205]. The choice and optimization of the catalyst is a key-step in the development of such synthesis and a decisive contribution to this field has been provided by Nolan and coworkers [206-208]. Pommella et al. [202], exploited a two feed microreactor to synthesize a simple arylamine by B-H amination using a palladium-N-heterocyclic carbene (NHC) complex as catalyst

1.6 Scope of the thesis

In this work, many multiphase systems related issues such as emulsion phase inversion, droplet interfacial properties and microfluidic reactive flows will be investigated by rheological (bulk

and interfacial), microfluidic and confocal microscopy means. Regarding emulsion phase inversion, a detailed experimental campaign will be conducted in order to identify the key-parameters acting on emulsion properties, confocal microscopy and microfluidics will be exploited as an optical sectioning tool to highlight the finest morphological detail of the emulsion; eventually rheological measurements will be used to relate macroscopical properties to the microscopical features of the emulsion. Droplet interfacial properties will be measured by microfluidic means and compared with well-established techniques such as pendant drop tensiometry. Eventually, a four-feed microreactor will be developed in order to synthesize an arylamine by coupling a secondary amine with an arylbromide via Buchwald-Hartwig synthesis. Microreactor performance insight will be provided in terms of reaction kinetics and conversion degree.

2 Theoretical Background

2.1 Phase behavior and its role in phase inversion

Phase behavior plays an essential role in studying emulsions properties. In general, amphiphilic molecules like surfactants or phospholipids show characteristic cooperative association in aqueous solutions leading to supermolecular structures such as micelles in a given surfactant concentration range. Hydrophobic interactions are the driving force of the phenomenon and are important for a thermodynamic description[209, 210]. The polar head groups of surfactants are indeed hydrated to allow appreciable water-amphiphile contact in the micelles [209]. An isotropic micellar solution is also named L_1 [211] or L_2 if made of reverse micelles [211]. For higher surfactant concentrations surfactant self-assembly leads to lyotropic liquid crystalline phases, i.e., larger equilibrium structures with high degree of organization such as hexagonal (long rods of surfactants forming hexagonal pillars, H_I or H_{II} if made of reverse micelles) [209, 212], reverse anisotropic nematic N_2 [213], discontinuous cubic (spherical aggregates packed with a cubic symmetry) [209], bicontinuous cubic (spherical interconnected aggregates packed with a cubic symmetry), Q or V, with relevant example in case of inverse cubic bicontinuous structure like gyroid G type (*Ia3d* denoted Q^{230}), diamond D type (primitive lattice *Pn3m* [214] denoted Q^{229}) and the primitive type (body centered lattice *Im3m* denoted Q^{224})[212]. In turn, these different structures give rise to differences in macroscopic properties, such as viscosity, which is lower in discontinuous structures with respect to bicontinuous ones [212]. Some of the most ubiquitous structures are lamellar (where sheets of amphiphiles are separated by thin water layers, Lα), sponge-like (interconnected lamellar phases, L_3), vesicles [175, 176, 215], also known as L_4 phases [216] when unilamellar, and bicontinuous microemulsion phases (D) [217-221]. Most of these phases sometimes display peculiar optical properties such as birefringence

[51][175, 176, 211, 222-224] and are often in equilibrium with a micellar phase. A possible way to rationalize amphiphile aggregation is based on the critical packing parameter (*V/la*)[225], where *V* is the volume of the surfactant hydrophobic group, *l* the length of the hydrocarbon chain, *a* the cross-sectional area of the surfactant hydrophobic core. When CPP=1, surfactant film has no tendency to curve and surfactant bilayers are favored. In particular, planar aggregates are found in the range ½<CPP≤1, whereas, for CPP<<1, micelles having hydrocarbon chains towards the internal part are favored, showing cylindrical aggregates for ⅓<CPP<½ and spherical ones for CPP<⅓. Reverse micelles, i.e. with water inside, are favored for CPP>1.

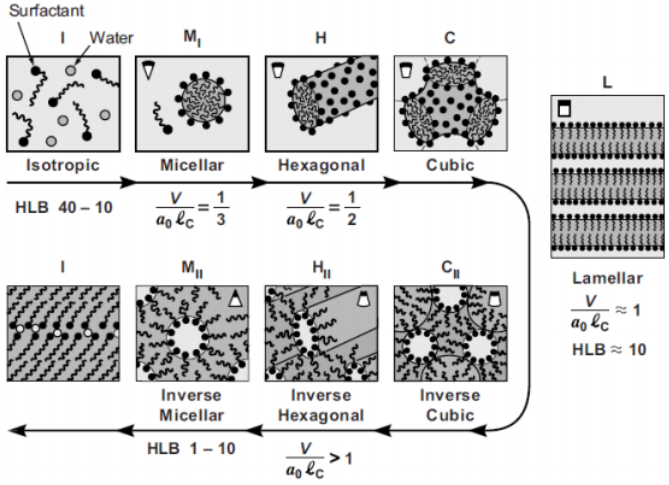

Fig. 14: Several phase structure at different critical packing parameter and HLB [225].

A classification for systems showing microemulsion phases in the case of surfactants-water-oil system has been given by Winsor [226] who stated the existence of four cases:

type 1: the surfactants are soluble in water and an o/w microemulsion is formed (Winsor I). The water phase is rich of surfactants and coexist with an oil phase where surfactants are only present as monomers at small concentration.

type 2: the opposite case of the first. The surfactant is oil soluble and a w/o microemulsion is formed, being this phase in equilibrium with a water phase with tiny amount of surfactants (Winsor II).

type 3: a three phase system where a surfactant rich middle phase is an equilibrium with two excess phases, one aqueous and one organic both having small amount of surfactants within them (Winsor III or middle phase microemulsion).

type 4: a single phase isotropic micellar solution, formed by using a sufficient quantity of amphiphile.

A seminal work on the role of phase behavior in phase inversion is due to Kozo Shinoda [36, 227] who studied temperature related phase behavior issues during phase inversion. He found that non-ionic surfactants are affected by temperature induced modification of the hydrophilic head, making non-ionic surfactant more hydrophobic and oil soluble by increasing temperature,

thus inducing a change in the curvature of the surfactant interfacial arrangement [36] (Figure 15). In particular, he reported a zero interfacial tension and flat curvature nearby the inversion zone [36]. Building on these results, a large number of studies have been performed [228].

Phase diagram in form of triangles where each vertex represents one of the component (oil, water and surfactant or mixture of them) are often exploited to describe the phase behavior. In PIT, the starting system is a water-in-oil emulsion (or viceversa) with nonionic surfactants and by changing the temperature the phases are inverted, so that the point representing the system on the phase diagram changes accordingly. In between the two emulsions, a so-called single phase region (possibly in equilibrium with an excess oil and water phase) extending from the water side to the oil side of the phase diagram corresponds to the intermediate system morphology, which is described as one of the phases already mentioned, such as a bicontinuous microemulsion [229] or a lamellar phase Lα. Both are favored due to their zero average curvature [230]. By the way, the bicontinuous microemulsion that could rise during the inversion process is really relevant for applications because able to develop nanoemulsion by its dilution [231] or is exploited as template for nanoparticles production [232-234]. In the inversion process, the transition from oil-in-water morphology to a bicontinuous microstructure and eventually to water droplets in an oil phase can be attributed to a change of the curvature of the amphiphilic monolayer from convex to concave passing through flat as depicted in Fig. 1 for a PIT process [230].

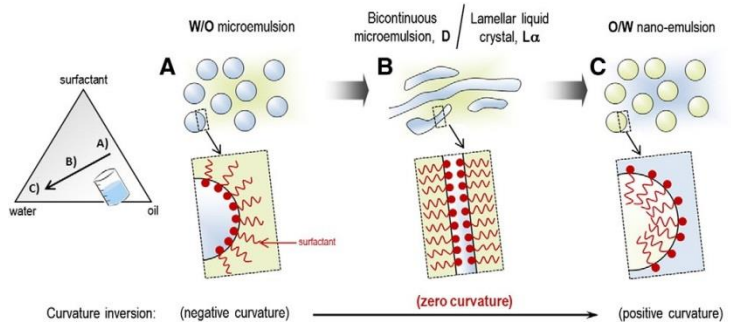

Fig.15: Emulsion inversion pathway with related interface curvature (image taken from reference [230])

The interfacial tension is sensitive to the change of curvature and optimum solubilization of oil into the aqueous phase is obtained at minimum interfacial tension occurring when the interface is flat [229]. Non-ionic surfactants have ethylene oxide (EO) groups as hydrophilic head. The interaction of EO groups with water decreases by increasing temperature and modifies the configuration of the EO groups usually inducing a shrinkage of their area [235]. As a result, CPP increases thus favoring a curvature change. Similarly, Strey [236] reported that for non-ionic surfactants within the CiEj (alkyl polyglycolethers [237], also known as CiEOj, or Brij) family, the mean interfacial curvature H (defined as $H= (c_1+c_2)/2$, with c_1 and c_2 principal curvatures) changes monotonically with temperature from positive (Winsor I system) to negative (Winsor II system) passing through a bicontinuous microemulsion (Winsor III system, or D phase) corresponding to a minimum in the interfacial tension. A similar pathway is also

suggested by Solans and coworkers [230, 238], who in addition highlighted the possibility to get a lamellar liquid crystalline phase Lα associated with the zero curvature domain. Anton et al. [74] proposed that fine oil droplets are produced by surfactant molecules migration from the organic phase to the aqueous phase which happens when the two immiscible phases are put in contact [74, 239]. The relevance of phase behavior in the development of phase inversion has been proposed for ionic nanoemulsions [240] as well. Pizzino et al. also reported the influence of phase behavior on emulsion of $C_{10}E_4$, water and n-heptane with further investigation on water oil ratio effect and temperature [241]. All these ways to interpret phase inversion are based on Shinoda's seminal work.

Regarding systems exploiting a mixture of ionic and non-ionic surfactants the intermediate phase has been found to be more likely an high internal phase emulsion or a structure resembling that of a polyhedral foam rather than a bicontinuous microemulsion [229]. Moreover, apart from varying temperature, a change in the interfacial tension could be obtained by adding a co-surfactant to the solution [229], thus exploiting the so-called synergism effect [236] where the use of a couple of surfactants lowers the interfacial tension with respect to a system having only one surfactant. This synergic effect to induce phase inversion is also exploited in PIC (see below), where one of the components is gradually added to the system while mixing [230]. In conclusion, the PIT process can be summarized in the following steps as recently done by Friberg et al. [242]: by decreasing temperature, once the upper temperature of the PIT range is reached, the original water in oil phase becomes a bicontinuous microemulsion in equilibrium with an oil rich phase with low amount of surfactants and water. In a way, this intermediate phase is swollen having absorbed part of the water and it disintegrates partly giving rise to small oil droplets when leaving the PIT range.

Concerning PIC, Wang et al. [243] and Roger et al. [244] stated that a hydration-driven change of curvature upon water addition which reduces oil solubilization leading to oil supersaturation and droplet nucleation, is the fundamental step in PIC (catastrophic) emulsification development [243, 244].Thus, a mechanism analogous to the temperature-induced curvature change in PIT has been proposed to explain PIC as well. Similarly, in previous works, other authors have indicated that adding water leads to the formation of water droplets which get easily elongated by the action of mixing flow thanks to the vanishing value of interfacial tension [238, 245, 246] and merge together to give lamellar structures eventually decomposing in fine oil droplets (Fig. 16).

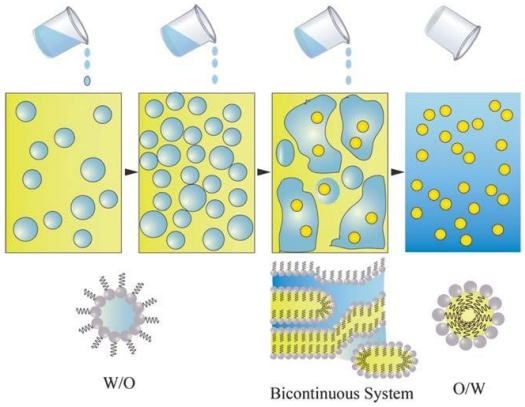

Fig. 16 Emulsion PIC pathway (image taken from reference [66])

Mercuri et al. [247] mix oil with surfactant to water in one step and observe a swelling of the organic phase which gives rise to regions of w/o microemulsions and then liquid crystalline phases at the droplet boundaries [239, 247]. Eventually, fragments of such lyotropic liquid crystalline phases break off from the droplet boundary migrating into the aqueous phase, thus dissociating into fine oil droplets. The differences in the observed behavior and in the proposed mechanisms can be partially attributed to the fact that the corresponding experiments were done at different values of a few important parameters in phase inversion emulsification, i.e., water addition rate, oil to surfactant ratio, oil content and phase behavior of the system. Hence, further work is needed in order to generalize the fine oil droplets formation mechanism involved in PIC phase inversion [239].

Phase inversion evolution (along with the effect of phase behavior) also affects the morphology of the final emulsion, which is an important parameter for industrial applications, being related, for example, to emulsion stability. For example, it is reported how, in an agitated vessel, a five times greater water addition rate acts to change nanoemulsion size from about 90 nm to 130 nm [230, 248]. Other key variables affecting the final emulsion morphology are: i) oil type [239], ii) surfactants type [239], iii) surfactants to oil ratio [239, 246, 249], iv) initial surfactant location [239], v) water to oil ratio [250]. Peculiar phase inversion pathways can be optimized in order to obtain microemulsions, nanoemulsions and bicontinuous emulsions with desired features [26, 40, 231, 246, 248, 251-257].

2.2 Phase Inversion in Emulsification maps

A macroscopic physico-chemical approach has been widely exploited by Salager and Sajjadi [35, 250, 258, 259] in order to describe the inversion phenomenon. For the sake of clarity, we shortly review some basic definitions that are commonly encountered when dealing with emulsification maps. A “normal” emulsion obeys to the so called Bancroft’s rule [35] (“the phase in which an emulsifier is more soluble constitutes the continuous phase”), whereas an “abnormal” emulsion does not [35]. HLB (hydrophilic lipophilic balance), a concept introduced by Griffin in 1949 [260] and then partially revised by Davies [261]is an index of the affinity of

a surfactant towards the oil (HLB <10) or towards the water (HLB>10). According to this classification, any oil-water emulsion, depending on the oil nature, has an ideal HLB to be stable. Thus an optimal formulation could be obtained by choosing properly the surfactant HLB. Alternative ways to obtain an optimal formulation are triggering the affinity of the surfactant towards the phase to be stabilized by changing temperature [35] (if the surfactant is temperature sensitive), or changing salinity, or alcohol content, or adding particles.

Salager et al. aimed at taking into account the physicochemical and composition variables of the system by introducing a generalized variable called SAD (surfactant affinity difference).“Formulation variables” depend on the nature of the components [250], while “composition variables” are the compounds weight or volume fractions [250].The SAD is the difference between the standard chemical potentials of the surfactant in the oil and water phase [250]:

$$SAD = \mu_{w*} - \mu_{0*} = \Delta G_{oil\text{-}water} = -RT \ln Kp \quad (3)$$

This relationship can be expressed as a function of the formulation variables, which for systems containing ionic and non-ionic surfactants respectively becomes [250]:

$$SAD/RT = \ln(S) - K * ACN - f(A) + \sigma - a_T \Delta T + Constant \quad (4)$$

$$SAD/RT = \alpha - EON + b*S - k * ACN - \phi(A) + c_T \Delta T + Constant \quad (5)$$

where the formulation variables are Kp (the partition coefficient of the surfactant between water and oil at the corresponding temperature), *S* (the salinity, wt% NaCl in the aqueous phase), ACN (the alkane carbon number or the equivalent EACN if the oil is not an alkane (hence, is depending on the oil phase in general), *f(A)* and $\phi(A)$ (functions of the alcohol type and content), σ and α (the characteristic parameters of the surfactant structure, where α depends on the lipophilic group of the surfactant), EON (the average number of ethylene oxide groups per molecule of nonionic surfactants), *b*, *k*, *K*, a_T, c_T (empirical constants that depend on the nature of the system) and ΔT (temperature deviation from 25°C). The value of the “Constant” is the SAD/RT calculated at the “optimum formulation” and its calculation can be found in the work of Salager et al. [84] as well. A formulation-composition bidimensional map shows how the composition of the mixture at which the emulsion inverts changes with SAD. In a nutshell, when SAD is positive the surfactant has more affinity for the oil and the favored emulsion is a normal emulsion, in particular an o/w microemulsion Winsor type I, but when the content of the "preferred continuous phase" for the surfactant is too low, the favored emulsion becomes an oil in water emulsion, i.e., an abnormal emulsion. The contrary in case when SAD is negative, whereas SAD=0 when the affinity for the phases is equal. Again, the interfacial tension is minimum for SAD=0 (balanced system).

In later works [258, 259] the SAD variable has been replaced by a more general formulation concept, the so called HLD (hydrophilic-lipophilic deviation from the optimum formulation obtainable by the HLB number), because for nonionic surfactants SAD is different from zero at

the optimum formulation. It is defined as HLD= (SAD-SAD_{ref})/RT where SAD_{ref} refers to the optimum formulation [262]. The HLD is a dimensionless parameter that characterize the behavior of a surfactant within a specific surfactant-oil-water mixture and depends on surfactant type, oil type, and aqueous phase properties such as pH, ionic strength and co-solvent [239]. For HLD<0 surfactant has more affinity for water, and form micelles that can stabilize o/w emulsion. The opposite occurs for HLD>0. When HLD=0 the affinity is towards both the aqueous and the oil phase and a bicontinuous microemulsions or liquid crystalline phase can be formed [239]. A formulation composition map with the HLD on the y axis and the water to oil ratio on the x axis can be exploited to rationalize an emulsification process based on phase inversion [239]. The HLD equation, for a system containing a ionic and non-ionic surfactant respectively is as follows [93,98]:

$$\mathrm{HLD} = \ln S - k\,\mathrm{ACN} + \sigma - a_T\,(T\text{-}25) \quad (6)$$

$$\mathrm{HLD} = k * \beta + b*S - k * \mathrm{ACN} + t\,(\mathrm{T}\text{-}25) + a * A \quad (7)$$

where $\beta = (\alpha - \mathrm{EON})/k$

α, k and t are surfactants parameters, b and a are constants characteristic of each type of salt and alcohol, S and A, the salt and alcohol concentration. The use of HLD it is convenient because at the "optimal formulation" HLD=0.

In the diagram below (Fig. 17), a bidimensional formulation-composition map is showed, where B indicates an oil rich phase, C a water rich phase and A an intermediate phase and + and – terms refer to HLD sign.

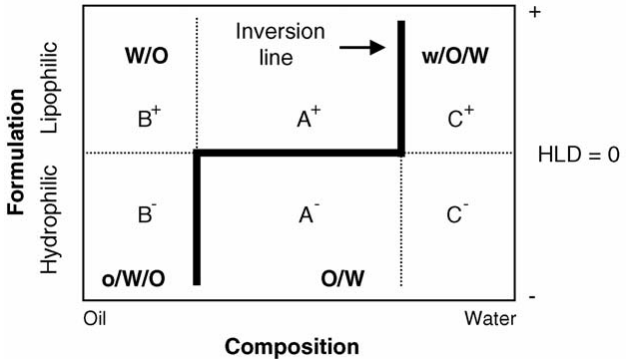

Fig. 17: Bidimensional formulation–composition map illustrating emulsion types (image taken from reference [263])

Moving vertically in the diagram represents a variation in the formulation of the system, while moving horizontally represents a variation in composition, i.e. water to oil ratio. The horizontal line corresponding to HLD=0 is referred to the flat curvature where the interfacial tension is minimum (Windsor III). Following the inversion line, which appears as a stair on the diagram, a transitional phase inversion is a process occurring between two kinetically stable normal emulsions (A^+, A^-, B^+, C^-), whereas a catastrophic phase inversion involves a transition between a normal and an abnormal emulsion (B^- and C^+) [35].

When water to oil ratio is varied between B^- and C^+ (abnormal emulsions) or between A^+ e C^+ to cross the inversion line (according to a catastrophic inversion), phase inversion could suffer a

delay (emulsion inversion does not take place immediately) due to multiple emulsion formation. It follows that vertical lines are replaced by an "uncertainty area" on the diagram, i.e., is not possible to exactly identify inversion line vertical branches location, but it is known that they fall in a certain region of the map identified by a triangular shaded area. These areas may also be seen as zones of hysteresis. A coupled variation of formulation and composition can slant the vertical branches of the inversion line, but doesn't affect the horizontal branch, which can be narrowed by lowering surfactants concentration, by increasing stirring energy or viscosity of one of the phases [250].

As stated by Salager et al., experimental work is still needed to characterize the effect of the mixing protocol onto catastrophic phase inversion emulsification and some efforts in this respect have been done in recent years by Salager and coworkers by studying some effects. Regarding the effect of stirring intensity on the catastrophic inversion frontier [264], it has been reported that for an intermediate stirring the inversion frontier is reached straightforward while for low stirring or high stirring regimes the formation of multiple emulsions could delay the inversion process. Moreover, the effect of the internal phase addition rate has been shown to be relevant in inversion frontier. If addition is slow the phase inversion can happen in smaller or larger time scales depending on the formation of multiple emulsions. For high addition rate the phase inversion seems to be delayed but happens in short time scales without displaying multiple emulsion morphology [265]. The conditions to trigger emulsion from abnormal to normal have been investigated in general [266]. The inversion from abnormal o/w to normal w/o emulsions by stirring and without the internal phase addition [263] has been also shown to be affected by multiple emulsion development. The use of continuous stirring has been exploited to generate high internal phase emulsions [267].

2.3 Multiple emulsions during phase inversion

As mentioned above, multiple emulsions genesis during catastrophic phase inversion has been investigated by many authors [268-272], and recently Liu et al. [251] summarized different explanations suggested by Groeneweg et al [272], Sajjadi et al. [273] and Klahn [274] et al. Groeneweg et al. attributed multiple emulsion formation to the enclosing of the film between colliding droplets, with the film becoming the inner droplet. Sajjadi et al. attributed the inclusion of the dispersed phase into the continuous one to the shear-induced deformation of the droplets. The observation of Sajjadi [273] is based on a previous idea of Ohtake et al. [275] and is consistent with the droplet shear deformation theory developed by Taylor [276] (where it is showed that shear droplet deformation increases with droplet diameter and decreases with interfacial tension). It is considered that surfactant at droplet interface can develop a concave interface, and that these concavities are enhanced by deformation thus permitting the continuous phase to migrate into the internal one. Klahn et al. [274] have also taken into account the importance of the escape process of the inclusion during multiple emulsion formation within

phase inversion phenomena, reporting that the inclusion must be counteracted by an escape process of inner droplets back into the continuous phase, depending on the drainage time scale of the film between the inclusion of an o/w droplet. If the drainage is fast enough on the time-scale of the inclusion-interface contact, escape will take place and will hamper phase inversion.
Mira et al. [264] attributed multiple emulsion creation during inversion to the low curvature interfaces which exhibit high local deformation, thus favoring the encapsulation of other droplets. Such emulsification pathway is far from thermodynamic equilibrium and the effect of the water addition rate should be relevant. Nevertheless, this parameter is usually neglected in most of the work dealing with catastrophic phase inversion. Bouchama et al. pioneered the study of the effect of the volume by which the dispersed phase is added on catastrophic emulsification. The latter should be not confused with the addition rate. E.g., by keeping the same addition rate (in terms of ml/min), the addition of water drop by drop can affect the system depending on the drop volume. Bouchama et al. reported that if water is added to a mixture of oil and surfactant by pouring continuously an amount less than the 0.2% of the entire mixture volume, the inversion locus happens for higher water volume fraction respect to the case of a larger amount of water addition and is independent from addition rate and stirring intensity, whereas, for larger aliquots of water addition, inversion is anticipated (it occurs for lowers volume fractions) by increasing addition rate or, equivalently, by increasing stirring energy. Bouchama et al. attributed this behavior to the formation of multiple emulsions, i.e., the inclusion of continuous phase in the droplets. During the formation of multiple emulsion there is a self-amplifying growth of the dispersed phase until inversion occurs. When water is added by larger volume, the probability to create multiple emulsion is enhanced increasing addition rate, thus permitting an inversion of the phases for lower water volume fraction added. An opposite effect has been reported by Zambrano et al. [265]. In this case, the higher addition rate caused a delayed but more rapid phase inversion whereas, for lower addition rate, inversion is anticipated but takes longer time scale. The authors attributed this different behavior to the formation of multiple emulsion that occurs in the case of low addition rate only. The disagreement between the two works could be due to many reasons, e.g., surfactants type and concentration exploited was different as well as the oil type and the water/oil ratio. It is clear that quantitative prediction of phase inversion time delay and overall time of inversion are limited to specific systems and experimental conditions. Nevertheless, the formation of multiple emulsion seems to play a relevant role in catastrophic phase inversion [277], as reported since the works on of Brooks and Richmond [270, 271] regarding systems containing surfactants. Bouchama et al. [30] well summarized the seminal contributions of Brooks and Richmond and Pacek et al. regarding the role of multiple emulsion formation during inversion. In particular, Brooks and Richmond stated that the effective volume fraction of the dispersed phase is higher than its actual volume when multiple emulsion are formed thus permitting phase inversion for lower dispersed phase

volume fraction respect to the cases where multiple emulsions are not formed. Pacek et al.[278] stated that inversion is possible when continuous phase droplets entrapped into the inner part of the multiple droplets reach a critical packing volume. Eventually, Jahanzad et al. [253] identified the formation of multiple emulsion as a prerequisite for phase inversion. Phase inversion could also be triggered by varying pH of the system. Besnard et al. [114] recently showed multiple emulsions formation just before emulsion inversion when pH is varied from 1.5 to 7.3 in a sytem water-toluene stabilized by a copolymer, i.e., PS_{48}-*b*-(PS_{31}-*co*-$PDMAEMA_{60}$).

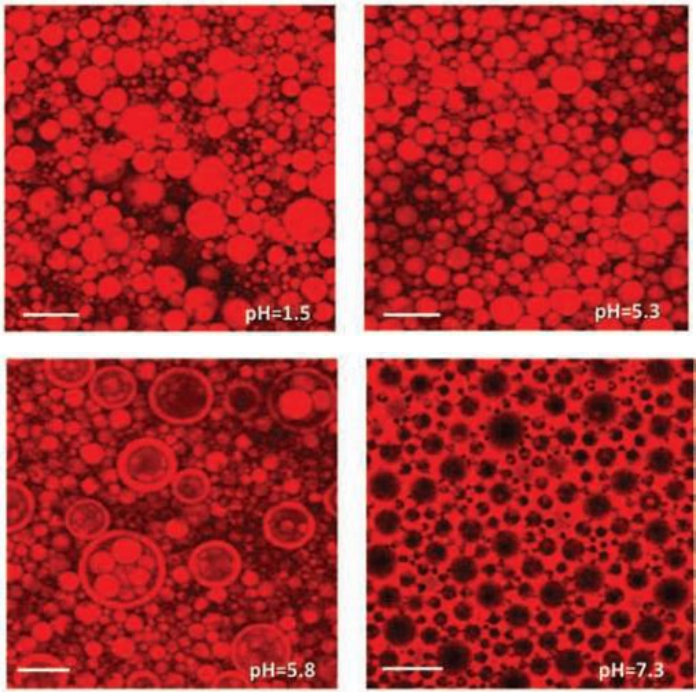

Fig.18: Fluorescent microscopy images. Evidence of multiple emulsions formation prior to phase inversion. The oil phase is red labeled by Nile Red. Scale bars represent 20 μm (image taken from reference [279])

2.4 The role of interfacial mechanical properties

The interfacial physical properties, such as bending, flexibility and elasticity, are not explicitly considered in the phase behavior approaches described above. These properties, however, are expected to play a key role in emulsion formation and phase behavior as shown by the work of Helfrich or based on his approach [236, 280-284], such as the ones by De Gennes and Taupin [245], Zemb [285-288] and coworkers, Gompper and coworkers [289, 290] and Cates [291-293] and coworkers. The Helfrich approach is based on the assumption that the bending energy is the most relevant property for the interface mechanical properties and its contribution to interfacial tension, in the case of bicontinuous microemulsion (the typical intermediate phase during inversion) can be expressed as proposed by Strey [236]:

$$\sigma = 2H^2(k+\bar{k}) + \bar{k}c_1c_2 \qquad (8)$$

where k is the bending rigidity (also known as bending elastic modulus, bending modulus or splay), $\bar{k}$ the saddle splay modulus (or saddle splay elastic constant), c_1 and c_2 the principle curvatures and H the mean curvature. De Gennes and Taupin approach is based on the role of persistence length on interface flexibility. The work of Gompper and Cates is mainly based on the elasticity theory of Ginzburg and Landau. It is intriguing to note that similar approaches have been also used to describe membrane properties in general, e.g., in the case of bilayer interfaces which are found in biological cells, such as red blood cells [174, 294-298] and lipid membranes [299-305]. In figure 19 a schematic representation of compression and expansion forces resulting from a bilayer bending.

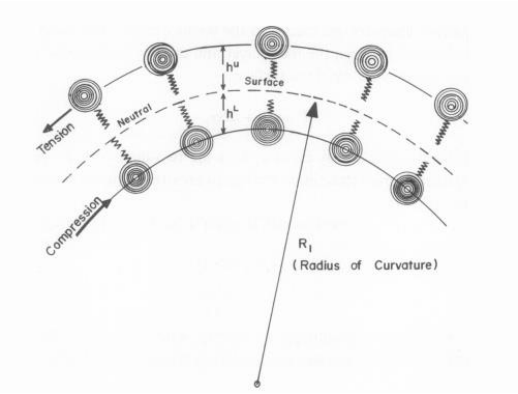

Fig. 19: Curvature schematic of a bilayer (image taken from reference [298])

Concerning the Helfrich approach, Kabalnov and Wennerstrom [306], revisited the oriented wedge theory previously developed by Harkins and Langmuir [306] (the original "oriented wedge theory" was also exploited by Harkins and Keith [307] to explain the inversion of emulsions, an approach that was however criticized later [306]), tried to outline the role of phase behavior, interfacial physical properties such as bending rigidity and spontaneous curvature in the evolution of PIT method. To quantify the role of interface bending rigidity and curvature they exploited the Helfrich's approach [280]. Here, a relevant role is attributed to the bending elasticity of the interfacial surfactant layer that is taken into account in the spontaneous curvature H_0. According to this theory, the inversion pathway is divided in the following steps: 1) oil in water emulsion, 2) emulsion breakage, 3) water in oil system. The passage from one step to the other is dictated by the change in spontaneous curvature elicited by variation of the bending elasticity. The capability of such argument seems to be very powerful in order to understand each phenomena related to phase inversion, e.g., some relations between rigid surfactant monolayer or multilamellar stabilized system and multiple emulsion development can be found. Also the relation between bending and coalescence rate can be explained by this theory.

2.5 Agitated Vessel: effect of process and material properties

From a macroscopic point of view, often useful in industrial emulsification processes, phase inversion has been interpreted and modeled by many authors as a dualistic dynamical

phenomenon between droplets coalescence and break-up [33, 37, 308, 309]. In the light of this consideration, phase inversion has been studied in agitated vessel and tube flow to predict morphology (average droplet diameter and mean Sauter diameter d_{32} so far) of the emulsion obtained. Phase inversion affects mass, momentum and heat transfer efficiency so it is of fundamental relevance to be studied.

Generally, in an agitated vessel, break-up is predominant nearby the impeller zone and inhibited in wall proximity, being the opposite for coalescence. Phase inversion is reached when coalescence rate overwhelm break-up rate over the majority of the vessel. In such a process-related approach, the role of temperature, flow regime, wetting, interfacial tension, viscosity, density, geometry and material of the vessel and of the impeller on breakup and coalescence has been discussed and reviewed [30, 33, 37, 277, 309-312].

In a system of two immiscible liquids a range of volume fractions exists beyond which both components may be the continuous phase. This range is known as "ambivalent range", the extension of which depends on how the dispersion is produced, on the volume fractions of the dispersed phase and the initial energy level of the system [33].The region of ambivalence is a metastable region, thus, any perturbation of the system can result in a reversal of the phase boundaries. There is a large range of volume fraction (between 0.3 oil in water and 0.3 water in oil) where each phase can be the continuous one depending on how the dispersion is produced [37]. In the work of Yeo et al. the example of water-hexane system is reported. The ambivalence region is delimited by two curves, the upper and the lower one. Above the upper curve, dispersion of water in hexane will occur, while below the lower curve of ambivalence, a dispersion of hexane in water will be present. It is clear that for a fixed amount of hexane nearby the ambivalence zone, hexane will tend to be the continuous phase by increasing the agitation speed. Above a certain value, the agitation speed will not affect more this phenomena, i.e., ambivalence curves are initially monotonically decreasing by increasing the agitation speed but after a certain point they become independent on the agitation speed.

Some efforts, since the studies of Ostwald [30, 33], have been done in order to understand which is the critical transition for the inversion of the dispersed phase into the continuous one. In the work of Ostwald it is assumed that the transition occurs when the system reaches a critical packing of its inclusions, in this case the droplets. By assuming that droplets are rigid equal sized spheres, the phase inversion may occur as a complete coalescence of the dispersed phase, when the volume fraction of that phase reaches the maximum efficiency of aggregation. This volume fraction is given by the Ostwald index that corresponds to the efficiency of aggregation of the spheres in a cubic structure in which the particles cover 74% of the space available and the remaining 26% is occupied by the external phase. In this theory, both droplet deformability and the formation of multiple emulsions, thus lowering the expected volume fraction for which phase inversion occurs, is not taken into account. Apart from the limitation of

using equal sized droplets, this model does not provide prediction on phase inversion induced solely by increasing agitation speed or by the action of flow.

2.5.1 Stirring speed

The input power of the impeller (related to the cube of the rotation speed) transmits mechanical energy to the liquid in form of turbulent motion, causing the breakage of a phase into small droplets, thereby increasing the interfacial area between the two phases, and facilitating transfer of matter. Yeo et al. [33] have reported that the lower limit of ambivalence decreases as higher agitation speed is used; i.e. at higher agitation speed, phase inversion occurs at lesser amount of the dispersed phase. This trend has been explained by stating that a greater stirring speed provides a greater initial energy to the droplets, which leads to an increase in the phenomenon of coalescence, and therefore to a larger average size of the drops. The upper curve shows a shifting upward with increasing agitation speed. This trend of the curve of ambivalence has been explained by considering the secondary dispersions (multiple emulsions). The greater is the speed used, the smaller will be the droplets of the dispersed phase (water) that are formed and the greater will be their tendency to coalesce, reducing the amount of continuous phase (oil) that is trapped.

It is noted that the inversion of the dispersion of oil in water occurs at lower values of the dispersed phase respect to the inversion of the dispersion of water in oil and this has been explained by the presence of an electrostatic charge on the droplet (will be explained better in the next paragraph). Yeo et al. also reported that with increasing agitation speed, the difference between the average size of the oil drop in water and the average size of the droplet of water in oil, is reduced by an amount that is related to the amount of the external phase (oil) trapped in the dispersed phase (water) in a dispersion of oil in water, thus confirming the presence of secondary dispersions. In all cases, increasing the stirring speed of the inversion curve tends to an asymptotic value, i.e., the volume fraction of the organic phase reaches a constant value. For this transition, asymptotic linear relations of the organic phase for the two curves have been proposed as a function of the Weber number We, which is a dimensionless number relating inertia-induced droplet breakup with the restoring action of interfacial forces. The Weber number can be also seen as the ratio [37] $t_{break\text{-}up}/(\sigma/d_{droplet})$, where $t_{break\text{-}up}$ is the characteristic break-up time, σ is the interfacial tension, $d_{droplet}$ the droplet diameter. The asymptotic relations reported by Yeo et al. [33] are the following:

-higher inversion curve

$$\phi_{o,i}^{U} = 0.160 + 6.0x10^{-5} We_I \tag{9}$$

-lower inversion curve

$$\phi_{o,i}^{L} = 0.470 + 2.0x10^{-5} We_I \tag{10}$$

The impeller Weber is defined as follow:

$$We_I = \frac{\rho_c N^2 D_I^3}{\sigma} \tag{11}$$

where ρ_c is the density of the continuous phase (Kg/m^3), N is the rotation speed (r.p.m), D_I impeller diameter (m) and σ is the interfacial tension (N/m). Usually We is defined in terms of $v^2 l$ (v, fluid velocity; l, tube characteristic length) rather than $N^2 D_I^3$, but in agitated vessel is more convenient to use the impeller Weber. (9) and (10) are valid for We_I within 350-4000.

Usually many relations are available to characterize droplet break-up and what is usually given by these models is the range of sizes of the droplets produced and the Sauter mean diameter d_{32} [37]. The latter is defined as the area-volume mean and links the area of the dispersion to its volume or mass and is related to the specific surface area of the droplets, a, by the relation $a = 6\phi/d_{32}$, where ϕ is the volume fraction of the dispersed phase [37]. The effect of different types of impellers on droplet size is reported in the work of Nienow [37].

Mira et al. reported a series of studies showing the increased phase inversion point by increasing agitation speed both with and without surfactants. Coupling the role of surfactants and agitation speed, nontrivial results come out. As reported by Mira et al. [264], phase inversion could be favored either by low energy stirring and high energy stirring, being inhibited by intermediate energy stirring. The explanation they gave is based on the low curvature interfaces configuration in the low energy case due to the presence of big droplets. The presence of such droplets could favor multiple emulsion creation and hence phase inversion. In the case of high energy stirring big droplets and low curvature interfaces are not favored anymore but the high agitation energy speed-up the surfactant adsorption from the bulk to the interface thus permitting the formation of droplets inside droplets, which the authors consider as the leading inversion mechanism. In the intermediate energy stirring regime droplets are not big enough and surfactant adsorption also is not fast enough, thus, for both reasons, phase inversion is inhibited. However, a major role is also played by the HLD. When HLD<0 (that corresponds to HLB>11, i.e. hydrophilic system) the system is largely insensitive to rate of addition and stirring energy, because phase inversion is already fast enough due to faster surfactant adsorption of the hydrophilic surfactant. On the other hand, when HLD>0 (HLB<10) the system is largely affected by addition rate and stirring speed. Similar results have been reported also by Tyrode et al. [266]

2.5.2 Wetting

Wetting refers to the propensity of the vessel/impeller material to be wet by one of the phases [313]. Especially in the absence of surfactants, the vessel material can influence phase inversion

[33]. Wetting is affected by surface roughness [314], heterogeneity of the surface [314], temperature [314], trace elements [314] and is in turn related to viscosity, interfacial tension and density of the phases [314]. It was observed that wetting influences the frequency of collision of the droplets and thereby coalescence, resulting in a change of the inversion process [33]. In agitated vessel break-up occurs in the vicinity of the impeller while coalescence occurs initially in the region farthest from it. However, if the impeller is mainly wet from the dispersed phase, there is the possibility that droplets approaching the impeller can coalesce, thus affecting the mechanisms of coalescence and breakup [33]. In a stainless steel vessel/impeller, which is water-wetted, phase inversion from oil continuous to aqueous continuous occurs at much lower concentrations of oil when compared to a preferentially oil-wetted Plexiglass tank and impeller [37]. This aspect could be relevant in scale-up issue because usually lab-equipment are made of Plexiglass or glass while pilot and industrial scale are usually made of stainless steel (one should also take into account that area to volume ratio is higher in lab-scale equipment with respect to industrial one [37]).

2.5.3 Density

If the density of the aqueous phase and of the oil is similar, there are no particular effects on the phase inversion, whereas when high densities differences are present, phase inversion is promoted due to the increase in the relative velocities between dispersed and continuous phases [33]. If dispersed phase is less dense than the continuous one, the delay time to reach inversion gets shorter with increasing speed as the centrifugal force is strengthened, while if the dispersed phase is denser, the trailing vortices tend to centrifuge out the droplets and consequently delay time increases, limiting catastrophic inversion [37].

2.5.4 Viscosity

Usually, if the dispersed phase is more viscous than the matrix, break-up is slowed down [37]. High viscosity ratios between the phases cause secondary dispersions [33]. The tendency of a phase to disperse decreases with its viscosity. The increase in the viscosity of the two liquids, increases the time of drainage, corresponding to a lower coalescence rate that gives a wider ambivalence zone, thus inhibiting phase inversion. Moreover, the agitation is less efficient when the dispersed phase is next to the phase inversion locus. The system viscosity assumes a maximum value in the vicinity of the point of inversion, which is an indication of when the system is next to inversion.

2.5.5 Interfacial tension

As observed by Yeo et al. [33] the lower the interfacial tension, the greater the resistance of the system to the inversion, as a drop undergoes a break-up when the kinetic energy transmitted to droplet by turbulent eddies exceeds the droplet interfacial energy, which is linked to the interfacial tension. Therefore a reduction of the latter enhances droplet break-up. In addition a

lower interfacial tension causes a decrease of the drainage time of the film between two approaching droplets through the Marangoni effect, i.e. the continuous phase liquid flows back into the film to suppress interfacial tension gradients due to droplet deformation [315-318]. Hence surfactants hinder coalescence with respect to break-up causing an enlargement of the region of ambivalence and therefore a higher resistance of the system to the inversion. Even impurities, such as solid particles can change the inversion process by lowering the interfacial tension.

2.5.6 The role of electrostatic charge

In the review of Yeo et al. [33], the role of electrostatic charge has been thoroughly reported and is summarized here. The charge on the surface of the droplets may inhibit the coalescence process, since electrostatic effects due to the presence of hydroxide ions at the interface significantly stabilize the dispersions, irrespective of the presence or absence of surfactants. The presence of these ions allows to explain why the phase inversion of oil in water occurs at lower values of the inversion of water in oil. This asymmetric behavior assumed by a liquid-liquid system is due to the fact that the droplets carry a charge due to the great difference between the dielectric constants of the two immiscible phases. It is this difference that makes the interaction of the drops of oil in water different from the interaction of the drops of water in oil. The drops of oil in water show a repulsion due to overlap of electrical double layers who inhibit coalescence. Conversely, drops of water in oil do not exhibit this effect, and their higher coalescence efficiency can generate multiple emulsions.

2.5.7 Phase inversion time delay

Since the electrical conductivity of water-in-oil emulsions compared to oil-in-water ones differs by several orders of magnitude, the conductivity can be used to determine the type of emulsion and the area of phase inversion [33, 264]. Delay time (the time to reach the phase inversion point) can vary from zero (instant inversion) to infinity (the inversion does not occur, i.e., the dispersion is stable).

The inversion takes place in an extremely small range of time as seen from the steep variation of electrical conductivity at the inversion point. During the initial delay, droplet size grows with time. In proximity of the inversion point, a certain critical concentration of droplets is reached where coalescence ultimately leads to phase inversion. Hence, effects promoting break-up lead to an increase of the delay time, and the opposite happens when coalescence is favored. Intuitively, time delay is lower with higher agitation speed if coalescence is enhanced and it increases by increasing phase viscosity or surfactant concentration because both these variables inhibit coalescence rate. A proposed relationship to predict the delay-time is [33]:

$$t_I = 0.048 V^{0.66} \phi_d^{-0.33} D_{tr}^{-1.0} \tag{12}$$

ϕ_d the dispersed phase volume fraction, , V the vessel volume (m^3), D_{tr} is the turbulent diffusion coefficient that characterizes the eddies diffusion in a turbulent system and is obtained from this equation:

$$D_{tr} = \alpha' * \bar{\varepsilon}^{0.33} * \lambda'^{1.33} \tag{13}$$

with $\bar{\varepsilon}$ the average energy supplied per unit mass (J/Kg), λ' eddy length (m) and α' dimensional constant. As reported in the section regarding multiple emulsions formation during inversion, the latter could affect time delay thus leading to results not predictable with the above described approach.

2.5.8 Predicting the phase inversion point

A theoretical link between the point of phase inversion and physico-chemical parameters would reduce the amount of trial and error to predict the inversion point of a given system. The various proposals for possible relationships, reported by Yeo et al. [33], are as follows:

i) The organic phase volume fraction at inversion ($\phi_{o,i}$) is inversely proportional to the power $P(Watt)$ delivered to the system [319]:

$$\phi_{o,i} = \phi'_{o,i} + \frac{\alpha}{P} \tag{14}$$

Where $\phi'_{o,i}$ is the asymptotic value of the organic phase volume fraction at high impeller speed (is a constant), and α is a constant

$$P = K\rho_m N^3 \text{ (power delivered to the system)} \tag{15}$$

$$\rho_m = \rho_d \varepsilon_d + \rho_c (1-\varepsilon_d) \text{ (mixture average density)} \tag{16}$$

Where K is a constant, ρ_m the mixture average density, ρ_d the dispersed phase density, ρ_c the continuous phase density, ε_d the dispersed phase volume fraction.

ii) a relation to estimate ambivalence region width W based on the criterion that the curves of the upper and lower inversion are linearly related to Weber number and (see (9) and (10)) is directly affected by interfacial tension σ:

$$W = \phi^U_{o,i} - \phi^L_{o,i} = (0.094 * N - 64.0) * \sigma^{-(0.82+0.6610^{-3}*N)} \tag{17}$$

iii) based on the criterion that the total energy of the system should be minimized and thus the phase inversion is a spontaneous process, two relations are proposed for the higher $\phi^U_{o,i}$ and lower curves of inversion $\phi^L_{o,i}$

$$\phi_{o,i}^{U} = 1.32 \cdot 10^{6} * \left(\frac{\eta_d}{\eta_c}\right)^{0.32} \left(\frac{\Delta\rho}{\rho_c}\right)^{-0.11} Fr_I^{0.71} \mathrm{Re}_I^{1.06} We_I^{-0.25} \tag{18}$$

$$\phi_{o,i}^{L} = 12.2 * \left(\frac{\eta_d}{\eta c}\right)^{0.31} \left(\frac{\Delta\rho}{\rho_c}\right)^{0.04} Fr_I^{0.13} \mathrm{Re}_I^{0.22} We_I^{-0.03} \tag{19}$$

η_c is the continuous phase viscosity, the η_d dispersed phase viscosity, ρ_c the continuous phase density, $\Delta\rho$ the density difference between the phases. Fr_I is the impeller Froude number $Fr_I = N^2 D_I^{\ 3}/g$ and relates inertia with gravity. Re_I is the impeller Reynolds. D_I is the impeller diameter, g the gravitational acceleration.

iv) The limits of the region of ambivalence depend primarily on the coefficient of kinematic viscosity between the two phases, and the volume fraction of the dispersed phase inversion is given by the following relationship

$$\frac{\phi_{d,i}}{1-\phi_{d,i}} = \sqrt{\frac{\eta_d}{\eta_c}} \tag{20}$$

Where η_c is the continuous phase viscosity, the η_d dispersed phase viscosity, $\phi_{d,i}$ the dispersed phase volume fraction at the inversion point. The relation and is obtained assuming that the coalescence drives phase inversion and is affected by viscous forces rather than inertial ones. All of these expressions do not take into account the mass transfer which affects the limits of ambivalence region and phase inversion.

Yeo et al. [320] exploited a stochastic model to predict the phase inversion locus using a Monte Carlo technique, but its validity fails to catch the ambivalence region. However, Yeo et al. [321] later developed a simple analysis for agitated vessels based on the criterion of the interfacial minimization thus providing a relation capable to localize the inversion locus also in the presence of the ambivalent region (we will describe in the next section how the concept of "interfacial minimization" has been exploited by many authors to model phase inversion, in particular from Brauner and Ullmann [308] to describe phase inversion in tube flow):

$$\frac{\phi_{o,i}}{1-\phi_{o,i}} = \frac{d_{32\ o/w}}{d_{32\ w/o}} \tag{21}$$

$\phi_{o,i}$ is the inversion holdup, d_{32} the mean Sauter mean diameter, appropriately calculated for each morphology [321]. They found qualitative agreement with the experimental results of Selker & Sleicher [322]. The model is not able to take into account the effect of the agitation

speed, so is limited to the case where the agitation speed is high enough to prevent settling. As the same authors stated, further developments of the model, such as the use of viscosity model adequate for each case, could be done in order to fit a larger set of experimental results. Hu et al. [312, 323] developed a two region model where a relation for break-up rate and coalescence rate are provided. Here it is assumed that phase inversion happens when coalescence frequency overwhelm breakup frequency. A particular radial distribution function has been exploited in order to take into account coalescence in the case of concentrated droplets. The effect of interfacial tension, viscosity, density and impeller size on the width of the ambivalent region is considered in the model. Good agreement has been found for the upper limit of the ambivalent zone, whereas the lower one is often underestimated.

Salager et al. [250, 258, 266] argued that this kind of kinetic competing phenomena approach (i.e., breakup vs coalescence), even if satisfactory from a mere physical point of view, is still difficult to handle for quantitative features, being dependent on too many variables yet not fully mastered.

2.6 Tube Flow

In the chemical and petroleum industries, mixtures of oil and water are transported for long distances in horizontal pipes by means of pumping systems. During pipeline transportation of very viscous crude oil, water is introduced in order to reduce pumping energy required to transport oil through the ducts. Moreover, to extract oil from oil wells, aqueous solutions (viscoelastic surfactant solutions, nanoemulsions etc.) are always injected into the reservoir to push out oil. So water is ubiquitous and in some conditions a water in oil mixture can revert into an oil in water one during pipeline flow. The design of these ducts and of the pumping equipment requires an analysis of the flow patterns of the two phases and the related pressure drop. There are several flow patterns each of which is governed by different mechanisms and pressure gradients. A further complication is the non-Newtonian rheological behavior of oil-water systems. The phase inversion plays a key-role in all of the above mentioned applications and flow pattern developments. In the oil industry the lack of adequate relations to predict phase inversion hinders process optimization [38].

The main flow patterns of oil-water systems in a tube can be classified as follows:

Segregated flow: the two phases of the fluid flow in separate layers on both surfaces

Slug Flow: in which a liquid phase flows like a confined spherical or elongated droplet in another liquid phase

Dispersed flow: in which a fluid is dispersed into droplets within a continuous phase of another fluid

Yeo et al. [33], reviewed phase inversion in tube flow and in agitated vessel. More recently, Brauner and Ullmann [308] reviewed phase inversion in tube flow and they also reported, in the same paper, a novel developed model describing phase inversion in tubes. This model exploit

the so-called surface free energy minimization approach (a literature review on the previous works that exploited such approach can be found in the work of Brauner and Ullmann) coupled with a model for droplet size in dense dispersions. The main idea is that the system switch the morphology from oil-in-water (water-in-oil) towards water-in-oil (oil-in-water) once the opposite morphology is associated with a lower free energy. Their considerations start with the definition of the oil-water surface energy (per unit volume of the mixture):

$$E_{ow} = \frac{6\sigma\varepsilon_d}{d_{32}} \tag{22}$$

Where σ is the oil-water interfacial tension (considered the same in the case of water-in-oil dispersion), ε_d is the dispersed phase volume fraction, d_{32} the Sauter mean drop diameter. Then, a formulation for the overall surface energy in case of an oil-water dispersion is given:

$$E_{S_{ow}} = \frac{6\sigma\varepsilon_o}{(d_{32})_{o/w}} + s\sigma_{ws} \tag{23}$$

Where ε_o is the oil volume fraction, $(d_{32})_{o/w}$ is the Sauter mean diameter in the oil in water dispersion, σ_{ws} the water-solid surface tension coefficient and s the surface area per unit volume, with s = 4/D for smooth pipe. An analogous relation is given for the water-oil dispersion where the oil volume fraction is replaced by the water volume fraction, i.e., $(1-\varepsilon_o)$, the water in oil dispersion Sauter mean diameter considered as well as oil-solid surface tension coefficient. In both overall surface free energy relations is assumed that solid surface is completely wetted by the continuous phase. At the phase inversion point both morphologies, i.e., oil-in-water and water-in-oil are dynamically stable, hence the respective overall surface energies are equal. Moreover, considering Young's equation:

$$\sigma_{os} = \sigma_{ws} + \sigma cos\theta \tag{24}$$

where θ is the liquid-solid wettability angle, σ_{ws} the water-solid surface tension, σ_{os} the oil-solid surface tension, a relation for phase inversion point could be obtained:

$$\varepsilon_o^I = \frac{[\sigma/d_{32}]_{w/o} + \frac{s}{6}\sigma cos\theta}{[\sigma/d_{32}]_{w/o} + [\sigma/d_{32}]_{o/w}} \tag{25}$$

Where ε_o^I is the oil volume fraction at the inversion point, $0 \leq \theta < 90°$ corresponds to a surface which is preferentially wetted by water (hydrophilic surface), whereas for $90° < \theta \leq 180°$ the oil is the wetting fluid (hydrophobic surface). d_{32} can be approximated to $d_{32}=d_{max}/k_d$, with k_d, a constant depending on the fluids system, falling in the range 1.5-5. Considering that Azzopardi & Hewitt [324] reported a k_d value equal to 5 when the system is composed of a large number of droplets, assuming that interfacial tension is constant also after phase inversion and given the solid-liquid wettability negligible effects (i.e., θ=90° or s nearby zero that holds for large pipe diameter, where d_o, d_w << D_{tube}). Brauner and Ullmann came up with a simplified relation for the phase inversion point:

$$\varepsilon_o^I = \frac{d_o/d_w}{1+d_o/d_w} \tag{26}$$

With d_o and d_w representing the maximum drop size in the oil-water and in the water-oil dispersion respectively. The final part of the model development is related with the possible relations for d_o and d_w. The authors exploited the continuous phase d_{max} provided by H-model developed by Brauner [325]. In this relations, d_o and d_w both depend on mixture velocity, pipe geometry, surface tension, whereas the ratio between them does not. Eventually, a simple version of the phase inversion point equation could be written:

$$\varepsilon_o^I = \frac{\bar{\rho}\bar{v}^{0.4}}{1+\bar{\rho}\bar{v}^{0.4}} \tag{27}$$

$\bar{v}$ is the kinematic viscosity ratio of the two phases, i.e., v_o/v_w, $\bar{\rho}$ the ratio between the two phases density. Brauner and Ullmann compared their model to previously published experimental works both in laminar and turbulent flow and found qualitative agreement. The authors made also some model arrangements in order to fit experimental data of phase inversion in static mixer (published by Tidhar et al. [326]) and found quantitative agreement. One of the limitation of such approach is the absence of surfactants assumption, hence the typical role of phase behavior cannot be faced by similar models.

Ngan et al. [327] suggested an intuitive method to predict phase inversion in tube based on the idea that phase inversion happens at the phase fraction where the difference in viscosities between the two possible dispersions, oil continuous and water continuous is zero. The authors exploited a large set of viscosity correlation (as a function of the dispersed volume fraction) in order to fit experimental data and found that viscosity models of concentrated suspension and solution are good enough to fit the inversion locus. Also this model could be hardly exploited in system containing large amount of surfactants where usually viscosity behavior is completely different by changing surfactant type. Poesio and Beretta [309] interpreted phase inversion in a tube by using what they called a "minimal dissipation approach". The development of the model is based on the idea that the system chooses the configuration having the minimal energy cost, i.e., the one with lower pressure drop. Here, the basic idea is similar to the one proposed by Brauner and Ullmann [308], where it is analogously stated that the system invert in order to minimize the overall surface free energy. Starting from a water-in-oil emulsion in turbulent flow and then diluting with water, after a certain dispersed phase volume fraction, the pressure drop of the water-in oil system is much higher than the corresponding oil-in-water mixture having the same percentage of oil, so the system tends to invert phases from water-in-oil into oil-in-water. In a nutshell, by adding one phase into another in tube flow, pressure drop arises and phase inversion is occurring when the pressure drop maximum is reached, after this point pressure drops back until the final morphology is obtained (an oil-in-water if the initial emulsion was water-in-oil). This evidence has been showed also by Piela et al. [328]. Poesio and Beretta calculated pressure drop starting from the consideration that:

$$\Delta p = L \cdot dp/dx \tag{28}$$

where Δp is the pressure drop, L the tube length, and dp/dx the derivative of pressure over the space. The latter expressed as:

$$\frac{dp}{dx} = 2f_m \frac{\rho_m U_m^2}{D} \tag{29}$$

where $U_m = 4\left(\frac{\dot{m}_0}{\rho_0} + \frac{\dot{m}_w}{\rho_w}\right)/\pi D^2$ is the mixture velocity, $\rho_m = \rho_w \epsilon_w + \rho_0 \epsilon_0$, is the mean mixture density, D is the pipe diameter, ϵ_w the volume fraction of water and $\epsilon_0 = 1 - \epsilon_w$ the volume fraction of oil. For the mixture friction factor they assumed, similar to Blasius:

$$f_m = \frac{C}{Re_m^n} \tag{30}$$

with C and n depending on flow regime and the mixture Re number defined by using an effective viscosity. If the flow is laminar $Re_m \leq 2300$ C=64 and n=1, if the flow is turbulent $Re_m \geq 2300$, C=0.079, and n= 0.25.

For the viscosity they exploited a relation proposed by Ball and Richmond [329]:

$$\mu_m = \mu_c \left(1 - K_{\epsilon_d}\right)^{-5/(2K)} \tag{31}$$

Where μ_c is the continuous phase viscosity, ϵ_d the discrete phase hold-up, and $1/K$ can be interpreted as the maximum packing fraction and is retained nearby 1 for densely packed monodispersed deformable droplets. Hence, $1/K$ is 1. Once all these variables are defined, dp/dx is calculated as a function of hold-up volume fraction. The calculation is done twice, the first time, starting from the water-in-oil phase and increasing water volume fraction, the second time starting from the oil-in-water phase by increasing oil volume fraction. The two so-obtained curves cross each other for a certain volume fraction, and this volume fraction is taken as the phase inversion point. Analytically, it comes out that the phase inversion point can be calculated by the following expression:

$$\epsilon_w^I = \frac{1}{1+\left(\frac{\mu_0}{\mu_w}\right)^{2/5}} \tag{32}$$

$$\epsilon_0^I = \frac{1}{1+\left(\frac{\mu_0}{\mu_w}\right)^{-2/5}} \tag{33}$$

These expression are valid both for laminar and turbulent flow, and do not depend on density of the phases, velocity and tube diameter. As pointed out by the authors what is missing is to take into account wettability and interfacial tension, thus not allowing to predict the existence of the ambivalent region.

Poesio and Beretta [309] compared their modelling approach with the experimental data given by Arirachakaran [330], Nadler and Mewes [331] and Brauner and Ullmann [308] finding a

good agreement only with Nadler and Mewes. Poesio and Beretta compared also their model with the pipe flow experimental data of many authors, collected by Brauner and Ullmann. Here, the discrepancy between the minimal approach dissipation rate and the experimental data is much higher than the above mentioned cases mainly because the model does not consider the existence of the ambivalence region. Poesio and Beretta tried also to model ambivalent region by using a two parameter (K_1 and K_2, dependent on material wettability and maximum droplet packing) viscosity formulation obtained by fitting experimental data of Ioannou et al. [332]. They found good agreement of their model (containing the novel formulation for viscosity) and data of Iannou et al., also in the ambivalent region, but they limited the comparison of the novel model formulation only to the experimental data of Iannou et al. It seems that the minimal approach dissipation rate could be good enough for a rough prediction of phase inversion in tube, with limitations for the prediction of the ambivalent region. Moreover, we cannot say whether this model could be suitable for system rich of surfactants.

The hampering issue in development of phase inversion theoretical modeling is the difficulty into identify the leading mechanism responsible for the inversion. As pointed out by Hu et al. [333] , one key-step could be identified in the evolution of drop size during the process. Population balance equations (PBE) [334] describes how populations of "entities" interact with their environment, generally assumed to be continuous. Such "entities" could be particles, droplets [335], or ensemble of systems of state being represented by a vector. The overall description of the system is provided by the equations of conservation of mass, momentum and energy (related to the continuous phase), coupled with the PBE (related to the "entities" phase). Usually, detailed description of the fluid dynamics and mixing is required to solve PBE within computational fluid dynamics code [336]. Moving from this considerations, Hu et al. [333] applied population balance equations to model phase inversion in tube thus showing a qualitative agreement of the simulated droplet size with the experimental one. The existence of the ambivalent region in terms of the distance from the tube inlet, rather than function of the dispersed volume fraction, has been also predicted by their simulations. PBE have not yet exploited to predict phase inversion when surfactants phase behavior plays a key-role, and we cannot even say if they are suitable for this aim. Usually, PBE are not capable of dealing with the surfactants interfacial behavior.

Piela et al. [328, 337, 338] studied phase inversion in tube without added surfactants. They studied the phenomena in direct, continuous and discontinuous experiments. In a direct experiment the two phases are fed simultaneously in the tube. In the continuous way, the dispersed phase is injected gradually into the other phase, until it becomes the continuous one. In the discontinuous approach a pure water phase is flowing through the pipe, and at a certain moment it is changed to a pure oil phase (or vice versa), so that in a certain region of the mixing zone phase inversion will occur. They demonstrated how the continuous feeding way is

useful to induce phase inversion at higher values of the dispersed phase respect to the direct experiment; moreover, they showed, by taking images of the morphology at transition, that both continuous, discontinuous and direct feeding have the same morphological transitions, with the dispersed phase present always as a dispersion of nearly spherical droplets at the starting and at the end of the inversion process. On the contrary, the intermediate phase has a morphology rich of multiple droplets and "pockets" containing droplets, with an evolution towards the inverted isolated droplets morphology induced mainly by coalescence, break-up and escaping phenomena. They also stated in a later work [339] that the creation of such morphology, i.e., multiple emulsions of oil in water in oil droplets (the so called "pockets") along with a dispersion of clean oil drops in water is due to the presence of surface active substance already present in the liquids, with an affinity towards oil rather than water. During the continuous experiment they showed that the critical volume fraction of the dispersed phase (the volume fraction to achieve inversion) is not dependent on Reynolds number, Froude number, Weber number and on the dispersed phase injection velocity as long as the latter is sufficiently large (2 m/s) [311, 337, 339]. Piela et al. [337] also showed that the ambivalence region is unique for a specific water-oil mixture. Their final statement is that phase inversion critical volume fraction is dependent only on the injected phase volume fraction and that the effect of surfactant [339] is only to shift the ambivalent range and does not alter the linear relationship between critical volume fraction and injected phase volume fraction. It has to be noted that the surfactant used by Piela et al. was at low concentration, nearby CMC; it is not clear whether larger surfactant concentrations could have an impact on the ambivalent region.

Piela et al. [311] exploited the classical Ginzburg-Landau mean-field theory of phase transitions in thermodynamics to describe phase inversion phenomenon. The external filed driving phase transition is considered to be the shear stress caused by the pressure drop over the pipe. By considering the friction factor f as function of the injected phase volume fraction, they modeled the existence of the ambivalent region. They found agreement between experimental ambivalence region and predicted one [311], thus corroborating the experimental results that for such a mixture the ambivalence region depends on the injected phase volume fraction and it is independent on the Reynolds, Froude, and Weber numbers and also independent on the injection rate, as long as the mixture velocity is large enough. Moreover, they pointed out that when the oil type is changed or when a surfactant is added, the ambivalence region changes and two new experiments (one starting from oil and the other from water) need to be performed. However, this model was not compared with other literature studies, especially when large amount of surfactant are exploited.

Recently, the key-role of coalescence during phase inversion has been elucidated by microfluidic means by Bremond et al. [340]. However, surfactant concentration used was 0.3%

wt and given the use of a larger surfactant amount for phase inversion emulsification, further investigations are needed to understand what happens in concentrated amphiphile regimes.

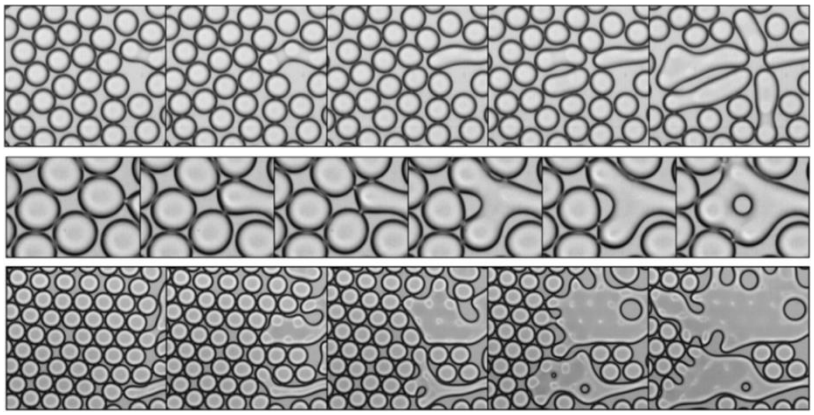

Fig. 20: Coalescence during phase inversion process, emulsion with hydrophobic surfactant Span80 (image taken from reference [298, 340])

2.7 Droplet in microfluidic channel

Concerning interfacial tension measurement of the emulsion flowing in the chip produced by soft-litography, a dynamical interfacial tension measurement model, based on the previous work of Rallison [341-343] developed by Hudson et al. [344, 345] was used:

$$\alpha\eta_c\left(\frac{5}{2\eta+3}\dot{\varepsilon}-u\frac{\partial D}{\partial x}\right)=\sigma\frac{D}{a_0} \qquad (34)$$

$$\alpha=\left(\frac{(2\eta+3)(19\eta+16)}{40(\eta+1)}\right) \qquad (35)$$

η is the ratio between the water viscosity (dispersed phase) and the oil viscosity (continuous phase), D is the deformation parameter (the difference of major and minor axis of the deformed droplet, respectively a and b, divided by their sum), x is the droplet position along the flow axis, ε is the extension rate, σ is the interfacial tension, a_0 is the undeformed droplet radius.

By transitional droplet edge detection (from the deformed droplet shape to the undeformed one), is possible to plot the left hand meber of the Eq. (34) vs D/a_0. The slope of of the line fitting experimental data gives the value of the interfacial tension between oil and water phase.

A correction on droplet deformation has been adopted. Confined droplet are much more deformed with respect to unconfined ones. The confinement correction consist into reduce the deformation parameter in order to get rid of the confinement effect. Mulligan et al.[346] reported the value of droplet deformation parameter for a droplet in confined and unconfined case in similar geometry with respect to us.

2.8 Pendant Drop

The study of the adsorption of surfactants and rheology at liquid/liquid interfaces is interesting for many technological applications, including oil recovery, emulsification procedures, pharmaceuticals, food and counter-flow extraction [347]

The basis of this method reside Young-Laplace equation, which in conditions of thermodynamic equilibrium expresses a relationship between the curvature of an interface and the pressure difference between the two fluids at that point, according to a coefficient that is precisely the interfacial tension:

$$\Delta p = \sigma \left(\frac{1}{R_1} + \frac{1}{R_2}\right) \qquad (36)$$

In which Δp is the pressure between the two phase, interfacial tension and R_1 and R_2 curvature radii. A thorough description of the technique can be found elesewhere (see cited articles of Miller et al.)

Fig 21: a pendant drop in a pendant drop apparatus – rising drop configuration.

By a thin needle is made literally hang a drop of the fluid to higher density in a vessel containing the fluid to lower density (in this way it is avoided that the drop curtain formed to rise upward to density difference). One can also work in the “reverse” mode, using a bent needle to "U", with the end facing upwards instead of downwards suspended and taking a drop of the fluid to lower density in a vessel containing the fluid to higher density: this variant of the method, whose theoretical treatment is identical to the first case, is called Rising Drop or Emerging Drop. The drop will assume a well-defined shape in function of its size, temperature, pressure difference between the two phases and interfacial tension, and then with the addition of various hypotheses not so restrictive, it is possible with a few simple experimental measurements (and more complex mathematical calculations) to obtain the value of IFT.

A pendant drop (a rising drop, more precisely) technique has been used in this work to characterize adsorption behavior of a non-ionic surfactant, Brij58, at soybean oil vs water interface. Also interfacial rheology has been performed. Brij58 (also known as polyethylene glycol hexadecyl ether or polyoxyethylene (20) cethyl ether or $C_{16}EO_{20}$ or $C_{16}E_{20}$) is a hydrophilic nonionic surfactant. Brij surfactants, in general, have a lot of applications in pharmaceutical industries, detergency and emulsification.[348, 349]

Interfacial properties of Brij surfactants have been widely studied in the literature by pendant drop technique, capillary pressure tensiometry. While, some insights on Brij58 adsorption behavior and its interfacial properties at high concentrations still lack. [237, 350, 351].

3 Experimental Section

3.1 Materials

Light mineral oil, Drakeol7®, was purchased by Penreco, polyoxyethylene sorbitan monooleate, C64H124O26, (1.06-1.09 g/ml, 1310 g/mol, Tween 80) and sorbitan monolaurate, $C_{18}H_{34}O_6$, (1.032 g/ml, 346.46 g/mol, Span 20) were used as emulsifiers and purchased by Sigma Aldrich. Deionized water from Millipore was used throughout. Water is added dropwise to a solution of oil and surfactants and mixed in a beaker on a magnetic stirrer at low energy (about 250 rpm) and at room temperature (T ~ 23 °C). Eventually, any sample is taken from the beaker and analysed in microfluidic channel or by placing some drop of the sample on glass slides. Alternatively, a beaker with a thin bottom glass slide (125 micron) is used directly under the confocal microscope to visualize directly the morphology of the obtained emulsion.

Regading microfluidic and pendant drop interfacial tensiometry interfacial tensiometry the non-ionic surfactant Brij58, soybean oil and water were exploited. The surfactant Brij58 (average MWn=1124 g/mol, HLB=16) was purchased by Sigma-Aldrich®. Soybean oil was purchased by Sigma-Aldrich® and, to get rid of its impurity, it has been purified with Florisil® resins (Fluka, 60-100 mesh, by Carl Roth) prior to start the experimental measurement procedure. A mixture of oil and Florisil® in proportion 2:1 w/w was shaken mildly for 3 h and then filtered with Millex® filters (0.1μm PDVF). Ultrapure water, obtained by using a Milli-Q water purification system (0.054 μS), was used. All glassware was washed with sulfuric acid and Milli-Q water before drying in the oven. The measurements were done with the drop profile analysis tensiometer PAT-1 (Sinterface, Germany). A hook needle, which contain the lesser dense phase (soybean oil), was placed inside a cuvette containing the aqueous surfactant solution. Surface dilatational rheology results are obtained from the surface tension response to a sinusoidal area oscillation.

By soft-litography technique has been possible to obtain a very small chip (see fig. 22) made of polydimethylsiloxane (PDMS) containing the microchannels having convergent-divergent geometry.

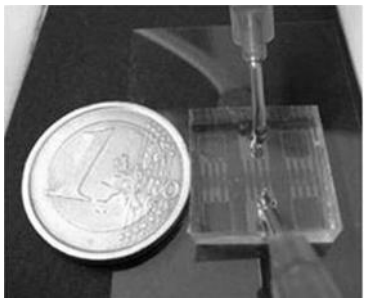

Fig. 22: Microfluidic chip

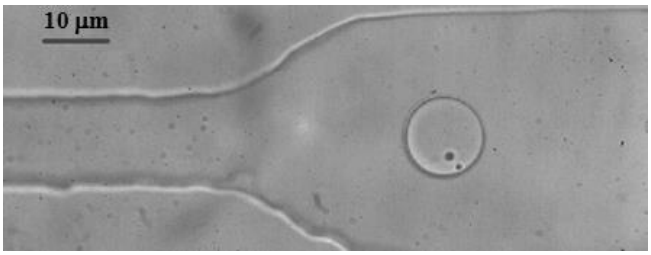

Fig. 23: Microfluidic channel

A convergent-divergent geometry is needed to obtain a divergent flow able to deform droplet. Microchannel section is rectangular and the smallest microchannel section is 8 µm x 15 µm. Afterwards, a hole for the inlet and one for outlet was created in the chip. Micropump was used to realize the requested pressure drop. An emulsion of soybean oil in water containing 1% wt of Brij58 has been tested in the microfluidic channel for the IFT measurement. A pure interface second solution, i.e., distilled water in silicone oil (η= 20 cSt) has been tested as well.

The components of Buchwald–Hartwig arylamination in microreactor considered in this work consist in an aryl bromide coupled with a secondary amine in an toluene using a Palladium-based pre-catalyst and a metal alkoxide as base to form an arylamine. The aryl bromide ((R)-8-Bromo-5-methyl-1,2,3,4-tetrahydronaphthalen-2-ylamine)-(S)-1-(phenylethyl)amine) (**1**) has been obtained by mixing (*R*)-8-Bromo-5-methyl-1,2,3,4-tetrahydronaphthalen- 2-yl)-(*S*)-1-(phenylethyl)amine Hydrochloride (**2**) (20 g, 52.6 mmol) with H_2O (32 mL, 1.6 mL/g) and 50% NaOH (aq) (12 mL, 152.5 mmol) in a round-bottomed flask fitted with a reflux condenser and a magnetic stirrer. Toluene (100 mL, 5 mL/g) was added, and the resulting mixture has been heated to 60 °C and stirred. At first, the mixture appears to be very heterogeneous. Once the material has been dissolved, the mixture has been cooled to room temperature and the stirring has been stopped. At this point two liquid layers are present. By pouring them into a separating funnel it has been possible to remove the bottom aqueous layer. The top layer (organic) has been distilled under vacuum by using rotary evaporator in order to remove toluene and any water remaining. This provided **1** as a crystalline solid. The Palladium-based pre-catalyst [Pd(IP*r*)(cin)Cl] (**3**) has been prepared according to a procedure reported in a previous paper [352]. Potassium tert-pentoxide (KOtAm) was received as a solution 1.7 M in toluene (Aldrich) and used as base, 1-methylpiperazine (Aldrich, 99%), 4,4'- di-tert-butylbiphenyl (Aldrich, 99%) and toluene (Aldrich, anhydrous, 99.8%) have been used as purchased.

3.2 Methods

3.2.1 Rheological measurements

The rheological measurements of the sample were carried out at room temperature by two stress controlled rotational rheometer. An MCR 301 rheometer (Anton Paar Instruments). A cone-plate 1°/75 mm geometry was used loading 2,5 ml of solution. The second stress-controlled rheometer is a Bohlin Instruments CVO 120, with cone-plate geometry, D=60mm, 4°. Both continuous and oscillatory flow tests were performed.

3.2.2 Microchannel flow

The analysis of the fluid dynamics od droplets under capillary flow was performed by using an experimental apparatus made up of silica micro-capillaries with a circular section. Those were bought by Polymicro Technologies. In particular, the experiments were run by using micro-capillaries with an inner diameter Dc equals to 100 μm respectively. A syringe pump (Harvard 11 Plus) was used in order to inject the HLAS solution in the micro-capillaries. The syringe pump and the micro-capillaries were connected by suitable connections. Images of emulsion flowing inside the micro-capillaries were acquired by a high speed video camera (Phantom 640) and analysed later. During all the experiments, observations were performed in bright field and confocal microscopy, using 63x optics. Finally the whole apparatus is placed on a vibration-isolated table as shown in Figure 24.

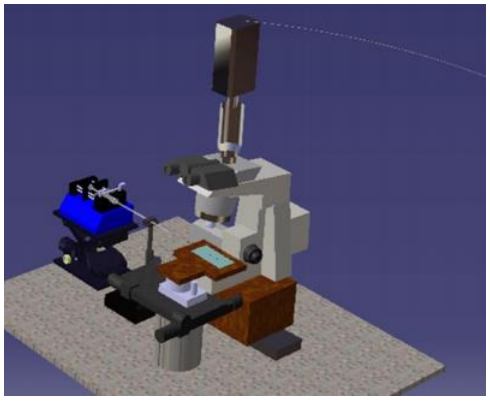

Fig. 24. Experimental apparatus used for the capillary flow.

3.2.3 Confocal microscopy

An investigation of the emulsion morphology was performed by the Laser Scanning Confocal Microscopy (LSCM) technique. A fluorescent marker, Rhodamine B , 1 μg/ml, was added to emulsion to make the hydrophilic part fluorescent. Another fluorescent marker, Nile Red 1 μg/ml, was added to highlight the hydrophobic part of the solution. A 3D reconstruction of the

emulsion using a commercial software of image analysis software package (Image Pro Plus 7) has also been done. The confocal microscope was a Zeiss LSM 5 PASCAL. It is made by the transmitted light microscope Axiovert 200 M equipped with a high resolution digital camera AxioCam and a high magnification optics (63x) were used. The module of the laser comprises a first Ar laser emitting at three different wavelengths (458,488, 514 nm) and a second HeNe laser emitting at a wavelength of 543 nm. The scanning module comprises a confocal pinhole with a variable diameter and a channel equipped with high sensitivity PhotoMultiplier Tubes (PMT) for the detection of the signal. There is also an additional channel for detecting the transmitted light.

3.2.4 Continuous flow reactor

The components of Buchwald–Hartwig arylamination considered in this work consist in an aryl bromide coupled with a secondary amine in toluene using a palladium-based pre-catalyst and a metal alkoxide as base to form an arylamine. The aryl bromide ((R)-8-Bromo-5-methyl-1,2,3,4-tetrahydronaphthalen-2-ylamine)-(S)-1-(phenylethyl)amine) (**1**) has been obtained by mixing (*R*)-8-Bromo-5-methyl-1,2,3,4-tetrahydronaphthalen-2-yl)-(*S*)-1-(phenylethyl)amine Hydrochloride (**2**) (20 g, 52.6 mmol)with H_2O (32 mL, 1.6 mL/g)and 50% NaOH (aq) (12 mL, 152.5 mmol) in a round-bottomed flask fitted with a reflux condenser and a magnetic stirrer. Toluene (100 mL, 5 mL/g) was added, and the resulting mixture has been heated to 60 °C and stirred. At first, the mixture appears to be very heterogeneous. Once the material has been dissolved, the mixture has been cooled to room temperature and the stirring has been stopped. At this point two liquid layers are present. By pouring them into a separating funnel it has been possible to remove the bottom aqueous layer. The top layer (organic) has been distilled under vacuum by using rotary evaporator in order to remove toluene and any water remaining. The latter process provided **(1)** as a crystalline solid. The palladium-based pre-catalyst [Pd(IPr)(cin)Cl] **(3)** has been prepared according to a procedure reported in a previous paper [352]. Potassium tert-amylate(KOtAm) was received as a solution 1.7 M in toluene (Aldrich) and used as base, the amine, i.e., 1-methylpiperazine (Aldrich, 99%), 4,4'- di-tert-butylbiphenyl (Aldrich, 99%) and toluene (Aldrich, anhydrous, 99.8%) have been used as purchased.

1 μL of the effluent is injected in splitless mode in a Shimadzu GC-FID 2010 GC, equipped with a non-polar capillary column (BPX5 10 m, i.d. 0.1 mm 0.1 lm film thickness from SGE) and He as gas carrier. The linear velocity is 50 cm/s, and the injector and FID detector temperature is set to 320 °C and 360 °C, respectively.

4 Results and Discussions

4.1 Phase Inversion Emulsification

By phase inversion composition methodology, long term stable nanoemulsions characterized by very low average diameter, i.e. 170 nm, and narrow droplet size distribution has been obtained. At such so small size, it has been possible to observe droplets Brownian motion.

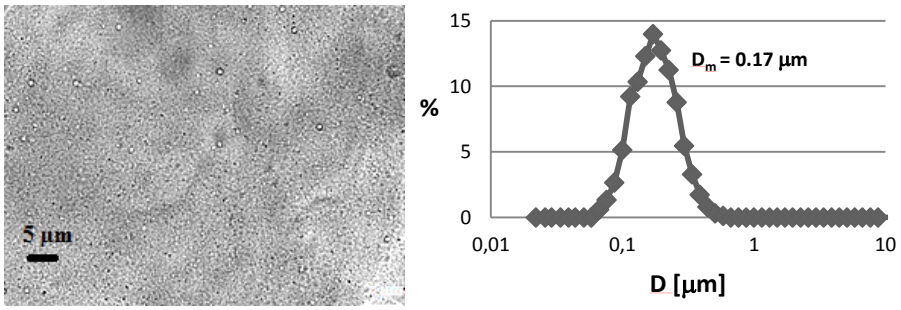

Fig. 27: optical image of the finished emulsion and correspondent droplet size distribution, water weight fraction is 76%.

According to the aforementioned method, emulsion have been produced by adding water dropwise to the solution of oil and surfactants, in this way an initial w/o emulsion has been formed.

In order to obtain emulsion as much as possible stable, three main parameters have been varied, i.e., surfactant ratio (mass ratio between the two surfactants), oil to water ratio (mass ratio between oil and water), surfactant to oil ratio (mass ratio between surfactants and oil). Most stable emulsion have been found for surfactant ratio equal to 1, oil to water equal to 0.24, and surfactant to oil ratio equal to 0.33.

Compounds used for emulsion phase inversion test are Newtonian, as outlined by rheometry tests (see fig. 28):

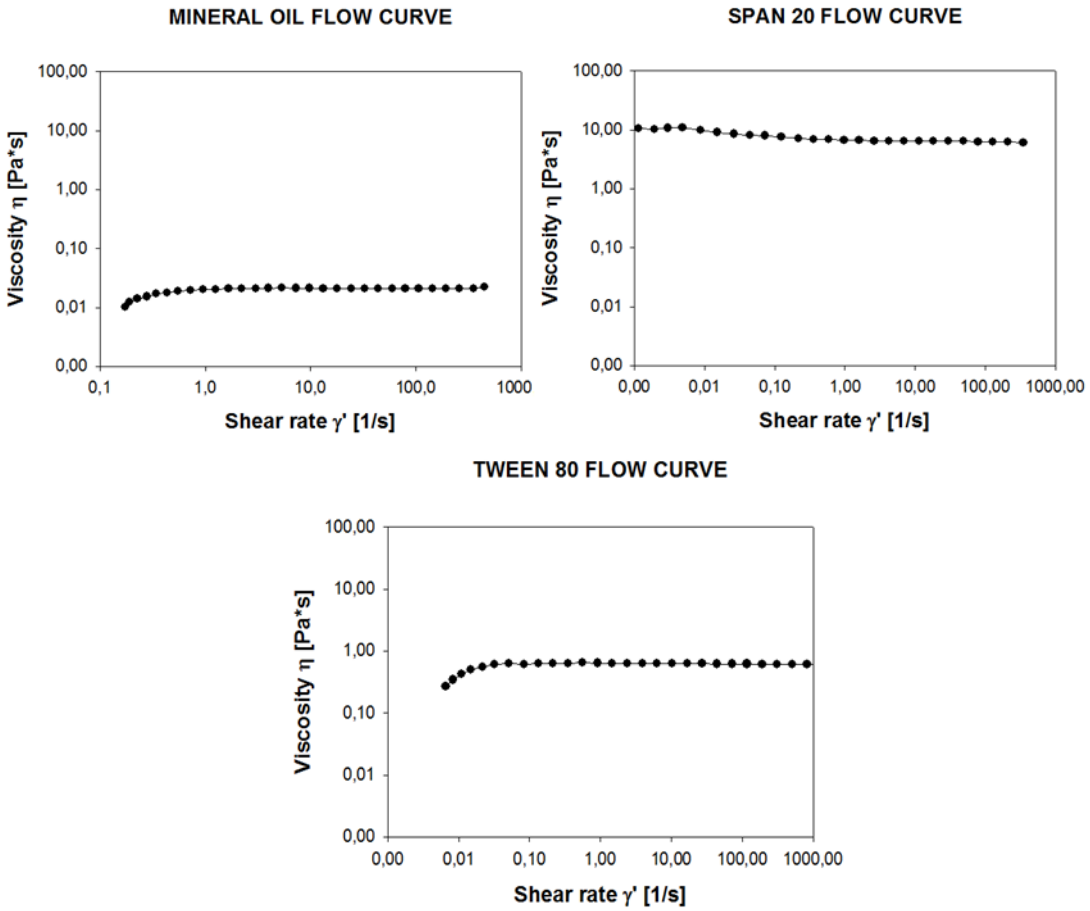

Fig. 28: Flow curves of the mineral oil, and the non-ionic surfactants.

The emulsion preparation starts with a solution 75%wt minearl oil, 12,5 % wt Span 20, 12,5%wt Tween 80. The mixture oil plus surfactants is Newtonian and remains Newtonian till the amount of water added reaches the 10%wt of the overall solution.

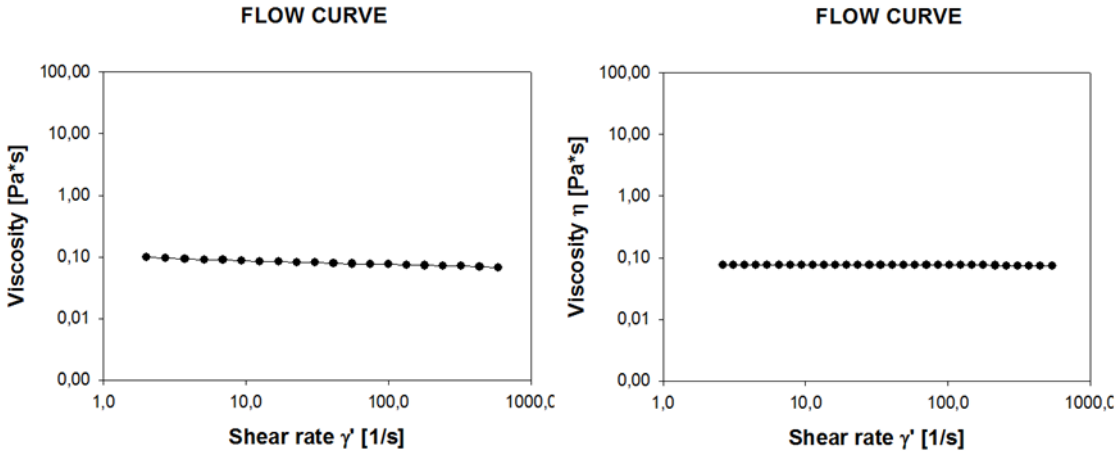

Fig 29: On the left, flow curve of the initial mixture, i.e., oil plus surfactants. On the right, flow curve of the sample with 5%wt of water added. It is evident the Newtonian behavior of both.

At 10%wt of water added non-newtonian behavior starts to be exhibited (see fig. 30), By adding a fluorescent dye into the aqueous phase (Pommella et al., 2012) (thus, the aqueous phase is red colored and the oil phase is dark), confocal light scanning microscopy was useful to follow emulsion morphology evolution induced by a linear and continuous increase in water concentration.

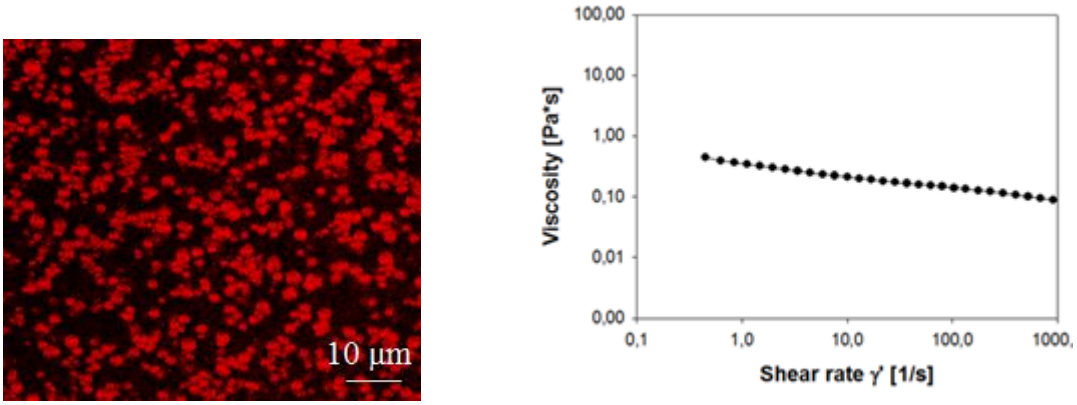

Fig. 30: on the left: static image of the emulsion at rest when water added is at 10%wt, population of isolated droplets. On the right, evidence of non-Newtonian behavior of the sample.

Despite the gradual alimentation of water, a sudden change in morphology, often named "catastrophic" event, was observed around the 20 wt% of water concentration, thus showing a bicontinuous morphology structure. Proceeding with the water feeding, the bicontinuous structure disappeared quite fast, leading to the formation of an o/w emulsion. Therefore, around to the 20 wt% of water concentration, phase inversion has been reached. Rheometry test at the phase inversion point showed a non-Newtonian behavior (see the shear thinning in the flow curve, fig. 31) and the visco-elastic behavior of the sample due to the interconnected structures typical of bicontinuous structures, well outlined by parallelism of linear viscoelasticity parameters, G' (elastic modulus) and G'' (viscous modulus) with G' > G'' in the frequency sweep test without preshear, with the same considerations in the test with pre-shear but with G''>G' (see fig. 32).

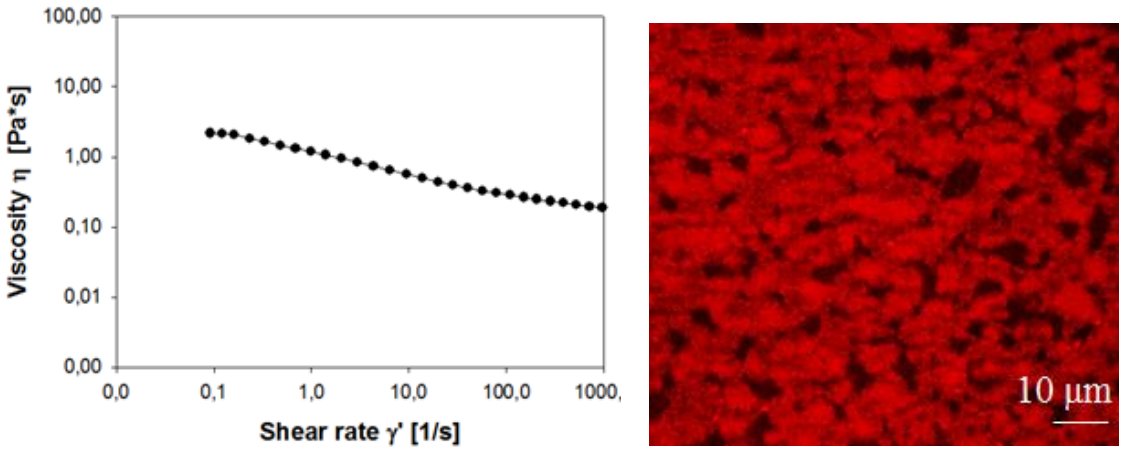

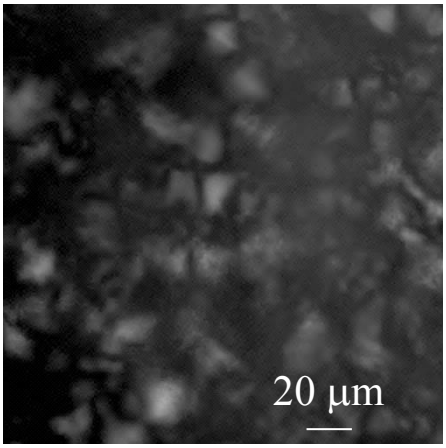

Fig. 31: On the top left: flow curve of the sample at 20% wt of water. Shear thinning behavior. On the top right, confocal miscopy image, emulsion at rest, population of crowded, overlapped droplets. On the bottom, polarized optical image of the emulsion at rest showing birefringence pattern typical of a liquid crystalline phase.

By using a glass cylindrical microchannel having 100 micron of internal diameter, it has been possible to obtain an optical sectioning of the emulsion at 20%wt flowing (soon after stopped emulsion flow within it), thus unraveling tiny details of the microstructure. An interconnected bicontinuous structure is evident (fig. 31 bis).

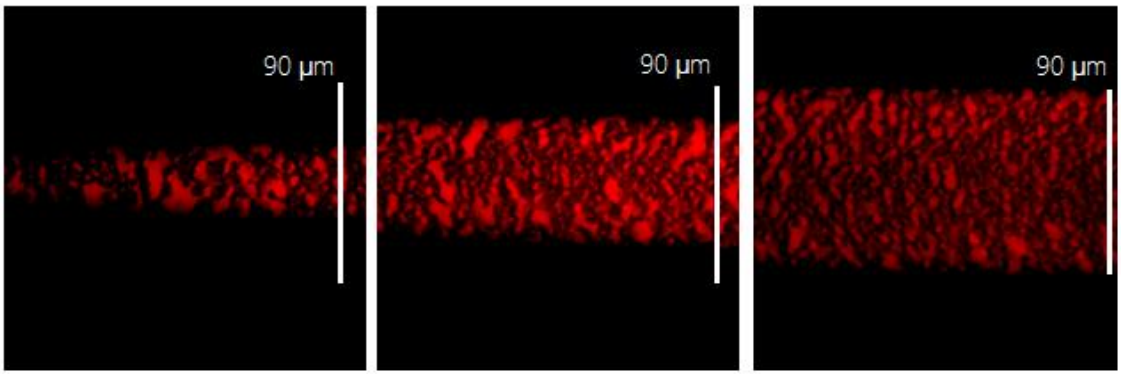

a)

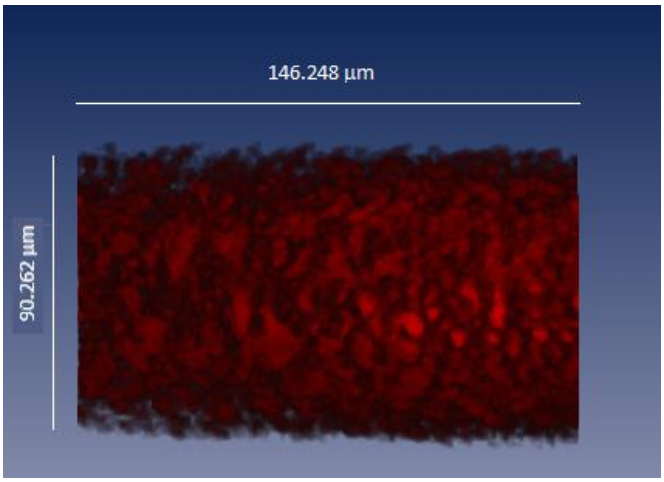

b)

Fig. 31 bis: a) optical sectioning by laser scanning confocal microscopy of the emulsion at 20% of water added. On the left, an optical slice nearby the bottom of the microchannel. On the right, an optical slice nearby the maximum cord legth, i.e., the diameter. b) a 3D reconstruction obtained by z-stack image acquisition.

The sample at 20% of water added has particular rheological behavior. We remind that here the composition is as follows: 20% water, 10% Span 20, 10% Tween 80, 60% mineral oil. Here, the effect of a strong flow, that has been simulated by applying a preshear before the oscillatory measurement, is to induce G''>G' (the opposite with respect to the case without preshear, see figure 32). Hence, a more viscous system has been obtained. Nevertheless, if one take a look to the normal stresses, the first normal stress difference N_1 appears to be highly positive as outlined by the Weissenberg effect, (being the first normal stress difference the difference between *Txx* and *Tyy* respectively the first and the central component of the stress tensor). In the latter, microfluidics has been a unique tool to demonstrate the origin of such rheological behavior. As we can see in the figure 33, where we fed a rectangular glass microchannel with the fluid, the evident effect of flow is to disaggregate the clusters of droplets, shrink droplet size and align the so-obtained small droplets. An alignment of such structure corresponds to a an increase in the first normal stress difference[353].

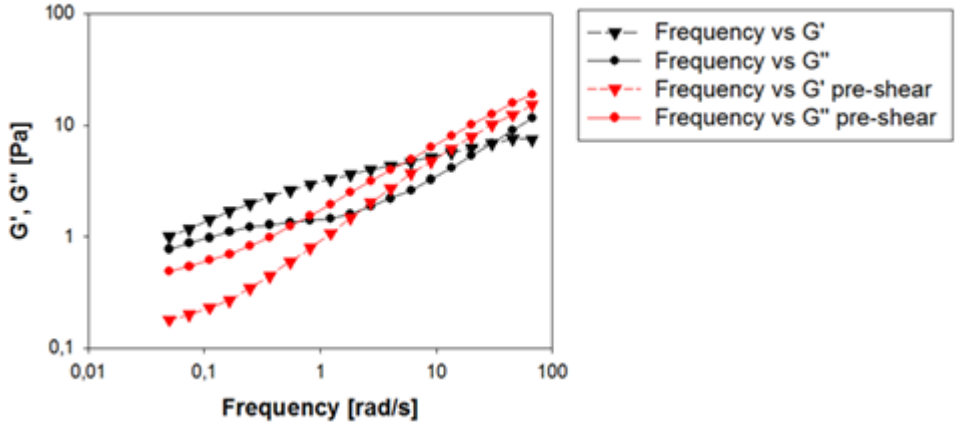

Fig 32: Frequency sweep of the sample with 20%wt of water. With a preliminary preshear of 500 s^{-1} for 30 s and without preshear.

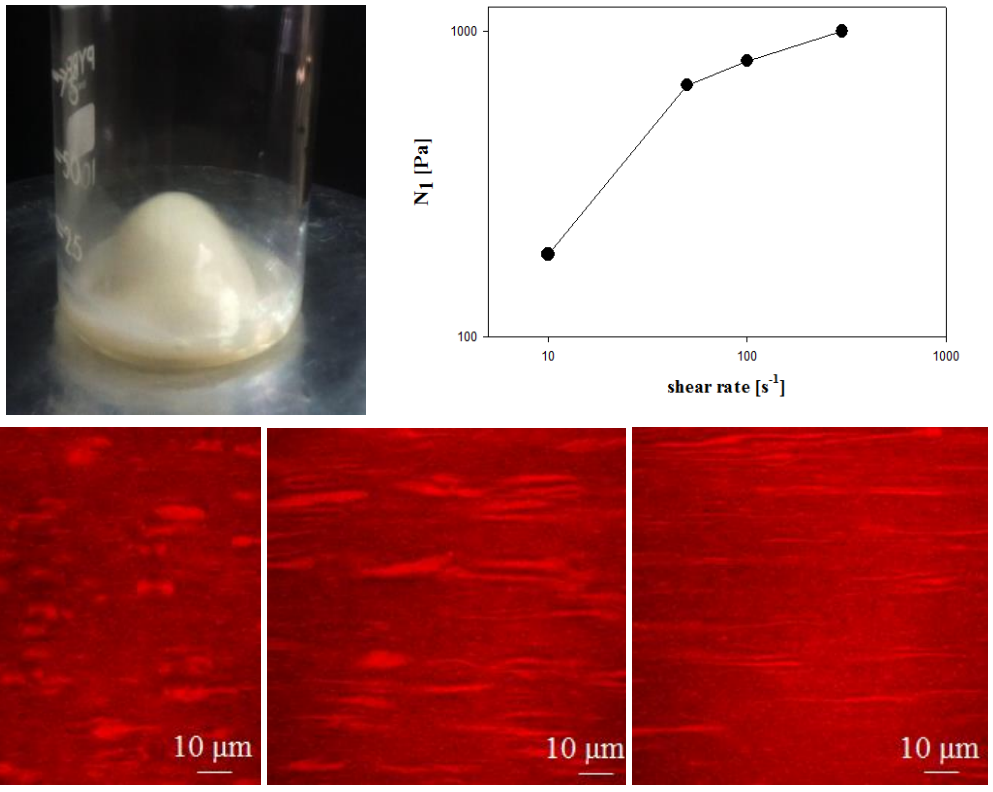

Fig 33: On the top left, an image of the beaker where the sample at 20%wt water is produced. Note viscoelastic effect, i.e, Weissenberg effect. On the top right we plotted first normal stress difference, N_1, of the sample vs shear rate. Every point has been acquired after 30 s about to get a steady state value. On the bottom, flow startup of the sample at 20% water added. The mechanism of droplet shrinkage and alignment is outlined thanks to a rectangular microfluidic channel (50 micron x 1 mm) under the field of view of confocal microscope.

At 50%wt of added water, emulsion is inverted and much more dispersed than the initial one. Here rheological behavior is slightly shear thinning (see fig. 34).

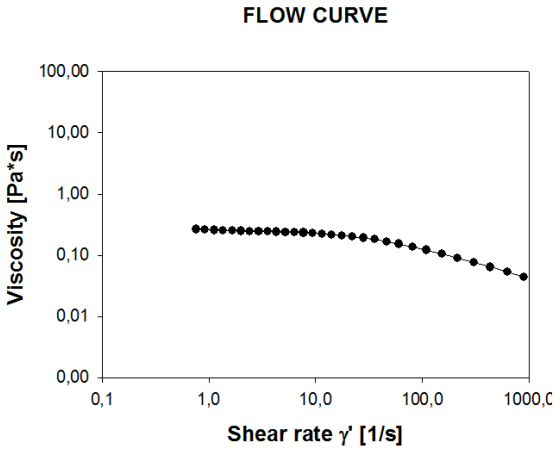

Fig 34: emulsion at 50% of water added. Shear thinning in the final part of the flow curve.

The small-sized droplet-like morphology of such sample could be seen in fig.35.

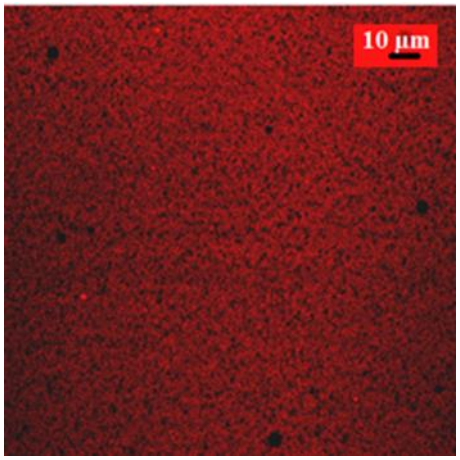

Fig. 35: confocal image, water weight fraction is 50%.

Then, water has been fed until to the final water concentration. By a zoom of the confocal image at 76%wt of water it has been possible to visualize the presence of droplets in droplets (fig. 37). Maybe, the intermediate bicontinuous structure could favor trapping of one phase into the other, leading to the formation of droplet in droplet inclusion. The obtained nanoemulsion has a composition: 75% water, 3% Span 20, 3% Tween 80, 19% mineral oil.

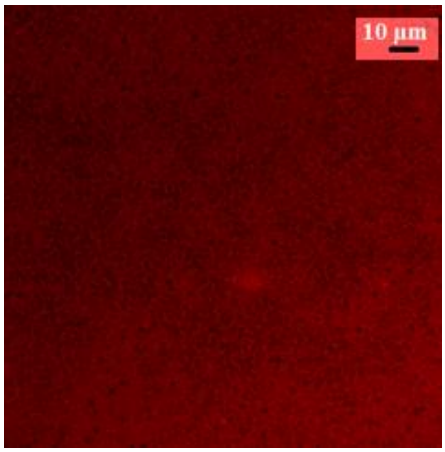

Figure 36: confocal image when water weight fraction is 76%.

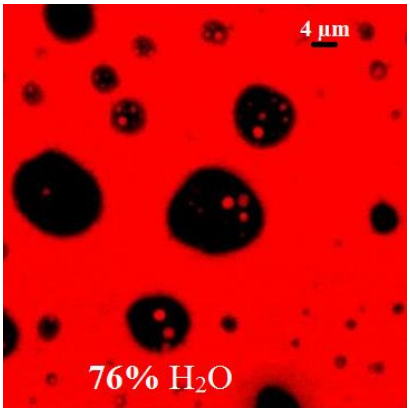

Fig. 37: confocal image, water weight fraction is 76%, zoom of the Figure 7. Note multiple emulsions

The rheological behavior of the final emulsion is clearly Newtonian (see fig. 38).

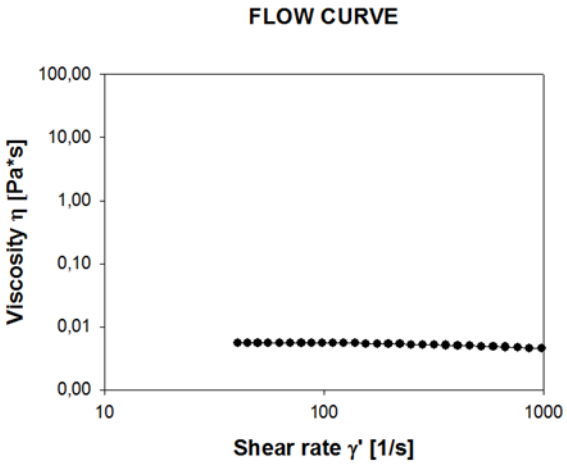

Fig 38: A Newtonian behavior is showed by the final nanoemulsion produced, where the water is 76%wt.

Resuming emulsification pathway in a nutshell, there is an initial increase in viscosity of the sample, till a maximum close to the phase inversion point, followed by a monotonic decrease till the final composition. The overall viscosity behavior is depicted in fig. 39:

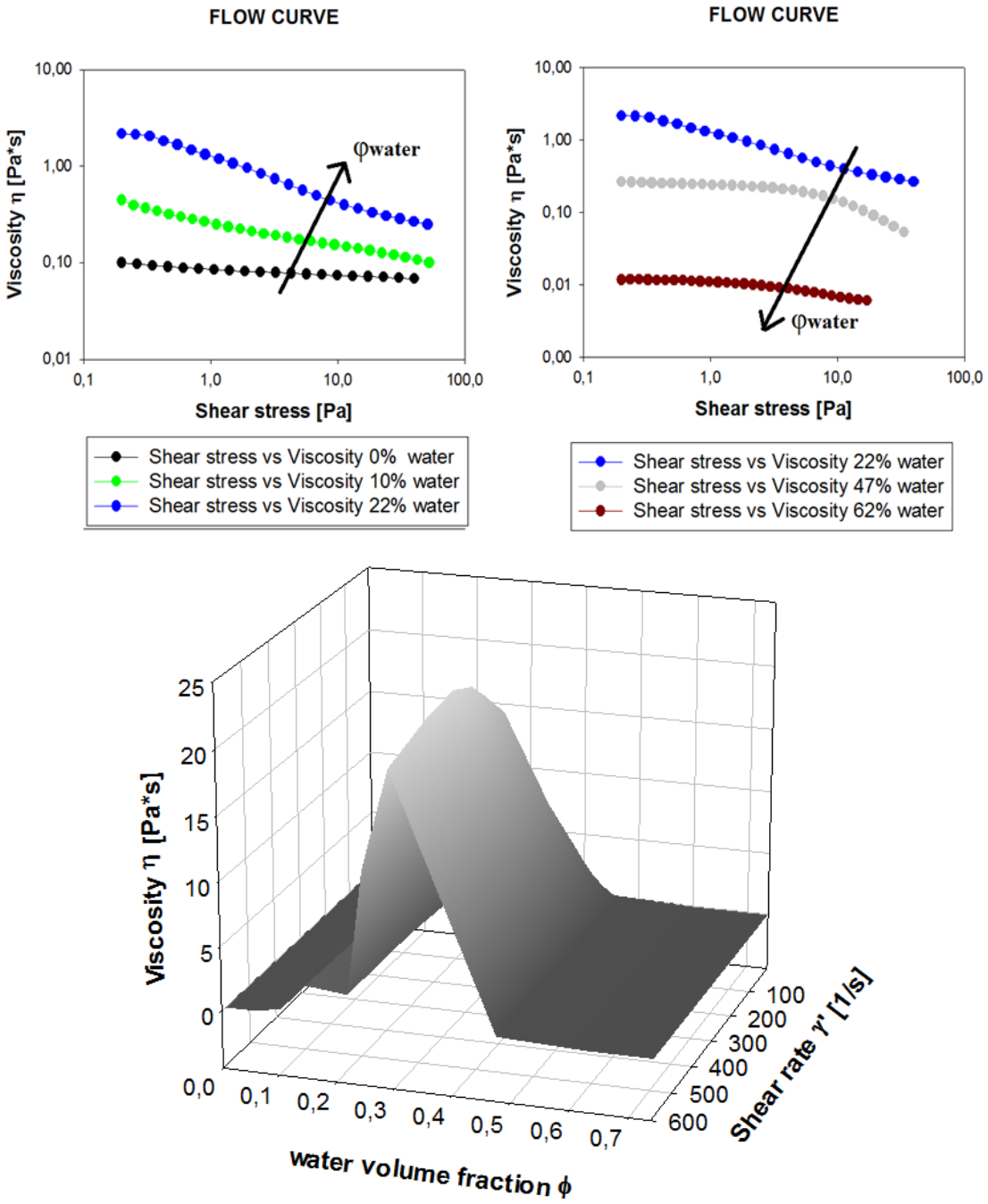

Fig. 39: Viscosity behavior during the emulsification pathway. The peak correspond to the viscoelastic solution at 20% of water.

4.2 Droplet Interfacial rheology

4.2.1 Microfluidic method

As soon droplet comes out from smallest microchannel section going then into the divergent and larger section (the microchannel has been shown in the methods section), droplet shape is first deformed then recovers the spherical shape. By image analysis of the transient droplet retraction process, it has been possible to experimentally measure the deformation parameter,

droplet position, droplet velocity. Fluids properties such as viscosities are known. Hence, the model described in theoretical background chapter could be exploited to perform the droplet interfacial tension measurement. Once data are collected, the first hand member of eq. 34:

$$\alpha\eta_c\left(\frac{5}{2\eta+3}\dot{\varepsilon}-u\frac{\partial D}{\partial x}\right)=\sigma\frac{D}{a_0}$$

can be reported on the *y* axis of a cartesian diagram where the term D/a_0 can be reported on the *x* axis. Thus, the slope of the obtained curve is equal to the interfacial tension. The experimental values of *D vs x*, and $\dot{\varepsilon}$ *vs x*, are fitted with a third order polynomial. In this way, the so-obtained polynomial function could be used directly in eq. 34. In addition, to get rid of an additional contribution to droplet deformation due to confinement, our *D* experimental data have been reduced by a value provided in a manuscript of Mulligan and Rothstein (as described in the method section), where the confined droplet superior deformation with respect to unconfined droplet case has been reported. According to the Hudson model, if we plot the first hand member of equation 34 against *D/ao* a line could be obtained being the slope of this line the droplet interfacial tension. Our results, showed a curve that could be fitted by two different lines with a different slope and we considered the detected interfacial tension as the average between the slope of the two fitting lines.

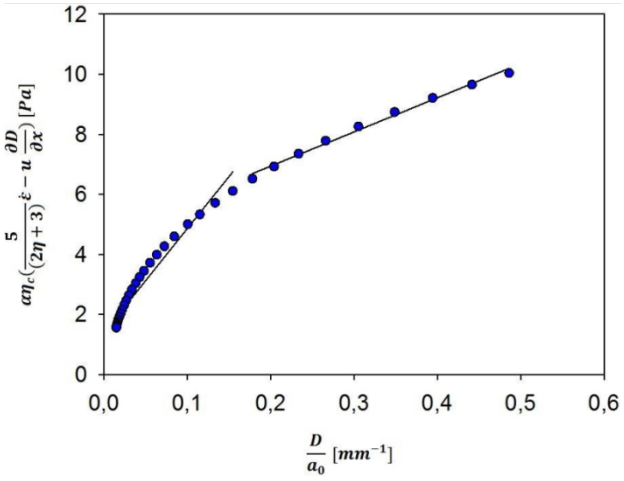

Fig. 40: Interfacial tension water in silicon oil 20 cSt.

In the case of the pure interface droplet (i.e., water in silicon oil, figure 40) , we obtained an interfacial tension value comparable with the one obtained from the literature, i.e., 23 mN/m measured vs 20 mN/m from the literature. In the case of droplet with an interface rich of surfactant (soybean oil in water +1% wt of Brij58), figure 41, we obtained a value much lower than the one reported in the literature thus we decided to further investigate the system by pendant drop and capillary pressure tensiometry, an argument that will be discussed in the next chapter.

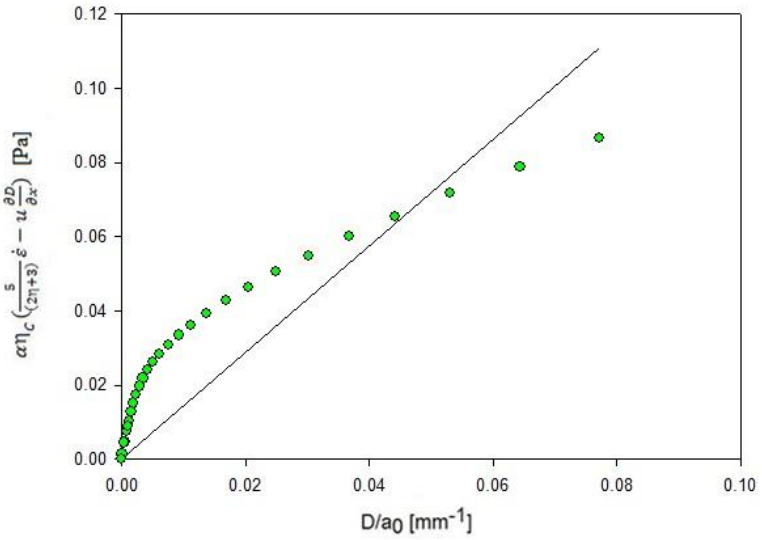

Fig. 41: Interfacial tension for soybean oil droplet in water+Brij58.

4.2.2 Pendant Drop

Pendant drop measurements and capillary pressure interfacial rheology have been performed at Max-Planck Institute für Kolloid- und Grenzflächenforschung, Potsdam, Germany under the supervision of Dr. Reinhard Miller.

We will initially show how dynamic interfacial tension of an oil droplet immersed in low concentrated water + Brij58 solution appears:

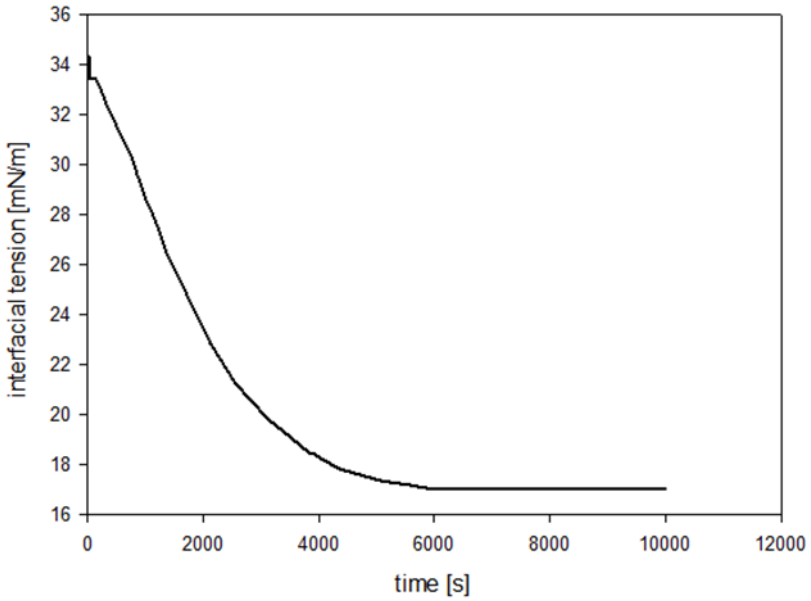

Fig. 42: interfacial tension vs time at 9*10-7 M of Brij58 in water.

Figure 42 shows the protocol used to study the adsorption process of adsorbed Brij58.

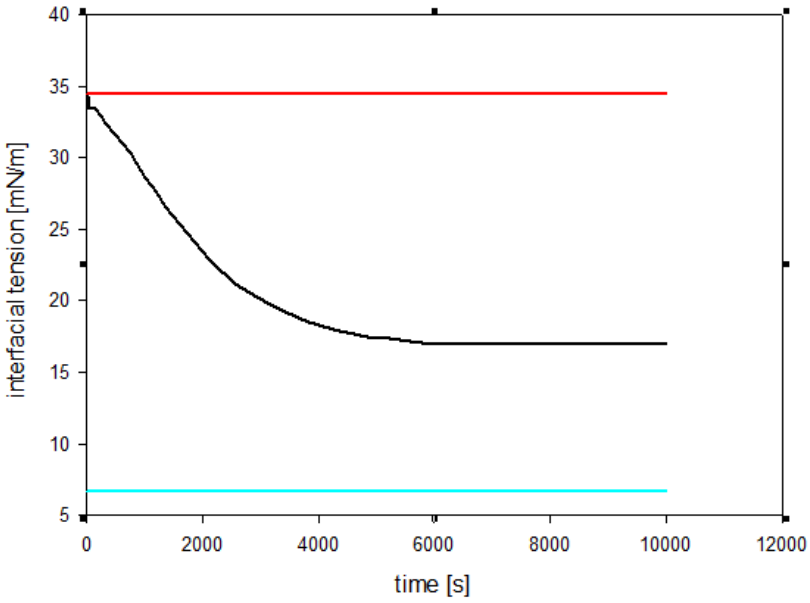

Fig. 43: Adsorption dynamics for 10-9 M Brij58 in water (red line), 9*10-7 M (black line), 4.5*10-3 M (cyan line).

Figure 43 shows the adsorption dynamic for different concentrations of Brij58 at the soybean oil-water interface. It is interesting to note that at $9*10^{-3}$ M the equilibrium interfacial tension, 6,5 mN/m, is reached within a few seconds. Moreover, at $4,5*10^{-3}$ M, the static interfacial tension is already 6,5 mN/m, thus probing that further addition of surfactant beyond a certain value does not affect static interfacial tension. The constant value at the lowest studied surfactant concentration probed the high purity of the studied soybean oil.

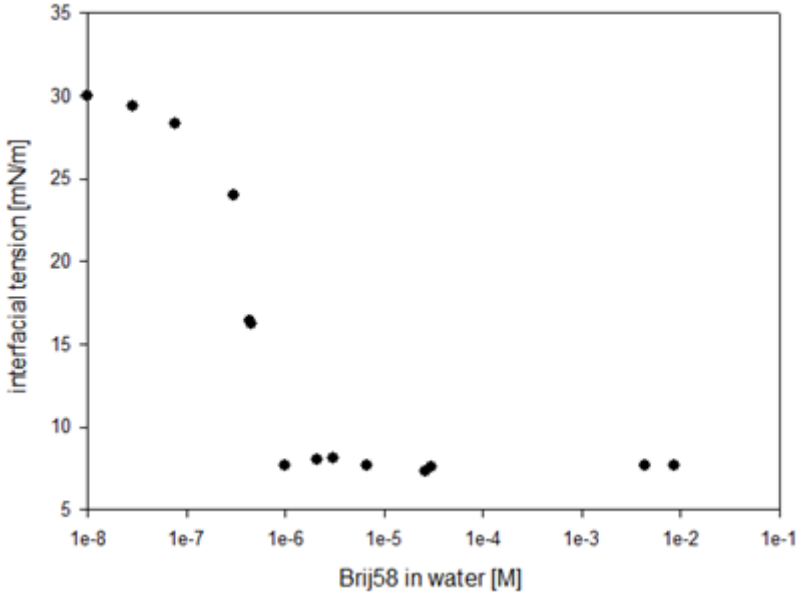

Fig. 44: interfacial tension adsorption isotherm for Brij58.

Fig. 44 shows interfacial tension adsorption isotherm for Brij58 at the interface soybean oil water. Critical micellar concentration is around 10^{-6} M.

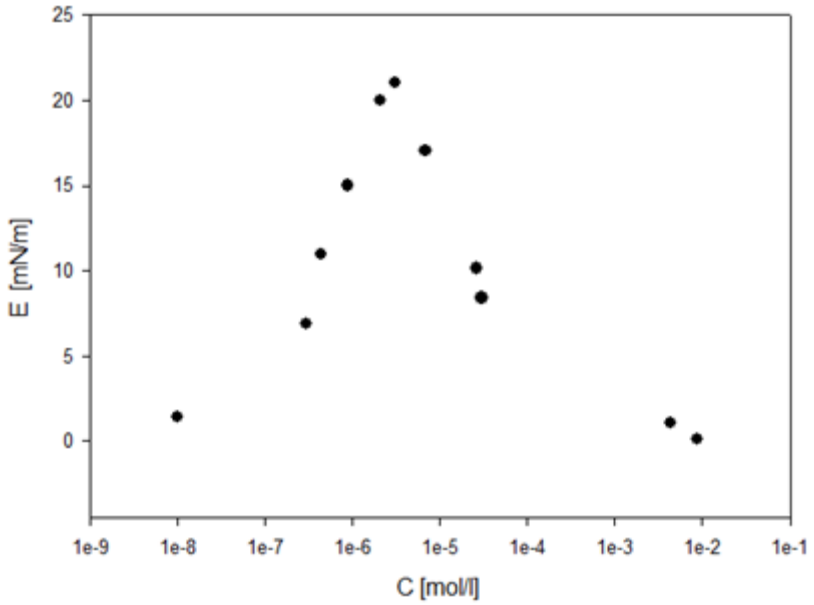

Fig. 45: Dilational interfacial elasticity vs Brij58 concentration at 0,1 Hz.

In Fig. 45 it is shown the droplet interface dilational elasticity vs Brij58 concentration, with a maximum between 10^{-6} M and 10^{-5} M. The dilational interface elasticity is zero at low surfactant concentration and zero at high surfactant concentration for two different reasons. At low concentration, surfactant is not enough to give elasticity to the interface. At the higher one, surfactant at the interface is too much to be diluted by expansion/compression at low frequencies typical of the pendant drop apparatus. Thus, surfactant interface packing is very tough and difficult to be displaced. This is a well-known phenomenon for C_mEO_n surfactants [237]. Pendant drop apparatus, where the maximum allowable frequency of deformation is more or less 1 Hz, are able to study interfacial rheology of emulsion with low concentration of surfactants.

By a preliminary study with capillary pressure tensiometer (CPT), which represent an evolution of the pendant drop system, it has been possible to test the interfacial elasticity of the droplet having 1% of surfactant concentration in the bulk phase. Such technique is capable to reach 100 Hz of oscillation and by properly getting rid of hydrodynamic effect one can come up with the interface elasticity of highly concentrated interface. Its description has been widely reported in the literature [354, 355]. In the next figure 46 is shown the value of the dilational interface elasticity E has obtained by CPT:

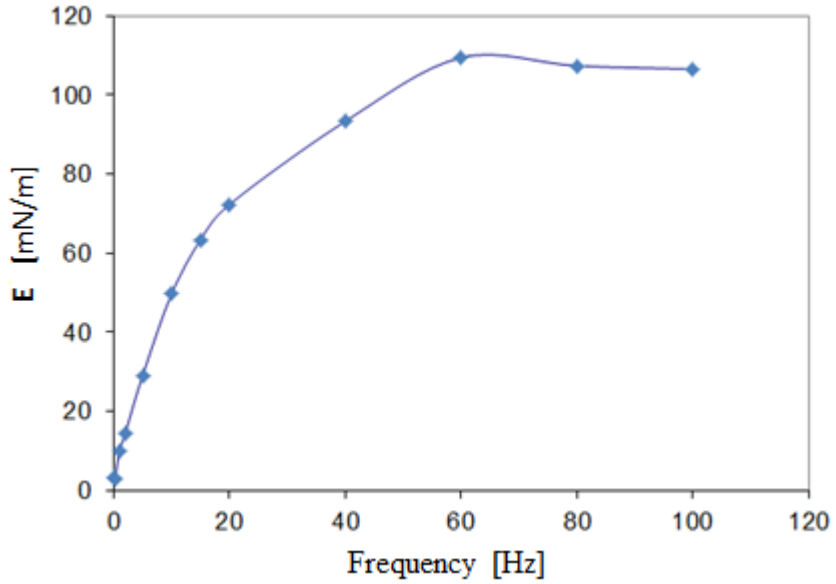

Fig. 46: Oil droplet dilational interface elasticity at high frequency, CPT measurement. Brij58 concentration in the water phase equal to 1% wt.

It is evident from such high dilational interface elasticity that key-role in droplet deformation is no more played only by interfacial tension but also by the aforementioned parameter and a microfluidic method based on the idea that droplet retraction is governed by interfacial tension solely it will obviously fail in the characterization of such dynamic.

4.3 Microreactor for cross-coupling reactive flows

In this work, the following reaction will be conducted [356, 357]:

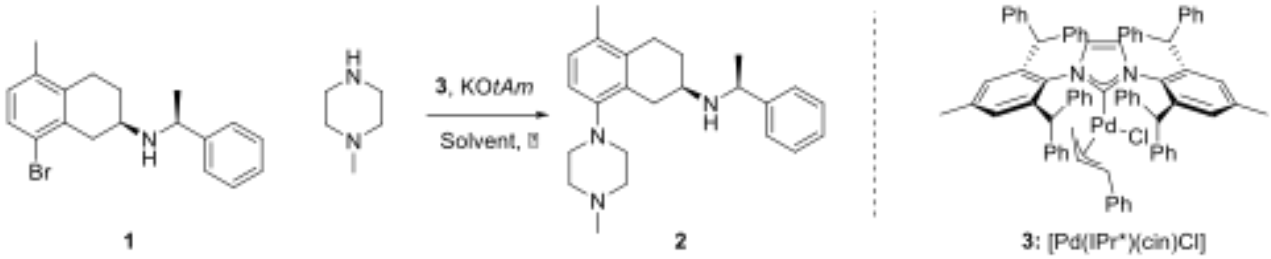

Scheme 1: left: amination reaction; right: palladium-based pre-catalyst.

A four-feed microreactor has been developed using our two-feed reactor, disclosed previously, as a benchmark to compare four-feed *vs* two-feed performance and to optimize overall reaction performance. In Figure 47, a brief graphical description of the two feed-configuration is provided. The details of the two-feed configuration has been reported in a previous paper dealing with a similar reaction[202].

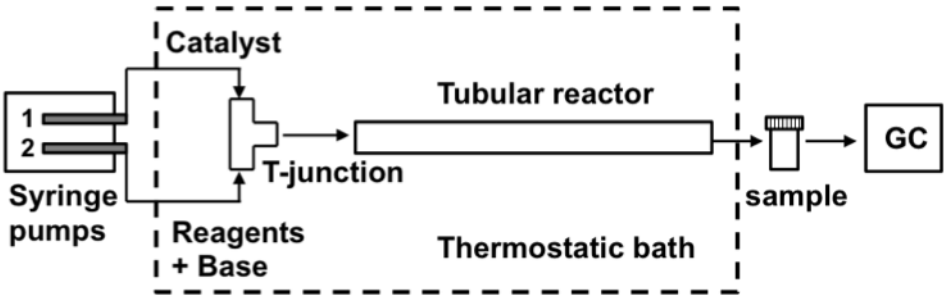

Figure 47: Scheme of the 2-feed continuous flow microreactor[202].

In such a configuration, a mixture of aryl bromide (**1**), amine (*N*-methylpiperazine), and base (potassium *tert*-amylate) is dissolved in toluene in the presence of an internal standard (4,4'- di-tert-butylbiphenyl) and fed in by syringe pump (Harvard Pump 11 Plus Dual). A solution of the catalyst (**3**) in toluene is loaded in a second syringe, placed on the same syringe pump, in order to impose the same flow rate. Both solutions were prepared inside a glove-box under inert atmosphere in the concentrations reported in Table I. The two syringes are connected to the stainless steel tubular reactor (inner diameter 2 mm, length 70 cm) by a stainless steel T-junction (inner diameter 1 mm), also used to ensure a suitable mixing of the two solutions. The concentrations reached in the tubular reactor are reported in Table I. In particular, a 1mol% (mmol of catalyst/mmol of Aryl bromide), corresponding to a molarity of 9.6 $*10^{-4}$ (mmol of catalyst/ml of solution) of (**3**) (relative to aryl bromide **1**) has been investigated, with 0.1 M of aryl bromide, 1.1 molar ratio of amine/aryl bromide and 1.05 molar ratio of base/aryl bromide. The microreactor and the T-junction are heated in a thermostatic bath at 50 °C, while both the syringes containing substrates and catalyst are kept at room temperature.

Table I: Molecular weights and concentrations in the syringes and in the reactor for the 2-feed configuration.

Syringe 1	**Mol weight**	**Quantity [mg]**	**mmol**
Catalyst	1172	23.44	0.02
Toluene	92.14	7.83 (9 ml)	0.085
Syringe 2	**Mol weight**	**Quantity [mg]**	**mmol**
Aryl bromide	344.29	688.58	2
N-Methylpiperazine	100.16	220.352	2.2
KO^{t}Am (Solution in toluene 1.7 M)	126.24	1110.912	2.1
4,4'-Di-tert-butylbiphenyl (I.S.)	266.42	18	0.0675
Toluene	92.14	6.765 (7.765 ml)	0.0733

Tubular Reactor				
Catalyst [% mol] (mol_{Cat}/mol_{ArBr})	**Catalyst** [M] ($mmol_{Cat}/ml_{Sol}$)	**ArBr** [M] ($mmol_{ArBr}/ml_{Sol}$)	**Met/ArBr** [mol/mol]	**KO^{t}Am/ArBr** [mol/mol]
1	$9.6*10^{-4}$	0.1	1.1	1.05

In the case of the four-feed microreactor, the catalyst, reagents, base and additional solvent have been separated into four different streams. The way in which the four streamlines are mixed has

been varied and its effect on conversion will be reported and discussed below. The typical concentrations for each stream are reported In Table II for the 4-inlet case.

Table II: Molecular weights and concentrations in the syringes and in the reactor for the 4-feed configuration.

Syringe 1	**Mol weight**	**Quantity [mg]**	**Quantity [mmol]**
Catalyst	1172	9.8/21.5/29.3/39.07	0.00836/0.0183/0.025/0.00333
Toluene	92.14	7.83 (9 ml)	0.0849
Syringe 2	**Mol weight**	**Quantity [mg]**	**Quantity [mmol]**
Aryl bromide	344.29	1147.63	3.333
N-Methylpiperazine	100.16	367.25	3.666
4,4'-Di-tert-butylbiphenyl (I.S.)	266.42	18	0.0675
Toluene	92.14	6.74 (7.754 ml)	0.0732
Syringe 3	**Mol weight**	**Quantity [mg]**	**Quantity [mmol]**
KO^{t}Am (Solution in toluene 1.7 M)	126.24	1930	3.645
Toluene	92.14	5.964 (6.85 ml)	0.0647
Syringe 4	**Mol weight**	**Quantity [mg]**	**Quantity [mmol]**
Toluene	92.14	7.83 (9 ml)	0.0849

Tubular reactor				
Catalyst [% mol] (mol_{Cat}/mol_{ArBr})	**Catalyst** [M] $*10^{-4}$ ($mmol_{Cat}/ml_{Sol}$)	**ArBr** [M] ($mmol_{ArBr}/ml_{Sol}$)	**Met/ArBr** [mol/mol]	**KO^{t}Am/ArBr** [mol/mol]
0.25/0.55/0.75/1	2.4/5.3/7.2/9.6	0.1	1.1	1.09

In order to make the two-feed tubular reactor more flexible in terms of variation of the component feed, allowing alteration of concentration or delayed feed of some components, a previously developed 2-feed continuous flow tubular microreactor[202] has been modified to incorporate four separate feeds. Such multi-feeding allows the independent control of all reagent streams. A variety of 4-inlet configurations have been investigated, as shown in Figure 48. Four syringes are placed two by two on two syringe pumps and are connected to the tubular reactor by using different junctions: i) a series of a T-junction and a cross-junction (both stainless steel, configuration 1); ii) two T-junctions feeding a third one connected to the reactor (configuration 2); a 4-inlets/1-outlet junction (stainless steel) in series with a porous membrane (porous size 20 μm), to facilitate mixing (configuration 3). The compounds fed in each syringe, together with the concentration are reported in Table II, where the final concentrations in the tubular reactor are reported. The reagents are injected into the microreactor with four syringes placed on two syringe pumps. In particular, the flow rate has been varied from 1.1 ml/h to 70 ml/h, in order to have different residence times and, consequently, different conversion degree. The microreactor and the T-junction are heated in a thermostatic bath at 50 °C, (not reported in the sketches for

the sake of brevity) while both the syringes containing substrates and catalyst are kept at room temperature.

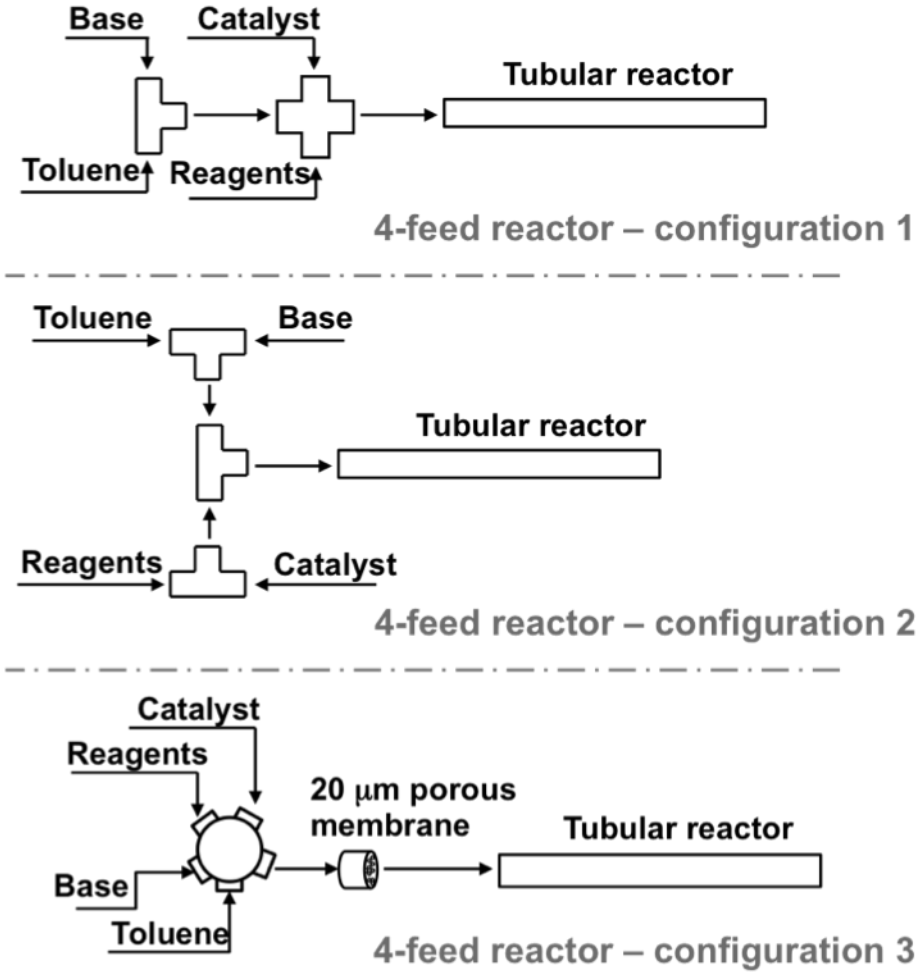

Figure 48: Schematics of different configuration used to increase the flexibility of the flow reactor.

In Figure 49, the conversion profile as a function of the fluid residence time within the reactor has been analyzed by gas chromatography for each four-feed configuration and compared with the two-feed reactor, for a given temperature (50° C) and 1 % mol of (**3**). The percentage conversion is referred to the aryl bromide, that is the limiting reactant, and it is calculated as $[(mol_{ArBr}^{IN} - mol_{ArBr}^{OUT})/ mol_{ArBr}^{IN}]*100$, where mol_{ArBr}^{IN} is the amount of ArBr before the reaction and mol_{ArBr}^{OUT} is the amount of ArBr after the reaction[358]. In order to highlight the occurring of blocking in the different setups, short residence times are reported. The overall conversion profile is reported for the case of the reaction run in the two-feed reactor, where the reaction reaches completion in 40 minutes, conversion being expressed in terms of percentage of aryl bromide converted. From the conversion obtained by using the four-feed reactor

arranged as in configuration 1 it is evident that the first data are available at ten minutes, as blocking of the reactor occurs at shorter residence time. A similar event happens for configuration 2 and 3. Thus, while in the two-feed configuration the reactor works without any blocking problems, the use of a four-feed configuration results in the blocking of the reactor at high flow rates (or, in other words, low residence time i.e., less than 10 minutes). This phenomenon could be attributed to a combination of two factors: the higher concentration of the catalyst as compared to the two-feed system, and the less efficient mixing, leading to incomplete solubilization of the solid compounds. Moreover, potassium bromide is a by-product of the reaction and its formation, even for low degree of conversion of the reagents, could also play a role in microreactor blocking. It should be noted that even when the reaction runs without any blocking (i.e. time higher than 10 minutes for conf. 1 and 3 and time higher than 15 minutes for conf. 2), the conversion is lower than is obtained in the two-feed system. In the table contained in Figure 49 the operating conditions and conversion for the four-feed configurations are reported.

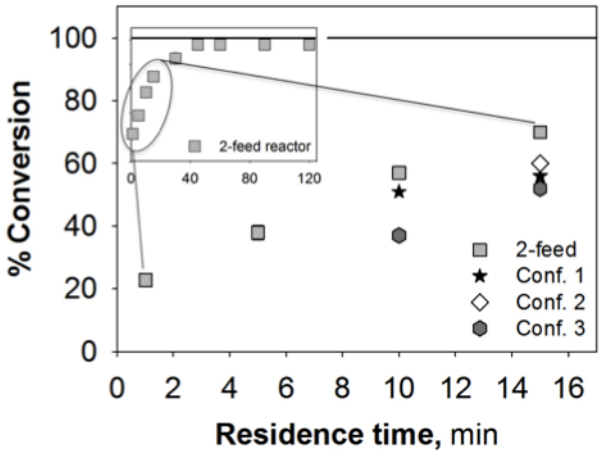

Configuration 1			Configuration 2			Configuration 3		
Time [min]	Flow rate [ml/hr]	% Conversion	Time [min]	Flow rate [ml/hr]	% Conversion	Time [min]	Flow rate [ml/hr]	% Conversion
7.5	4.4	Blocking	7.5	4,4	Blocking	7.5	4.4	Blocking
10	3.3	51 ↓	10	3.3	Blocking	10	3.3	37 ↓↓
15	2.2	56 ↓	15	2.2	60 ↓	15	2.2	52 ↓↓

Figure 49: Conversion degree as a function of time for the four-feed configurations showed in Figure 2 in comparison with the two-feed system at short residence time. The overall conversion of the reaction run in the two-feed reactor is reported in the inset. In the table, black arrows indicate that the conversion degree is lower (one arrow) and much lower (two arrows) compared with the two-feed reactor system

Thus, it was necessary to modify the way in which the microreactor feeding streams are connected in order to obtain a more efficient performance in terms of mixing (and hence of conversion), employing a revised four-feed system (configuration 4), which is shown in Figure 50. In this case, the mixing is performed in a stainless steel 2 mm i.d. junction, with four inlets

and one outlet, the reaction taking place in the stainless steel tubular microreactor. As previously described, the microreactor and the junction are heated in a thermostatic bath (three different temperatures, 50°C, 60°C and 70°C have been investigated), while the four syringes containing substrates, catalyst, base and solvent are at room temperature.

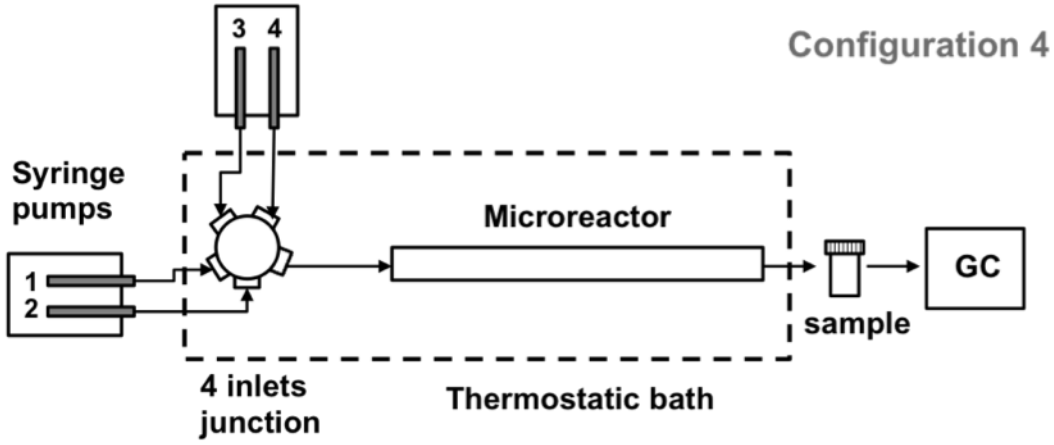

Figure 50: Scheme of the four-feed continuous flow microreactor developed and optimized in this work.

This configuration proved to be the most suitable one, returning performances equal to the simplest two-feed system, as shown in Figure 51, where the conversion as a function of residence time at 50 °C at the same final concentration (1 % mol catalyst, 0.1 M of **(1)**). The two sets of data show an identical reactivity in the two configurations. Indeed, the completion of the reaction has been observed with a time of 45 minutes at a catalyst concentration of 1mol%. Error bars represent the standard deviation of the measurements, which is mainly due to possible errors occurring during the weighing process of the reagents. The presence of potential by-products is precluded by the absence of any significant peaks with the exception of the given reagents and the expected product in the chromatograms. Reagent adsorption to the microreactor walls is negligible, as tested by conducting reactions involving the reagent mixture in the absence of the catalyst, and noting the constant concentrations. One of the differences between the two main configurations (i.e two and four feed) is the dilution of the reagents in the syringes. In order to retain the same overall concentration within the tubular reactor, the concentrations in the individual four-feed streams are higher with respect to the two-feed case. It is possible that the higher reagent concentrations within the syringes can lead to clogging of the microreactor at high flow rates where the retention time in the junction is lower than the characteristic time for diffusion. Configuration 3 gave the worst performance with respect to reactor blocking at high flow rates, despite being identical to configuration4 apart from the presence of a porous membrane. In configuration 3, the use of the porous membrane, exploited to promote efficient mixing, failed for this purpose, because of the very small (i.e., 20 μm) pore size in the membrane. In addition to this, such mixing worsens at high flow rates as this

hampers conversion, as reported in Figure 51, in which it is clear that the lower residence time results in a lower conversion degree.

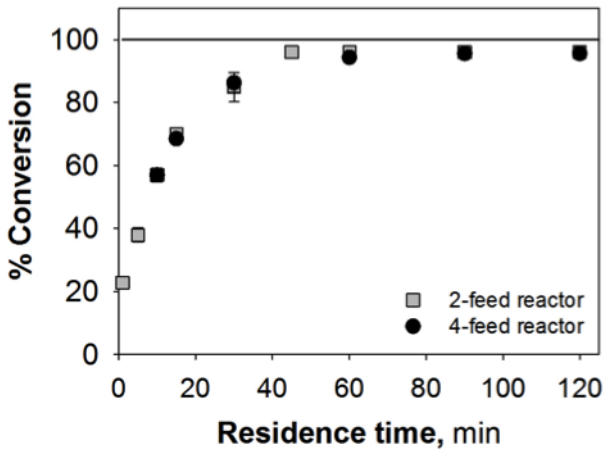

Figure 51: Comparison between 2-feed and 4-feed (configuration 4) reactor operating at 50°C with 0.1 mol% of pre-catalyst

Once the best microreactor streamlines configuration was identified, the reactor operating conditions were optimized. First, the effect of catalyst concentration on reaction rate was investigated. In Figure 52,the conversion profiles are shown for several pre-catalyst concentrations in the microreactor. It can be seen that increasing the catalyst loading allows better performance. In fact, at the highest catalyst loading (1-0.5 mol%), the reaction is almost complete (98%) after 60 min and 120 min respectively, while for lower catalyst concentration (0.25 mol%), complete conversion is never reached. Decreasing the catalyst concentration shows a dual advantage: first, the use of the microreactor allows the achievement of a sufficient level of reactivity by using a small amount of catalyst; second, the reduction in the amount of precious metal catalyst reduces the overall cost. It is worth noting that a reduction of expensive reagents is an important foundation of the sustainable chemistry approach. Thus, it is possible to run the reaction with half the amount of catalyst without having a detrimental effect on the process performance in terms of conversion and avoiding the blocking phenomenon. However, slightly longer residence times are required.

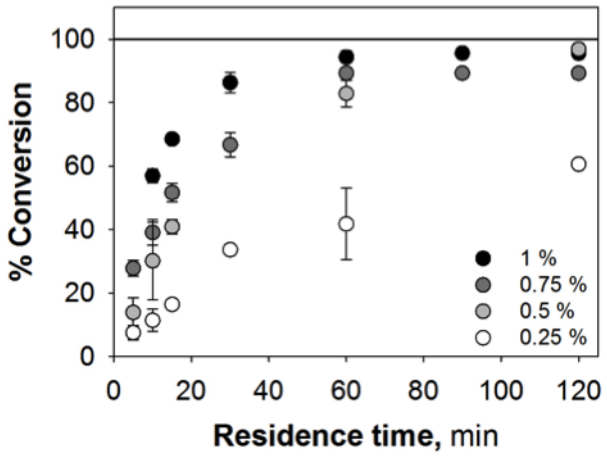

Figure 52: Conversion profiles for different catalyst loading at 50 °C with a concentration in the reactor of 0.1 M of Aryl bromide (toluene 32.6 mL). The continuous lines represents the full conversion.

Reaction rate is affected by aryl bromide concentration as well. We investigated four different concentrations in the range 0.01 – 0.1 M, the concentration of catalyst being constant at $9.6*10^{-4}$M (mmol of catalyst/mL of solution). The conversion of aryl bromide (**1**) as a function of the residence time is reported in Figure 53, highlighting that a decreasing concentration of (**1**) increases the reaction rate leading to a complete conversion in five minutes with 0.01 M of aryl bromide.

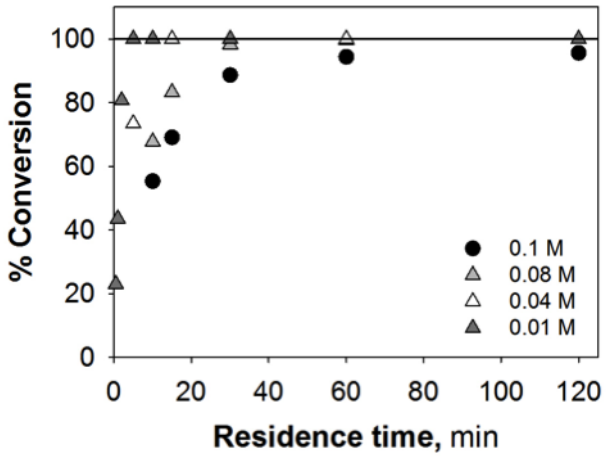

Figure 53: Conversion for different Aryl bromide concentration at 50 °C with a concentration in the reactor of $9.6*10^{-4}$ M of catalyst. The continuous lines represents the complete conversion.

Since the concentration of catalyst is kept constant, it is changing relative to the amount of ArBr (i.e. if at 0.1 M the concentration of catalyst is 1 mol% relative to ArBr, then at 0.01 M of ArBr, the same amount of catalyst is now 10 mol %). This could explain why a faster reaction rate at lower ArBr concentrations is found.

A typical approach for the reduction of reaction time is to perform reactions at higher temperatures. In the four-feed microreactor, full conversion is achieved in 10 minutes at 70 °C, whereas 1 hour is needed at 50 °C (Figure 54a). Because of the higher solubility of the solid compounds, a higher reaction temperature also prevents reactor blocking (also known as clogging), that is due to solid compounds bridging. Microreactor clogging is an issue often encountered when dealing with multiphase flow [202, 359-361]. Increasing the temperature in a microreactor and, at the same time, decreasing the catalyst concentration (Figure 54b) represents an enormous advantage since it is possible to obtain a very fast reaction (less than 20 minutes) with half the amount of catalyst, ensuring very precise controlled temperature, without by-product formation. This could minimize environmental impact when considering the energy contribution in a life-cycle analysis.

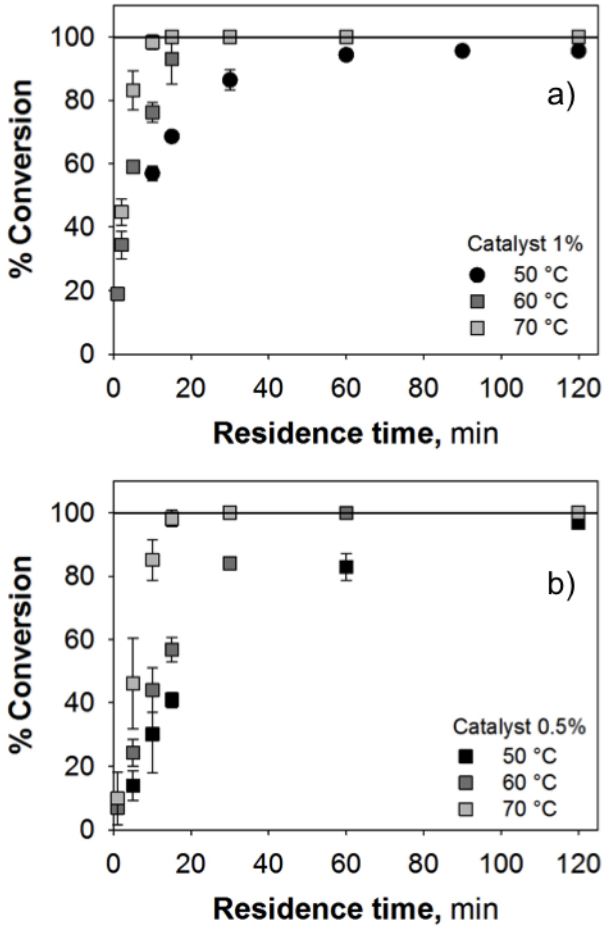

Figure 54: Conversion profiles for different temperature concentration in the reactor for 1% (top) and 0.5 % of catalyst (bottom). The continuous lines represent the complete conversion.

5 Conclusions

In this work, three multiphase systems related issues such as emulsion phase inversion, droplet interfacial properties and microfluidic reactive flows have been investigated by rheological (bulk and interfacial), microfluidic and confocal microscopy means.

Regarding emulsion phase inversion, a detailed experimental campaign have been conducted in order to identify the key-parameters acting on emulsion properties, confocal microscopy and microfluidics have been exploited as an optical sectioning tool to highlight the finest morphological detail of the emulsion; eventually rheological measurements were used to relate macroscopical properties to the microscopical features of the emulsion. Droplet interfacial properties have been measured by microfluidic means and compared with well-established techniques such as pendant drop tensiometry. Eventually, a four-feed microreactor has been developed in order to synthesize an arylamine by coupling a secondary amine with an arylbromide via Buchwald-Hartwig reaction.

During emulsion phase inversion, the emulsion morphology has been characterized in detail by direct observation in confocal microscopy. Long term stable emulsions with great energy saving have been obtained. Higher emulsions stability is associated with both small droplet size and low polydispersity of the droplet size distribution. Confocal microscopy can be exploited to follow the time evolution of the phase inversion process. Confocal imaging clearly shows bicontinuous structure formation in emulsification, that signs the two phases point of inversion. Furthermore, this bicontinuous one, could trap one of the two phase into the other, thus creating inclusion of droplets in droplets. Rheological test showed an increased viscoelastic behavior in the proximity of the inversion, with different behavior showed between the in-flow emulsion and the static one, in which elastic modulus is overwhelming the viscous one in static condition, whereas is the opposite for the in-flow measurement (that could simulated by imposing a pre-shear to the sample). Fine glass cylindrical microchannel having 100 micron of internal diameter, coupling with laser scanning confocal microscopy gave the opportunity to investigate tiniest detail of multiphase system morphology.

In the second part, a method to measure interfacial tension in microfluidic divergent flow of emulsion was shown. Lowering of the interfacial tension due to droplet confinement has been noted and taken into account by scaling droplet deformation parameter. Results are comparable with literature data only in the case of pure droplet interface, while in the case of interface covered or partially covered with surfactants, microfluidic technique is not able as pendant drop to evaluate properly interfacial tension, maybe due to the effects of interfacial Marangoni flow and wetting effect in confined droplet flow as well as the effect of droplet interface elasticity that are not taken into account in the microfluidic model.

Eventually we developed a microreactor for arylamine synthesis. The use of a continuous flow tubular microreactor provides minimization of potential hazards, due to the small internal volume of the reactor, and allows safe operation at high process temperatures. These features are recognized as fundamental in sustainable flow chemistry. In this work, a home-made continuous flow microreactor has been optimized for the Buchwald–Hartwig aryl amination, using a homogeneous well-defined palladium NHC complex. The aryl bromide exploited is a key intermediate in pharmaceutical process and the optimization of the operating conditions along with the microfluidic synthesis of the related arylamine is reported for the first time in this work. Pommella et al.[202] demonstrated the significant performance of a microreactor compared to a batch process in the synthesis of a related molecule. Thus, to the best of our knowledge, we have reported for the first time a flow synthesis of an important pharmaceutical intermediate with an optimized process configuration in which independent streams allow for perfect process handling and control of the chemical synthesis.

A comparison between a classical two-feed reactor and a novel, more flexible four-feed flow system has been provided, as well as an optimization of the operating parameters. The investigation of the effect of catalyst concentration on the degree of conversion has shown that it is possible to reach full conversion even with low catalyst loadings, thus making the process of particular interest in terms of cost, both for the low quantity of catalyst required and the reduced energy burden of the microfluidic approach. An increase of the reaction temperature, together with the decrease of catalyst concentration, allows high levels of reactivity at precisely controlled temperatures, due to optimal heat transfer provided by the microreactor as a result of the smaller surface to volume ratio with respect to batch and flow macroreactor. Moreover, a slight increase in reaction temperature gave full conversion in very short residence times, thus permitting a minimized environmental impact in terms of energy contribution in life-cycle analysis.

In addition, we provided a complete methodology to optimize cross-coupling reaction by using a home-made continuous flow microreactor. The choice of such a microfluidic approach meets requirements of green chemistry, in terms of productivity, process handling, economics savings and operations safety.

Bibliography

[1] S. Guido, M. Simeone, Binary collision of drops in simple shear flow by computer-assisted video optical microscopy, Journal of Fluid Mechanics, 357 (1998) 1-20.
[2] S. Caserta, L. Sabetta, M. Simeone, S. Guido, Shear-induced coalescence in aqueous biopolymer mixtures, Chemical engineering science, 60 (2005) 1019-1027.
[3] P. Taylor, Ostwald ripening in emulsions, Advances in colloid and interface science, 75 (1998) 107-163.
[4] T.J. Wooster, M. Golding, P. Sanguansri, Impact of oil type on nanoemulsion formation and Ostwald ripening stability, Langmuir, 24 (2008) 12758-12765.
[5] F. Leal-Calderon, F. Thivilliers, V. Schmitt, Structured emulsions, Current Opinion in Colloid & Interface Science, 12 (2007) 206-212.
[6] G. Marrucci, A theory of coalescence, Chemical engineering science, 24 (1969) 975-985.
[7] R. MILLER, G. KRETZSCHMAR, ADSORPTION-KINETICS OF SURFACTANTS AT FLUID INTERFACES, Advances in Colloid and Interface Science, 37 (1991) 97-121.
[8] S.S. Dukhin, G. Kretzschmar, R. Miller, Dynamics of adsorption at liquid interfaces: theory, experiment, application, Access Online via Elsevier, 1995.
[9] L. Del Gaudio, P. Pandolfini, F. Ravera, J. Krägel, E. Santini, A.V. Makievski, B.A. Noskov, L. Liggieri, R. Miller, G. Loglio, Dynamic interfacial properties of drops relevant to W/O-emulsion-forming systems: A refined measurement apparatus, Colloids and Surfaces A: Physicochemical and Engineering Aspects, 323 (2008) 3-11.
[10] R. Miller, V.B. Fainerman, A.V. Makievski, J. Krägel, D.O. Grigoriev, V.N. Kazakov, O.V. Sinyachenko, Dynamics of protein and mixed protein/surfactant adsorption layers at the water/fluid interface, Advances in Colloid and Interface Science, 86 (2000) 39-82.
[11] V. Ulaganathan, B. Bergenstahl, J. Krägel, R. Miller, Adsorption and shear rheology of β-lactoglobulin/SDS mixtures at water/hexane and water/MCT interfaces, Colloids and Surfaces A: Physicochemical and Engineering Aspects, 413 (2012) 136-141.
[12] R. Miller, R. Sedev, K.H. Schano, C. Ng, A.W. Neumann, RELAXATION OF ADSORPTION LAYERS AT SOLUTION AIR INTERFACES USING AXISYMMETRICAL DROP-SHAPE ANALYSIS, Colloids and Surfaces, 69 (1993) 209-216.
[13] R. Miller, D.O. Grigoriev, J. Krägel, A.V. Makievski, J. Maldonado-Valderrama, M. Leser, M. Michel, V.B. Fainerman, Experimental studies on the desorption of adsorbed proteins from liquid interfaces, Food Hydrocolloids, 19 (2005) 479-483.
[14] N. Mucic, A. Javadi, N.M. Kovalchuk, E.V. Aksenenko, R. Miller, Dynamics of interfacial layers—Experimental feasibilities of adsorption kinetics and dilational rheology, Advances in Colloid and Interface Science, 168 (2011) 167-178.
[15] R. Miller, On the solution of diffusion controlled adsorption kinetics for any adsorption isotherms, Colloid and Polymer Science, 259 (1981) 375-381.
[16] C. Kotsmar, V. Pradines, V.S. Alahverdjieva, E.V. Aksenenko, V.B. Fainerman, V.I. Kovalchuk, J. Krägel, M.E. Leser, B.A. Noskov, R. Miller, Thermodynamics, adsorption kinetics and rheology of mixed protein–surfactant interfacial layers, Advances in Colloid and Interface Science, 150 (2009) 41-54.
[17] A. Dan, G. Gochev, J. Krägel, E.V. Aksenenko, V.B. Fainerman, R. Miller, Interfacial rheology of mixed layers of food proteins and surfactants, Current Opinion in Colloid & Interface Science, 18 (2013) 302-310.
[18] E.V.A. Leser, V.B. Fainerman, R. Miller, Adsorption Characteristics of Ionic Surfactants at Water/Hexane Interface Obtained by PAT and ODBA, (2013).
[19] L.M.C. Sagis, Dynamic properties of interfaces in soft matter: Experiments and theory, Reviews of Modern Physics, 83 (2011) 1367.
[20] L.M.C. Sagis, P. Fischer, P.D. Anderson, Dynamics of complex fluid-fluid interfaces, The European Physical Journal Special Topics, 222 (2013) 1-5.
[21] L. Sagis, E. Scholten, Complex interfaces in food: Structure and mechanical properties, Trends in Food Science & Technology, 37 (2014) 59-71.
[22] L. Sagis, Dynamic behavior of interfaces: Modeling with nonequilibrium thermodynamics, Advances in colloid and interface science, 206 (2014) 328-343.
[23] A.G. Bykov, L. Liggieri, B.A. Noskov, P. Pandolfini, F. Ravera, G. Loglio, Surface dilational rheological properties in the nonlinear domain, Advances in colloid and interface science, (2014).
[24] L.M.C. Sagis, P. Fischer, Nonlinear rheology of complex fluid–fluid interfaces, Current Opinion in Colloid & Interface Science, (2014).
[25] M. Doi, T. Ohta, Dynamics and rheology of complex interfaces. I, The Journal of chemical physics, 95 (1991) 1242-1248.
[26] C. Solans, P. Izquierdo, J. Nolla, N. Azemar, M.J. Garcia-Celma, Nano-emulsions, Current Opinion in Colloid & Interface Science, 10 (2005) 102-110.
[27] M.Y. Koroleva, E.V. Yurtov, Nanoemulsions: the properties, methods of preparation and promising applications, Russian Chemical Reviews, 81 (2012) 21.
[28] D.J. McClements, Nanoemulsions versus microemulsions: terminology, differences, and similarities, Soft Matter, 8 (2012) 1719-1729.
[29] J. Salager, J. Morgan, R. Schechter, W. Wade, E. Vasquez, Optimum formulation of surfactant/water/oil systems for minimum interfacial tension or phase behavior, Soc. Pet. Eng. J, 19 (1979) 107-115.
[30] F. Bouchama, G.A. van Aken, A.J.E. Autin, G.J.M. Koper, On the mechanism of catastrophic phase inversion in emulsions, Colloids and Surfaces A: Physicochemical and Engineering Aspects, 231 (2003) 11-17.
[31] E. Dickinson, Thermodynamic aspects of emulsion phase inversion, Journal of Colloid and Interface Science, 87 (1982) 416-423.

[32] E. Dickinson, Interpretation of emulsion phase inversion as a cusp catastrophe, Journal of Colloid and Interface Science, 84 (1981) 284-287.
[33] L.Y. Yeo, O.K. Matar, E.S.P. de Ortiz, G.F. Hewitt, PHASE INVERSION AND ASSOCIATED PHENOMENA, 12 (2000) 66.
[34] G.E.J. Vaessen, H.N. Stein, The Applicability of Catastrophe Theory to Emulsion Phase Inversion, Journal of Colloid and Interface Science, 176 (1995) 378-387.
[35] S. Sajjadi, Nanoemulsion formation by phase inversion emulsification: on the nature of inversion, Langmuir, 22 (2006) 5597-5603.
[36] K. Shinoda, H. Saito, The effect of temperature on the phase equilibria and the types of dispersions of the ternary system composed of water, cyclohexane, and nonionic surfactant, Journal of Colloid and Interface Science, 26 (1968) 70-74.
[37] A. Nienow, Break-up, coalescence and catastrophic phase inversion in turbulent contactors, Advances in colloid and interface science, 108 (2004) 95-103.
[38] R. Orr, Phase inversion in heavy crude oil production, in: Proceedings of Teknas Conference on Heavy Oil Technology for Offshore Applications, 2009, pp. 14-15.
[39] J. Gutiérrez, C. González, A. Maestro, I. Sole, C. Pey, J. Nolla, Nano-emulsions: New applications and optimization of their preparation, Current Opinion in Colloid & Interface Science, 13 (2008) 245-251.
[40] M.M. Fryd, T.G. Mason, Advanced nanoemulsions, Annual Review of Physical Chemistry, 63 (2012) 493-518.
[41] Y. Li, Z. Zhang, Q. Yuan, H. Liang, F. Vriesekoop, Process optimization and stability of d-limonene nanoemulsions prepared by catastrophic phase inversion method, Journal of Food Engineering, 119 (2013) 419-424.
[42] S.L. Ee, X. Duan, J. Liew, Q.D. Nguyen, Droplet size and stability of nano-emulsions produced by the temperature phase inversion method, Chemical Engineering Journal, 140 (2008) 626-631.
[43] R. Santana, F. Perrechil, R. Cunha, High-and low-energy emulsifications for food applications: a focus on process parameters, Food Engineering Reviews, 5 (2013) 107-122.
[44] H.D. Silva, M.Â. Cerqueira, A.A. Vicente, Nanoemulsions for food applications: development and characterization, Food and Bioprocess Technology, 5 (2012) 854-867.
[45] P. Shah, D. Bhalodia, P. Shelat, Nanoemulsion: A pharmaceutical review, Systematic Reviews in Pharmacy, 1 (2010) 24.
[46] F. Sainsbury, B. Zeng, A.P. Middelberg, Towards designer nanoemulsions for precision delivery of therapeutics, Current Opinion in Chemical Engineering, 4 (2014) 11-17.
[47] G. Fack, C. Dubief, L. Nicolas-Morgantini, S. Restle, Method for preparing a cationic nanoemulsion and cosmetic composition, in, Google Patents, 2009.
[48] S. Sharma, K. Sarangdevot, Nanoemulsions For Cosmetics.
[49] O. Sonneville-Aubrun, J.-T. Simonnet, F. L'alloret, Nanoemulsions: a new vehicle for skincare products, Advances in Colloid and Interface Science, 108 (2004) 145-149.
[50] J. Komaiko, D.J. McClements, Optimization of isothermal low-energy nanoemulsion formation: Hydrocarbon oil, non-ionic surfactant, and water systems, Journal of colloid and interface science, 425 (2014) 59-66.
[51] V. Mohanraj, Y. Chen, Nanoparticles-a review, Tropical Journal of Pharmaceutical Research, 5 (2007) 561-573.
[52] N. Anton, J.-P. Benoit, P. Saulnier, Design and production of nanoparticles formulated from nano-emulsion templates—a review, Journal of Controlled Release, 128 (2008) 185-199.
[53] J. Rao, D.J. McClements, Stabilization of phase inversion temperature nanoemulsions by surfactant displacement, Journal of agricultural and food chemistry, 58 (2010) 7059-7066.
[54] Y. Chang, D.J. McClements, Optimization of Orange Oil Nanoemulsion Formation by Isothermal Low-Energy Methods: Influence of the Oil Phase, Surfactant, and Temperature, Journal of agricultural and food chemistry, 62 (2014) 2306-2312.
[55] G.P. Carino, J.S. Jacob, E. Mathiowitz, Nanosphere based oral insulin delivery, Journal of Controlled Release, 65 (2000) 261-269.
[56] L. Capretto, D. Carugo, S. Mazzitelli, C. Nastruzzi, X. Zhang, Microfluidic and lab-on-a-chip preparation routes for organic nanoparticles and vesicular systems for nanomedicine applications, Advanced drug delivery reviews, 65 (2013) 1496-1532.
[57] E. Esposito, S. Mazzitelli, R. Cortesi, M. Drechsler, L. Ravani, C. Nastruzzi, Analysis of the drug release profiles from formulations based on micro and nano systems, Current Analytical Chemistry, 9 (2013) 37-46.
[58] G. Fundueanu, E. Esposito, D. Mihai, A. Carpov, J. Desbrieres, M. Rinaudo, C. Nastruzzi, Preparation and characterization of Ca-alginate microspheres by a new emulsification method, International journal of pharmaceutics, 170 (1998) 11-21.
[59] K. Suzuki, K. Nishiyama, E. Takeuchi, S. Shim, S. Satoh, Preparation of polystyrene nanoparticles including fluorescent and hydrophobic materials by polymerization at phase inversion temperature, Polymers for Advanced Technologies, (2014).
[60] B. Heurtault, P. Saulnier, B. Pech, J.-E. Proust, J.-P. Benoit, A Novel Phase Inversion-Based Process for the Preparation of Lipid Nanocarriers, Pharmaceutical Research, 19 (2002) 875-880.
[61] K.S. Soppimath, T.M. Aminabhavi, A.R. Kulkarni, W.E. Rudzinski, Biodegradable polymeric nanoparticles as drug delivery devices, Journal of controlled release, 70 (2001) 1-20.
[62] J. Panyam, V. Labhasetwar, Biodegradable nanoparticles for drug and gene delivery to cells and tissue, Advanced drug delivery reviews, 55 (2003) 329-347.
[63] E. Acosta, Bioavailability of nanoparticles in nutrient and nutraceutical delivery, Current Opinion in Colloid & Interface Science, 14 (2009) 3-15.
[64] S. Mayer, J. Weiss, D.J. McClements, Vitamin E-enriched nanoemulsions formed by emulsion phase inversion: Factors influencing droplet size and stability, Journal of Colloid and Interface Science, 402 (2013) 122-130.
[65] M.X. Quintanilla-Carvajal, B.H. Camacho-Díaz, L.S. Meraz-Torres, J.J. Chanona-Pérez, L. Alamilla-Beltrán, A. Jimenéz-Aparicio, G.F. Gutiérrez-López, Nanoencapsulation: a new trend in food engineering processing, Food Engineering Reviews, 2 (2010) 39-50.
[66] D.J. McClements, Edible nanoemulsions: fabrication, properties, and functional performance, Soft Matter, 7 (2011) 2297-2316.
[67] Y. Yang, D.J. McClements, Encapsulation of vitamin E in edible emulsions fabricated using a natural surfactant, Food Hydrocolloids, 30 (2013) 712-720.
[68] Y. Yang, D.J. McClements, Vitamin E bioaccessibility: Influence of carrier oil type on digestion and release of emulsified α-tocopherol acetate, Food Chemistry, 141 (2013) 473-481.
[69] A.H. Saberi, Y. Fang, D.J. McClements, Stabilization of vitamin E-enriched mini-emulsions: Influence of organic and aqueous phase compositions, Colloids and Surfaces A: Physicochemical and Engineering Aspects, 449 (2014) 65-73.

[70] J.-B. Tagne, S. Kakumanu, D. Ortiz, T. Shea, R.J. Nicolosi, A nanoemulsion formulation of tamoxifen increases its efficacy in a breast cancer cell line, Molecular pharmaceutics, 5 (2008) 280-286.
[71] A. Myc, J.F. Kukowska-Latallo, A.U. Bielinska, P. Cao, P.P. Myc, K. Janczak, T.R. Sturm, M.S. Grabinski, J.J. Landers, K.S. Young, Development of immune response that protects mice from viral pneumonitis after a single intranasal immunization with influenza A virus and nanoemulsion, Vaccine, 21 (2003) 3801-3814.
[72] M. Kumar, A. Misra, A. Babbar, A. Mishra, P. Mishra, K. Pathak, Intranasal nanoemulsion based brain targeting drug delivery system of risperidone, International journal of pharmaceutics, 358 (2008) 285-291.
[73] Z. Wang, R. Pal, Enlargement of Nanoemulsion Region in Pseudo-ternary Mixing Diagrams for a Drug Delivery System, Journal of Surfactants and Detergents, 17 (2014) 49-58.
[74] N. Anton, T.F. Vandamme, The universality of low-energy nano-emulsification, International Journal of Pharmaceutics, 377 (2009) 142-147.
[75] C. Lovelyn, A.A. Attama, Current state of nanoemulsions in drug delivery, Journal of Biomaterials and Nanobiotechnology, 2 (2011) 626.
[76] A. Sulakvelidze, Z. Alavidze, J.G. Morris, Bacteriophage therapy, Antimicrobial agents and chemotherapy, 45 (2001) 649-659.
[77] P.P. Esteban, D.R. Alves, M.C. Enright, J.E. Bean, A. Gaudion, A. Jenkins, A.E. Young, T.C. Arnot, Enhancement of the antimicrobial properties of bacteriophage-K via stabilization using oil-in-water nano-emulsions, Biotechnology progress, (2014).
[78] D.J. Miller, T. Henning, W. Grünbein, Phase inversion of W/O emulsions by adding hydrophilic surfactant—a technique for making cosmetics products, Colloids and Surfaces A: Physicochemical and Engineering Aspects, 183 (2001) 681-688.
[79] J. MEYER, G. POLAK, R. SCHEUERMANN, Preparing PIC emulsions with a very fine particle size, Cosmetics and toiletries, 122 (2007).
[80] S.U. Pickering, CXCVI.-Emulsions, Journal of the Chemical Society, Transactions, 91 (1907) 2001-2021.
[81] A. Dinsmore, M.F. Hsu, M. Nikolaides, M. Marquez, A. Bausch, D. Weitz, Colloidosomes: selectively permeable capsules composed of colloidal particles, Science, 298 (2002) 1006-1009.
[82] B.P. Binks, S.O. Lumsdon, Catastrophic Phase Inversion of Water-in-Oil Emulsions Stabilized by Hydrophobic Silica, Langmuir, 16 (2000) 2539-2547.
[83] B.P. Binks, T.S. Horozov, Colloidal particles at liquid interfaces: an introduction, Colloidal Particles at Liquid Interfaces, Chapt, 1 (2006) 1-74.
[84] B.P. Binks, L. Isa, A.T. Tyowua, Direct Measurement of Contact Angles of Silica Particles in Relation to Double Inversion of Pickering Emulsions, Langmuir, 29 (2013) 4923-4927.
[85] R. Aveyard, B.P. Binks, J.H. Clint, Emulsions stabilised solely by colloidal particles, Advances in Colloid and Interface Science, 100 (2003) 503-546.
[86] M.R. Asadabadi, H. Abolghasemi, M.G. Maragheh, P.D. Nasab, Effect of silica nanoparticles on the phase inversion of liquid-liquid dispersions, Korean Journal of Chemical Engineering, 30 (2013) 733-738.
[87] D. Rousseau, Fat crystals and emulsion stability—a review, Food Research International, 33 (2000) 3-14.
[88] B.P. Binks, Particles as surfactants—similarities and differences, Current Opinion in Colloid & Interface Science, 7 (2002) 21-41.
[89] Z. Du, M.P. Bilbao-Montoya, B.P. Binks, E. Dickinson, R. Ettelaie, B.S. Murray, Outstanding stability of particle-stabilized bubbles, Langmuir, 19 (2003) 3106-3108.
[90] B. Binks, S. Lumsdon, Influence of particle wettability on the type and stability of surfactant-free emulsions, Langmuir, 16 (2000) 8622-8631.
[91] V. Garbin, Colloidal particles: Surfactants with a difference, Physics Today, 66 (2013) 68.
[92] B.P. Binks, R. Murakami, Phase inversion of particle-stabilized materials from foams to dry water, Nature materials, 5 (2006) 865-869.
[93] K.A. White, A.B. Schofield, P. Wormald, J.W. Tavacoli, B.P. Binks, P.S. Clegg, Inversion of particle-stabilized emulsions of partially miscible liquids by mild drying of modified silica particles, J Colloid Interface Sci, 359 (2011) 126-135.
[94] Z.-G. Cui, L.-L. Yang, Y.-Z. Cui, B. Binks, Effects of surfactant structure on the phase inversion of emulsions stabilized by mixtures of silica nanoparticles and cationic surfactant, Langmuir, 26 (2009) 4717-4724.
[95] B.P. Binks, J.A. Rodrigues, Influence of surfactant structure on the double inversion of emulsions in the presence of nanoparticles, Colloids and Surfaces A: Physicochemical and Engineering Aspects, 345 (2009) 195-201.
[96] Z. Yang, D. Zhao, M. Xu, Y. Xu, Mechanistic investigation on the formation of epoxy resin multi-hollow spheres prepared by a phase inversion emulsification technique, Macromolecular rapid communications, 21 (2000) 574-578.
[97] Z. Yang, Y. Xu, D. Zhao, M. Xu, Preparation of waterborne dispersions of epoxy resin by the phase-inversion emulsification technique. 1. Experimental study on the phase-inversion process, Colloid and Polymer Science, 278 (2000) 1164-1171.
[98] Z. Yang, Y. Xu, D. Zhao, M. Xu, Preparation of waterborne dispersions of epoxy resin by the phase-inversion emulsification technique. 2. Theoretical consideration of the phase-inversion process, Colloid and Polymer Science, 278 (2000) 1103-1108.
[99] Z. Yang, Y. Zhu, D. Qiu, H. Bu, Sub-Micron-Sized Waterborne Particles of Crosslinked Epoxy Resin Prepared by Phase-Inversion Emulsification, Macromolecular rapid communications, 22 (2001) 792-796.
[100] Z. Yang, D. Qiu, J. Li, Waterborne dispersions of a polymer-encapsulated inorganic particle nanocomposite by phase-inversion emulsification, Macromolecular rapid communications, 23 (2002) 479-483.
[101] M. Takenaga, Y. Serizawa, Y. Azechi, A. Ochiai, Y. Kosaka, R. Igarashi, Y. Mizushima, Microparticle resins as a potential nasal drug delivery system for insulin, Journal of controlled release, 52 (1998) 81-87.
[102] K. Haupt, K. Mosbach, Molecularly imprinted polymers and their use in biomimetic sensors, Chemical Reviews, 100 (2000) 2495-2504.
[103] A. Saniere, I. Henaut, J.F. Argillier, Pipeline transportation of heavy oils, a strategic, economic and technological challenge, Oil & Gas Science and Technology-Revue D Ifp Energies Nouvelles, 59 (2004) 455-466.
[104] M. Minale, S. Caserta, S. Guido, Microconfined Shear Deformation of a Droplet in an Equiviscous Non-Newtonian Immiscible Fluid: Experiments and Modeling, Langmuir, 26 (2010) 126-132.
[105] J.J.L. Higdon, Multiphase flow in porous media, Journal of Fluid Mechanics, 730 (2013) 1-4.
[106] R. Helmig, B. Flemisch, M. Wolff, A. Ebigbo, H. Class, Model coupling for multiphase flow in porous media, Advances in Water Resources, 51 (2013) 52-66.
[107] L. Kokal Sunil, B. Maini Brij, R. Woo, Flow of Emulsions in Porous Media, in: Emulsions, American Chemical Society, 1992, pp. 219-262.

[108] J. Torok, J. Toth, G. Gesztesi, Polydispersed O/W emulsions in porous media: Segregation at low-tension conditions, Journal of Colloid and Interface Science, 295 (2006) 569-577.
[109] V. Sibillo, G. Pasquariello, M. Simeone, V. Cristini, S. Guido, Drop Deformation in Microconfined Shear Flow, Physical Review Letters, 97 (2006) 054502.
[110] J.F. Roca, M.S. Carvalho, Flow of a drop through a constricted microcapillary, Computers & Fluids, 87 (2013) 50-56.
[111] S. Guido, V. Preziosi, Droplet deformation under confined Poiseuille flow, Advances in Colloid and Interface Science, 161 (2010) 89-101.
[112] S. Guido, Shear-induced droplet deformation: Effects of confined geometry and viscoelasticity, Current Opinion in Colloid & Interface Science, 16 (2011) 61-70.
[113] S. Cobos, M.S. Carvalho, V. Alvarado, Flow of oil-water emulsions through a constricted capillary, International Journal of Multiphase Flow, 35 (2009) 507-515.
[114] R.H. Davis, A.Z. Zinchenko, Motion of deformable drops through granular media and other confined geometries, Journal of Colloid and Interface Science, 334 (2009) 113-123.
[115] A.Z. Zinchenko, R.H. Davis, Emulsion flow through a packed bed with multiple drop breakup, Journal of Fluid Mechanics, 725 (2013) 611-663.
[116] V.R. Guillen, M.I. Romero, M.d.S. Carvalho, V. Alvarado, Capillary-driven mobility control in macro emulsion flow in porous media, International Journal of Multiphase Flow, 43 (2012) 62-65.
[117] H. Soo, C.J. Radke, Velocity effects in emulsion flow through porous media, Journal of Colloid and Interface Science, 102 (1984) 462-476.
[118] A. Cortis, T.A. Ghezzehei, On the transport of emulsions in porous media, Journal of Colloid and Interface Science, 313 (2007) 1-4.
[119] M.I. Romero, M.S. Carvalho, V. Alvarado, Experiments and network model of flow of oil-water emulsion in porous media, Physical Review E, 84 (2011) 046305.
[120] R. Hilfer, Macroscopic capillarity and hysteresis for flow in porous media, Physical Review E, 73 (2006) 016307.
[121] F.D.a.R. Hilfer, Generalized Buckley–Leverett theory for two-phase flow in porous media, New Journal of Physics, 13 (2011) 123030.
[122] S. Godefroy, P.T. Callaghan, 2D relaxation/diffusion correlations in porous media, Magnetic Resonance Imaging, 21 (2003) 381-383.
[123] W.J. Bryan J., Kantzas A.,, Measurement of emulsion flow in porous media: Improvements in heavy oil recovery, Journal of Physics: Conference Series, 147 (2009) 012058.
[124] M. Bavière, Basic concepts in enhanced oil recovery processes, Springer, 1991.
[125] J.-L. Salager, A.M. Forgiarini, J. Bullón, How to attain ultralow interfacial tension and three-phase behavior with surfactant formulation for enhanced oil recovery: a review. Part 1. Optimum Formulation For Simple Surfactant–Oil–Water Ternary Systems, Journal of Surfactants and Detergents, 16 (2013) 449-472.
[126] A. Mandal, A. Bera, K. Ojha, T. Kumar, Characterization of surfactant stabilized nanoemulsion and its use in enhanced oil recovery, in: SPE International Oilfield Nanotechnology Conference and Exhibition, Society of Petroleum Engineers, 2012.
[127] V. Santanna, F. Curbelo, T. Castro Dantas, A. Dantas Neto, H. Albuquerque, A. Garnica, Microemulsion flooding for enhanced oil recovery, Journal of Petroleum Science and Engineering, 66 (2009) 117-120.
[128] L. Del Gaudio, R. Bortolo, T.P. Lockhart, Nanoemulsions: a new vehicle for chemical additive delivery, in, Society of Petroleum Engineers.
[129] T. Austad, S. Strand, Chemical flooding of oil reservoirs 4. Effects of temperature and pressure on the middle phase solubilization parameters close to optimum flood conditions, Colloids and Surfaces A: Physicochemical and Engineering Aspects, 108 (1996) 243-252.
[130] J.-L. Salager, A.M. Forgiarini, Emulsion Stabilization, Breaking, and Inversion Depends upon Formulation: Advantage or Inconvenience in Flow Assurance, Energy & Fuels, 26 (2012) 4027-4033.
[131] A.D. Patel, Reversible invert emulsion drilling fluids: a quantum leap in technology, SPE Drilling & Completion, 14 (1999) 274-279.
[132] G.C. Maitland, Oil and gas production, Current Opinion in Colloid & Interface Science, 5 (2000) 301-311.
[133] C. Dalmazzone, C. Noïk, J.-F. Argillier, Impact of Chemical Enhanced Oil Recovery on the Separation of Diluted Heavy Oil Emulsions, Energy & Fuels, 26 (2012) 3462-3469.
[134] S.K. Wadhwa, Cross-linking system for water based well fracturing fluids, in, Google Patents, 1985.
[135] R.T. Whalen, Viscoelastic surfactant fracturing fluids and a method for fracturing subterranean formations, in, Google Patents, 2000.
[136] N.A. Spenley, M.E. Cates, T.C.B. McLeish, Nonlinear rheology of wormlike micelles, Physical Review Letters, 71 (1993) 939-942.
[137] J. Yang, Viscoelastic wormlike micelles and their applications, Current Opinion in Colloid & Interface Science, 7 (2002) 276-281.
[138] C.A. Dreiss, Wormlike micelles: where do we stand? Recent developments, linear rheology and scattering techniques, Soft Matter, 3 (2007) 956-970.
[139] Z. Chu, C.A. Dreiss, Y. Feng, Smart wormlike micelles, Chemical Society Reviews, 42 (2013) 7174-7203.
[140] G. Palazzo, Wormlike reverse micelles, Soft Matter, 9 (2013) 10668-10677.
[141] Z. Lin, J.J. Cai, L.E. Scriven, H.T. Davis, Spherical-to-Wormlike Micelle Transition in CTAB Solutions, The Journal of Physical Chemistry, 98 (1994) 5984-5993.
[142] S. Engelskirchen, D.P. Acharya, M. Garcia-Roman, H. Kunieda, Effect of C12EOn mixed surfactant systems on the formation of viscoelastic worm-like micellar solutions in sucrose alkanoate– and CTAB–water systems, Colloids and Surfaces A: Physicochemical and Engineering Aspects, 279 (2006) 113-120.
[143] V.K. Aswal, P.S. Goyal, P. Thiyagarajan, Small-Angle Neutron-Scattering and Viscosity Studies of CTAB/NaSal Viscoelastic Micellar Solutions, The Journal of Physical Chemistry B, 102 (1998) 2469-2473.
[144] T. Shikata, S.J. Dahman, D.S. Pearson, Rheo-Optical Behavior of Wormlike Micelles, Langmuir, 10 (1994) 3470-3476.
[145] A. Khatory, F. Lequeux, F. Kern, S.J. Candau, Linear and nonlinear viscoelasticity of semidilute solutions of wormlike micelles at high salt content, Langmuir, 9 (1993) 1456-1464.
[146] J.P. Rothstein, Transient extensional rheology of wormlike micelle solutions, Journal of Rheology, 47 (2003) 1227.

[147] A.A. Dehghan, M. Masihi, S. Ayatollahi, Evaluation of Chemicals Interaction with Heavy Crude Oil through Water/Oil Emulsion and Interfacial Tension Study, Energy & Fuels, (2013).
[148] N. Thampi, K. Ojha, U. Nair, Effect of Branched Alcohols on Phase Behavior and Physicochemical Properties of Winsor IV Microemulsions, Journal of Surfactants and Detergents, (2013) 1-11.
[149] K. Panthi, K.K. Mohanty, Effect of Alkaline Preflush in an Alkaline-Surfactant-Polymer Flood, Energy & Fuels, 27 (2013) 764-771.
[150] B. Engelke, M.S. Carvalho, V. Alvarado, Conceptual Darcy-Scale Model of Oil Displacement with Macroemulsion, Energy & Fuels, 27 (2013) 1967-1973.
[151] A.M. Johannessen, K. Spildo, Enhanced Oil Recovery (EOR) by Combining Surfactant with Low Salinity Injection, Energy & Fuels, (2013).
[152] J.-L. Salager, A. Forgiarini, J. Bullón, How to Attain Ultralow Interfacial Tension and Three-Phase Behavior with Surfactant Formulation for Enhanced Oil Recovery: A Review. Part 1. Optimum Formulation for Simple Surfactant–Oil–Water Ternary Systems, Journal of Surfactants and Detergents, 16 (2013) 449-472.
[153] V.C. Santanna, F.D.S. Curbelo, T.N. Castro Dantas, A.A. Dantas Neto, H.S. Albuquerque, A.I.C. Garnica, Microemulsion flooding for enhanced oil recovery, Journal of Petroleum Science and Engineering, 66 (2009) 117-120.
[154] V.C. Santanna, A.C.M. Silva, H.M. Lopes, F.A. Sampaio Neto, Microemulsion flow in porous medium for enhanced oil recovery, Journal of Petroleum Science and Engineering, 105 (2013) 116-120.
[155] L. Liggieri, R. Miller, Relaxation of surfactants adsorption layers at liquid interfaces, Current Opinion in Colloid & Interface Science, 15 (2010) 256-263.
[156] F. Mori, J.C. Lim, O.G. Raney, C.M. Elsik, C.A. Miller, Phase behavior, dynamic contacting and detergency in systems containing triolein and nonionic surfactants, Colloids and Surfaces, 40 (1989) 323-345.
[157] C. Stubenrauch, V.B. Fainerman, E.V. Aksenenko, R. Miller, Adsorption Behavior and Dilational Rheology of the Cationic Alkyl Trimethylammonium Bromides at the Water/Air Interface, The Journal of Physical Chemistry B, 109 (2005) 1505-1509.
[158] V.B. Fainerman, R. Miller, Surface Tension Isotherms for Surfactant Adsorption Layers Including Surface Aggregation, Langmuir, 12 (1996) 6011-6014.
[159] V.B. Fainerman, S.V. Lylyk, E.V. Aksenenko, N.M. Kovalchuk, V.I. Kovalchuk, J.T. Petkov, R. Miller, Effect of water hardness on surface tension and dilational visco-elasticity of sodium dodecyl sulphate solutions, Journal of Colloid and Interface Science, 377 (2012) 1-6.
[160] N. Mucic, N.M. Kovalchuk, E.V. Aksenenko, V.B. Fainerman, R. Miller, Adsorption layer properties of alkyltrimethylammonium bromides at interfaces between water and different alkanes, Journal of Colloid and Interface Science, 410 (2013) 181-187.
[161] N. Schelero, R. von Klitzing, V.B. Fainerman, R. Miller, Chain length effects on complex formation in solutions of sodium alkanoates and tetradecyl trimethyl ammonium bromide, Colloids and Surfaces A: Physicochemical and Engineering Aspects, 413 (2012) 115-118.
[162] D. Langevin, Rheology of Adsorbed Surfactant Monolayers at Fluid Surfaces, Annual Review of Fluid Mechanics, (2013).
[163] A. Bera, T. Kumar, K. Ojha, A. Mandal, Adsorption of surfactants on sand surface in enhanced oil recovery: Isotherms, kinetics and thermodynamic studies, Applied Surface Science, 284 (2013) 87-99.
[164] M.M. Khasanov, G.T. Bulgakova, A.G. Telin, A.T. Akhmetov, Non-equilibrium and Nonlinear Effects in Water-in-Oil Emulsion Flows in Porous Media, Energy & Fuels, 25 (2011) 1173-1181.
[165] D.M. Boersma, J. Bruining, H. Ronde, R.A. Gotlieb, Capillary behaviour of multi-phase systems in porous media, Journal of Petroleum Science and Engineering, 2 (1989) 141-147.
[166] R. Martínez-Palou, M.d.L. Mosqueira, B. Zapata-Rendón, E. Mar-Juárez, C. Bernal-Huicochea, J. de la Cruz Clavel-López, J. Aburto, Transportation of heavy and extra-heavy crude oil by pipeline: A review, Journal of Petroleum Science and Engineering, 75 (2011) 274-282.
[167] S.W. Hasan, M.T. Ghannam, N. Esmail, Heavy crude oil viscosity reduction and rheology for pipeline transportation, Fuel, 89 (2010) 1095-1100.
[168] N. Abdurahman, Y. Rosli, N. Azhari, B. Hayder, Pipeline transportation of viscous crudes as concentrated oil-in-water emulsions, Journal of Petroleum Science and Engineering, 90 (2012) 139-144.
[169] S. Ashrafizadeh, M. Kamran, Emulsification of heavy crude oil in water for pipeline transportation, Journal of Petroleum Science and Engineering, 71 (2010) 205-211.
[170] D. Langevin, S. Poteau, I. Hénaut, J. Argillier, Crude oil emulsion properties and their application to heavy oil transportation, Oil & gas science and technology, 59 (2004) 511-521.
[171] H.A. Stone, A.D. Stroock, A. Ajdari, Engineering flows in small devices: microfluidics toward a lab-on-a-chip, Annu. Rev. Fluid Mech., 36 (2004) 381-411.
[172] T.M. Squires, S.R. Quake, Microfluidics: Fluid physics at the nanoliter scale, Reviews of modern physics, 77 (2005) 977.
[173] G.M. Whitesides, The origins and the future of microfluidics, Nature, 442 (2006) 368-373.
[174] G. Tomaiuolo, Biomechanical properties of red blood cells in health and disease towards microfluidics, Biomicrofluidics, 8 (2014) 051501.
[175] A. Pommella, S. Caserta, V. Guida, S. Guido, Shear-Induced Deformation of Surfactant Multilamellar Vesicles, Physical Review Letters, 108 (2012) 138301.
[176] A. Pommella, S. Caserta, S. Guido, Dynamic flow behaviour of surfactant vesicles under shear flow: role of a multilamellar microstructure, Soft Matter, 9 (2013) 7545-7552.
[177] S.-Y. Teh, R. Lin, L.-H. Hung, A.P. Lee, Droplet microfluidics, Lab on a Chip, 8 (2008) 198-220.
[178] P. Garstecki, M.J. Fuerstman, H.A. Stone, G.M. Whitesides, Formation of droplets and bubbles in a microfluidic T-junction—scaling and mechanism of break-up, Lab on a Chip, 6 (2006) 437-446.
[179] R. Seemann, M. Brinkmann, T. Pfohl, S. Herminghaus, Droplet based microfluidics, Reports on progress in physics, 75 (2012) 016601.
[180] A.J. Demello, Control and detection of chemical reactions in microfluidic systems, Nature, 442 (2006) 394-402.
[181] S. Jakiela, P.M. Korczyk, S. Makulska, O. Cybulski, P. Garstecki, Discontinuous Transition in a Laminar Fluid Flow: A Change of Flow Topology inside a Droplet Moving in a Micron-Size Channel, Physical review letters, 108 (2012) 134501.
[182] R. Lindken, L. Gui, W. Merzkirch, Velocity measurements in multiphase flow by means of particle image velocimetry, Chemical engineering & technology, 22 (1999) 202-206.

[183] T.T. Al-Housseiny, P.A. Tsai, H.A. Stone, Control of interfacial instabilities using flow geometry, Nature Physics, 8 (2012) 747-750.
[184] T.T. Al-Housseiny, I.C. Christov, H.A. Stone, Two-phase fluid displacement and interfacial instabilities under elastic membranes, Physical review letters, 111 (2013) 034502.
[185] S.A. Setu, I. Zacharoudiou, G.J. Davies, D. Bartolo, S. Moulinet, A.A. Louis, J.M. Yeomans, D.G. Aarts, Viscous fingering at ultralow interfacial tension, arXiv preprint arXiv:1309.2770, (2013).
[186] E.O. Dias, J.A. Miranda, Taper-induced control of viscous fingering in variable-gap Hele-Shaw flows, Physical Review E, 87 (2013) 053015.
[187] D. Shou, J. Fan, M. Mei, F. Ding, An analytical model for gas diffusion though nanoscale and microscale fibrous media, Microfluidics and Nanofluidics, (2013) 1-9.
[188] M.A. Nilsson, R. Kulkarni, L. Gerberich, R. Hammond, R. Singh, E. Baumhoff, J.P. Rothstein, Effect of fluid rheology on enhanced oil recovery in a microfluidic sandstone device, Journal of Non-Newtonian Fluid Mechanics, 202 (2013) 112-119.
[189] C. Jiménez-González, P. Poechlauer, Q.B. Broxterman, B.-S. Yang, D. am Ende, J. Baird, C. Bertsch, R.E. Hannah, P. Dell'Orco, H. Noorman, Key green engineering research areas for sustainable manufacturing: a perspective from pharmaceutical and fine chemicals manufacturers, Organic Process Research & Development, 15 (2011) 900-911.
[190] C. Wiles, P. Watts, Continuous flow reactors: a perspective, Green Chemistry, 14 (2012) 38-54.
[191] L. Malet-Sanz, F. Susanne, Continuous flow synthesis. A pharma perspective, J. Med. Chem, 55 (2012) 4062-4098.
[192] J. Wegner, S. Ceylan, A. Kirschning, Ten key issues in modern flow chemistry, Chemical Communications, 47 (2011) 4583-4592.
[193] J. Wegner, S. Ceylan, A. Kirschning, Flow chemistry–a key enabling technology for (multistep) organic synthesis, Advanced Synthesis & Catalysis, 354 (2012) 17-57.
[194] G.S. Calabrese, S. Pissavini, From batch to continuous flow processing in chemicals manufacturing, AIChE journal, 57 (2011) 828-834.
[195] S.G. Newman, K.F. Jensen, The role of flow in green chemistry and engineering, Green Chemistry, 15 (2013) 1456-1472.
[196] J.i. Yoshida, H. Kim, A. Nagaki, Green and sustainable chemical synthesis using flow microreactors, ChemSusChem, 4 (2011) 331-340.
[197] E.K. Sackmann, A.L. Fulton, D.J. Beebe, The present and future role of microfluidics in biomedical research, Nature, 507 (2014) 181-189.
[198] K.S. Elvira, X.C. i Solvas, R.C.R. Wootton, The past, present and potential for microfluidic reactor technology in chemical synthesis, Nature chemistry, (2013).
[199] H. Song, D.L. Chen, R.F. Ismagilov, Reactions in droplets in microfluidic channels, Angewandte chemie international edition, 45 (2006) 7336-7356.
[200] H. Nowothnick, J. Blum, R. Schomäcker, Suzuki Coupling Reactions in Three-Phase Microemulsions, Angewandte Chemie International Edition, 50 (2011) 1918-1921.
[201] B.P. Mason, K.E. Price, J.L. Steinbacher, A.R. Bogdan, D.T. McQuade, Greener approaches to organic synthesis using microreactor technology, Chemical reviews, 107 (2007) 2300-2318.
[202] A. Pommella, G. Tomaiuolo, A. Chartoire, S. Caserta, G. Toscano, S.P. Nolan, S. Guido, Palladium-N-heterocyclic carbene (NHC) catalyzed C-N bond formation in a continuous flow microreactor. Effect of process parameters and comparison with batch operation, Chemical Engineering Journal, 223 (2013) 578-583.
[203] B. Ahmed-Omer, J.C. Brandt, T. Wirth, Advanced organic synthesis using microreactor technology, Organic & biomolecular chemistry, 5 (2007) 733-740.
[204] G.M. Greenway, S.J. Haswell, D.O. Morgan, V. Skelton, P. Styring, The use of a novel microreactor for high throughput continuous flow organic synthesis, Sensors and Actuators B: Chemical, 63 (2000) 153-158.
[205] J.P. Wolfe, S. Wagaw, J.-F. Marcoux, S.L. Buchwald, Rational development of practical catalysts for aromatic carbon-nitrogen bond formation, Accounts of chemical research, 31 (1998) 805-818.
[206] F. Izquierdo, S. Manzini, S.P. Nolan, The use of the sterically demanding IPr* and related ligands in catalysis, Chemical Communications, 50 (2014) 14926-14937.
[207] M.S. Viciu, R.A. Kelly, E.D. Stevens, F. Naud, M. Studer, S.P. Nolan, Synthesis, characterization, and catalytic activity of N-heterocyclic carbene (NHC) palladacycle complexes, Organic letters, 5 (2003) 1479-1482.
[208] N. Marion, O. Navarro, J. Mei, E.D. Stevens, N.M. Scott, S.P. Nolan, Modified (NHC) Pd (allyl) Cl (NHC= N-heterocyclic carbene) complexes for room-temperature Suzuki-Miyaura and Buchwald-Hartwig reactions, Journal of the American Chemical Society, 128 (2006) 4101-4111.
[209] H. Wennerström, B. Lindman, Micelles. Physical chemistry of surfactant association, Physics Reports, 52 (1979) 1-86.
[210] D. Chandler, Interfaces and the driving force of hydrophobic assembly, Nature, 437 (2005) 640-647.
[211] G. Vitiello, G. Mangiapia, E. Romano, M. Lavorgna, S. Guido, V. Guida, L. Paduano, G. D'Errico, Phase behavior of the ternary aqueous mixtures of two polydisperse ethoxylated nonionic surfactants, Colloids and Surfaces A: Physicochemical and Engineering Aspects, 442 (2014) 16-24.
[212] N. Garti, D. Libster, A. Aserin, Lipid polymorphism in lyotropic liquid crystals for triggered release of bioactives, Food & Function, 3 (2012) 700-713.
[213] R. Angelico, A. Ceglie, U. Olsson, G. Palazzo, Phase diagram and phase properties of the system lecithin-water-cyclohexane, Langmuir, 16 (2000) 2124-2132.
[214] I. Martiel, L. Sagalowicz, R. Mezzenga, Phospholipid-based nonlamellar mesophases for delivery systems: Bridging the gap between empirical and rational design, Advances in colloid and interface science, 209 (2014) 127-143.
[215] L. Gentile, M.A. Behrens, L. Porcar, P. Butler, N.J. Wagner, U. Olsson, Multilamellar Vesicle Formation from a Planar Lamellar Phase under Shear Flow, Langmuir, 30 (2014) 8316-8325.
[216] S. Chiruvolu, H.E. Warriner, E. Naranjo, S.H.J. Idziak, J.O. Rädler, R.J. Plano, J.A. Zasadzinski, C.R. Safinya, A phase of liposomes with entangled tubular vesicles, Science, (1994) 1222-1224.
[217] R. Strey, Microemulsion microstructure and interfacial curvature, Colloid and Polymer Science, 272 (1994) 1005-1019.
[218] S. Burauer, L. Belkoura, C. Stubenrauch, R. Strey, Bicontinuous microemulsions revisited: a new approach to freeze fracture electron microscopy (FFEM), Colloids and Surfaces A: Physicochemical and Engineering Aspects, 228 (2003) 159-170.
[219] T. Sottmann, C. Stubenrauch, Phase behaviour, interfacial tension and microstructure of microemulsions, Microemulsions: Background, New Concepts, Applications, Perspectives, ed. C. Stubenrauch, John Wiley & Sons, Oxford, (2009).

[220] M. Laupheimer, K. Jovic, F.E. Antunes, M.d.G.M. Miguel, C. Stubenrauch, Studying orthogonal self-assembled systems: phase behaviour and rheology of gelled microemulsions, Soft Matter, 9 (2013) 3661-3670.
[221] M. Laupheimer, T. Sottmann, R. Schweins, C. Stubenrauch, Studying orthogonal self-assembled systems: microstructure of gelled bicontinuous microemulsions, Soft matter, 10 (2014) 8744-8757.
S. Guido, Phase behavior of aqueous solutions of hydroxypropyl cellulose, Macromolecules, 28 (1995) 4530-4539.
[223] F.B. Rosevear, The microscopy of the liquid crystalline neat and middle phases of soaps and synthetic detergents, Journal of the American Oil Chemists' Society, 31 (1954) 628-639.
[224] F.B. Rosevear, Liquid crystals: the mesomorphic phases of surfactant compositions, J. Soc. Cosmetic Chemists, 19 (1968) 581-594.
[225] J.N. Israelachvili, Intermolecular and surface forces: revised third edition, Academic press, 2011.
[226] P.A. Winsor, Hydrotropy, solubilisation and related emulsification processes, Transactions of the Faraday Society, 44 (1948) 376-398.
[227] K. Shinoda, H. Arai, The Correlation between Phase Inversion Temperature In Emulsion and Cloud Point in Solution of Nonionic Emulsifier, The Journal of Physical Chemistry, 68 (1964) 3485-3490.
[228] S.E. Friberg, H. Sagitani, T.J. Lin, Kozo Shinoda, in Memoriam, Journal of Dispersion Science and Technology, 35 (2014) 1511-1511.
[229] L. Wolf, H. Hoffmann, Y. Talmon, T. Teshigawara, K. Watanabe, Cryo-TEM imaging of a novel microemulsion system of silicone oil with an anionic/nonionic surfactant mixture, Soft Matter, 6 (2010) 5367-5374.
[230] C. Solans, I. Solé, Nano-emulsions: Formation by low-energy methods, Current Opinion in Colloid & Interface Science, 17 (2012) 246-254.
[231] I. Solè, C. Solans, A. Maestro, C. González, J.M. Gutiérrez, Study of nano-emulsion formation by dilution of microemulsions, Journal of Colloid and Interface Science, 376 (2012) 133-139.
[232] E. Negro, R. Latsuzbaia, G.J.M. Koper, Bicontinuous Microemulsions for High Yield Wet Synthesis of Ultrafine Platinum Nanoparticles: Effect of Precursors and Kinetics, Langmuir, 30 (2014) 8300-8307.
[233] E. Negro, R. Latsuzbaia, A. de Vries, G. Koper, Experimental and Molecular Dynamics Characterization of Dense Microemulsion Systems: Morphology, Conductivity and SAXS, Soft Matter, (2014).
[234] E. Negro, M. Dieci, D. Sordi, K. Kowlgi, M. Makkee, G.J.M. Koper, High yield, controlled synthesis of graphitic networks from dense micro emulsions, Chemical Communications, 50 (2014) 11848-11851.
[235] C.A. Miller, Dissolution Rates of Surfactants, in: Interfacial Processes and Molecular Aggregation of Surfactants, Springer, 2008, pp. 3-24.
[236] R. Strey, Phase behavior and interfacial curvature in water-oil-surfactant systems, Current Opinion in Colloid & Interface Science, 1 (1996) 402-410.
[237] P. Ramírez, L.M. Pérez, L.A. Trujillo, M. Ruiz, J. Muñoz, R. Miller, Equilibrium and surface rheology of two polyoxyethylene surfactants (CiEOj) differing in the number of oxyethylene groups, Colloids and Surfaces A: Physicochemical and Engineering Aspects, 375 (2011) 130-135.
[238] A. Forgiarini, J. Esquena, C. González, C. Solans, Formation of Nano-emulsions by Low-Energy Emulsification Methods at Constant Temperature, Langmuir, 17 (2001) 2076-2083.
[239] F. Ostertag, J. Weiss, D.J. McClements, Low-energy formation of edible nanoemulsions: Factors influencing droplet size produced by emulsion phase inversion, Journal of Colloid and Interface Science, 388 (2012) 95-102.
[240] A. Maestro, I. Solè, C. González, C. Solans, J.M. Gutiérrez, Influence of the phase behavior on the properties of ionic nanoemulsions prepared by the phase inversion composition method, Journal of colloid and interface science, 327 (2008) 433-439.
[241] A. Pizzino, V. Molinier, M. Catté, J.F. Ontiveros, J.-L. Salager, J.-M. Aubry, Relationship between Phase Behavior and Emulsion Inversion for a Well-Defined Surfactant (C10E4)/n-Octane/Water Ternary System at Different Temperatures and Water/Oil Ratios, Industrial & Engineering Chemistry Research, 52 (2013) 4527-4538.
[242] S.E. Friberg, R.W. Corkery, I.A. Blute, Phase Inversion Temperature (PIT) Emulsification Process, Journal of Chemical & Engineering Data, 56 (2011) 4282-4290.
[243] L. Wang, K.J. Mutch, J. Eastoe, R.K. Heenan, J. Dong, Nanoemulsions Prepared by a Two-Step Low-Energy Process, Langmuir, 24 (2008) 6092-6099.
[244] K. Roger, B. Cabane, U. Olsson, Emulsification through Surfactant Hydration: The PIC Process Revisited, Langmuir, 27 (2010) 604-611.
[245] P.G. De Gennes, C. Taupin, Microemulsions and the flexibility of oil/water interfaces, The Journal of Physical Chemistry, 86 (1982) 2294-2304.
[246] P. Fernandez, V. André, J. Rieger, A. Kühnle, Nano-emulsion formation by emulsion phase inversion, Colloids and Surfaces A: Physicochemical and Engineering Aspects, 251 (2004) 53-58.
[247] A. Mercuri, A. Passalacqua, M.J. Wickham, R. Faulks, D.M. Craig, S. Barker, The Effect of Composition and Gastric Conditions on the Self-Emulsification Process of Ibuprofen-Loaded Self-Emulsifying Drug Delivery Systems: A Microscopic and Dynamic Gastric Model Study, Pharmaceutical Research, 28 (2011) 1540-1551.
[248] I. Solè, C.M. Pey, A. Maestro, C. González, M. Porras, C. Solans, J.M. Gutiérrez, Nano-emulsions prepared by the phase inversion composition method: Preparation variables and scale up, Journal of colloid and interface science, 344 (2010) 417-423.
[249] W. Liu, D. Sun, C. Li, Q. Liu, J. Xu, Formation and stability of paraffin oil-in-water nano-emulsions prepared by the emulsion inversion point method, Journal of Colloid and Interface Science, 303 (2006) 557-563.
[250] J.-L. Salager, L. Márquez, A.A. Peña, M. Rondón, F. Silva, E. Tyrode, Current phenomenological know-how and modeling of emulsion inversion, Industrial & engineering chemistry research, 39 (2000) 2665-2676.
[251] Y. Liu, E.L. Carter, G.V. Gordon, Q.J. Feng, S.E. Friberg, An investigation into the relationship between catastrophic inversion and emulsion phase behaviors, Colloids and Surfaces a-Physicochemical and Engineering Aspects, 399 (2012) 25-34.
[252] Y. Liu, S.E. Friberg, Role of liquid crystal in the emulsification of a gel emulsion with high internal phase fraction, Journal of Colloid and Interface Science, 340 (2009) 261-268.
[253] F. Jahanzad, G. Crombie, R. Innes, S. Sajjadi, Catastrophic phase inversion via formation of multiple emulsions: A prerequisite for formation of fine emulsions, Chemical Engineering Research and Design, 87 (2009) 492-498.
[254] F. Jahanzad, D. Josephides, A. Mansourian, S. Sajjadi, Dynamics of transitional phase inversion emulsification: effect of addition time on the type of inversion and drop size, Industrial & Engineering Chemistry Research, 49 (2010) 7631-7637.

[255] K. Roger, B. Cabane, U. Olsson, Formation of 10-100 nm size-controlled emulsions through a sub-PIT cycle., Langmuir, 26 (2010) 3860-3867.
[256] L. Yu, C. Li, J. Xu, J. Hao, D. Sun, Highly Stable Concentrated Nanoemulsions by the Phase Inversion Composition Method at Elevated Temperature, Langmuir, 28 (2012) 14547-14552.
[257] J.M. Morais, P.A. Rocha-Filho, D.J. Burgess, Influence of Phase Inversion on the Formation and Stability of One-Step Multiple Emulsions, Langmuir, 25 (2009) 7954-7961.
[258] J.L. Salager, A. Forgiarini, L. Márquez, A. Peña, A. Pizzino, M.P. Rodriguez, M. Rondón-González, Using emulsion inversion in industrial processes, Adv Colloid Interface Sci, 108-109 (2004) 259-272.
[259] J. Salager, Emulsion phase inversion phenomena, Surfactant science series, 132 (2006) 185.
[260] W.C. Griffin, Classification of Surface-Active Agents by 'HLB', in, Journal of the Society of Cosmetic Chemists, 1949, pp. 311-326.
[261] J.T. Davies, A quantitative kinetic theory of emulsion type, I. Physical chemistry of the emulsifying agent, in, Butterworths London, pp. 426.
[262] J.-L. Salager, N. Marquez, A. Graciaa, J. Lachaise, Partitioning of ethoxylated octylphenol surfactants in microemulsion-oil-water systems: influence of temperature and relation between partitioning coefficient and physicochemical formulation, Langmuir, 16 (2000) 5534-5539.
[263] M. Rondón-González, V. Sadtler, L. Choplin, J.-L. Salager, Emulsion inversion from abnormal to normal morphology by continuous stirring without internal phase addition: Effect of surfactant mixture fractionation at extreme water–oil ratio, Colloids and Surfaces A: Physicochemical and Engineering Aspects, 288 (2006) 151-157.
[264] I. Mira, N. Zambrano, E. Tyrode, L. Márquez, A.A. Peña, A. Pizzino, J.-L. Salager, Emulsion Catastrophic Inversion from Abnormal to Normal Morphology. 2. Effect of the Stirring Intensity on the Dynamic Inversion Frontier, Industrial & Engineering Chemistry Research, 42 (2002) 57-61.
[265] N. Zambrano, E. Tyrode, I. Mira, L. Márquez, M.-P. Rodríguez, J.-L. Salager, Emulsion catastrophic inversion from abnormal to normal morphology. 1. Effect of the water-to-oil ratio rate of change on the dynamic inversion frontier, Industrial & engineering chemistry research, 42 (2003) 50-56.
[266] E. Tyrode, I. Mira, N. Zambrano, L. Márquez, M. Rondón-Gonzalez, J.-L. Salager, Emulsion Catastrophic Inversion from Abnormal to Normal Morphology. 3. Conditions for Triggering the Dynamic Inversion and Application to Industrial Processes, Industrial & Engineering Chemistry Research, 42 (2003) 4311-4318.
[267] M. Rondon-Gonzalez, V. Sadtler, P. Marchal, L. Choplin, J.-L. Salager, Emulsion catastrophic inversion from abnormal to normal morphology. 7. Emulsion evolution produced by continuous stirring to generate a very high internal phase ratio emulsion, Industrial & Engineering Chemistry Research, 47 (2008) 2314-2319.
[268] P. Sherman, C. Parkinson, Mechanism of temperature induced phase inversion in O/W emulsions stabilised by O/W and W/O emulsifier blends, in: A. Weiss (Ed.) Emulsions, Steinkopff, 1978, pp. 10-14.
[269] M. Zerfa, S. Sajjadi, B.W. Brooks, Phase behaviour of non-ionic surfactant–p-xylene–water systems during the phase inversion process, Colloids and Surfaces A: Physicochemical and Engineering Aspects, 155 (1999) 323-337.
[270] B.W. Brooks, H.N. Richmond, Phase inversion in non-ionic surfactant—oil—water systems—II. Drop size studies in catastrophic inversion with turbulent mixing, Chemical Engineering Science, 49 (1994) 1065-1075.
[271] B.W. Brooks, H.N. Richmond, Dynamics of liquid—liquid phase inversion using non-ionic surfactants, Colloids and Surfaces, 58 (1991) 131-148.
[272] F. Groeneweg, W. Agterof, P. Jaeger, J. Janssen, J. Wieringa, J. Klahn, On the mechanism of the inversion of emulsions, Chemical Engineering Research and Design, 76 (1998) 55-63.
[273] S. Sajjadi, M. Zerfa, B. W. Brooks, Dynamic behaviour of drops in oil/water/oil dispersions, Chemical Engineering Science, 57 (2002) 663-675.
[274] J.K. Klahn, J.J.M. Janssen, G.E.J. Vaessen, R. de Swart, W.G.M. Agterof, On the escape process during phase inversion of an emulsion, Colloids and Surfaces A: Physicochemical and Engineering Aspects, 210 (2002) 167-181.
[275] T. Ohtake, T. Hano, K. Takagi, F. Nakashio, Effects of viscosity on drop diameter of W/O emulsion dipersed in a stirred tank, Journal of chemical engineering of Japan, 20 (1987) 443-447.
[276] G.I. Taylor, The mechanism of plastic deformation of crystals. Part I. Theoretical, Proceedings of the Royal Society of London. Series A, Containing Papers of a Mathematical and Physical Character, (1934) 362-387.
[277] L. Liu, O.K. Matar, E. Susana Perez de Ortiz, G.F. Hewitt, Experimental investigation of phase inversion in a stirred vessel using LIF, Chemical Engineering Science, 60 (2005) 85-94.
[278] A.W. Pacek, A.W. Nienow, I.P.T. Moore, On the structure of turbulent liquid—liquid dispersed flows in an agitated vessel, Chemical Engineering Science, 49 (1994) 3485-3498.
[279] L. Besnard, F. Marchal, J.F. Paredes, J. Daillant, N. Pantoustier, P. Perrin, P. Guenoun, Multiple Emulsions Controlled by Stimuli-Responsive Polymers, Advanced Materials, 25 (2013) 2844-2848.
[280] W. Helfrich, Elastic properties of lipid bilayers: theory and possible experiments, Zeitschrift für Naturforschung. Teil C: Biochemie, Biophysik, Biologie, Virologie, 28 (1973) 693.
[281] W. Helfrich, R.M. Servuss, Undulations, steric interaction and cohesion of fluid membranes, Il Nuovo Cimento D, 3 (1984) 137-151.
[282] W. Helfrich, Lyotropic lamellar phases, Journal of Physics: Condensed Matter, 6 (1994) A79.
[283] N. Nandi, D. Vollhardt, Helfrich's concept of intrinsic force and its molecular origin in bilayers and monolayers, Advances in colloid and interface science, 208 (2014) 110-120.
[284] Z. Shi, T. Baumgart, Dynamics and instabilities of lipid bilayer membrane shapes, Advances in colloid and interface science, 208 (2014) 76-88.
[285] T.N. Zemb, I.S. Barnes, P.J. Derian, B.W. Ninham, Scattering as a critical test of microemulsion structural models, in: M. Zulauf, P. Lindner, P. Terech (Eds.) Trends in Colloid and Interface Science IV, Steinkopff, 1990, pp. 20-29.
[286] T. Zemb, Flexibility, persistence length and bicontinuous microstructures in microemulsions, Comptes Rendus Chimie, 12 (2009) 218-224.
[287] M. Duvail, L. Arleth, T. Zemb, J.-F. Dufrêche, Predicting for thermodynamic instabilities in water/oil/surfactant microemulsions: A mesoscopic modelling approach, The Journal of chemical physics, 140 (2014) 164711.
[288] T.N. Zemb, The DOC model of microemulsions: microstructure, scattering, conductivity and phase limits imposed by sterical constraints, Colloids and Surfaces A: Physicochemical and Engineering Aspects, 129–130 (1997) 435-454.

[289] G. Gompper, S. Zschocke, Elastic properties of interfaces in a Ginzburg-Landau theory of swollen micelles, droplet crystals and lamellar phases, EPL (Europhysics Letters), 16 (1991) 731.
[290] G. Gompper, S. Zschocke, Ginzburg-Landau theory of oil-water-surfactant mixtures, Physical Review A, 46 (1992) 4836.
[291] D. Roux, C. Coulon, M.E. Cates, Sponge phases in surfactant solutions, The Journal of Physical Chemistry, 96 (1992) 4174-4187.
[292] D. Andelman, M.E. Cates, D. Roux, S.A. Safran, Structure and phase equilibria of microemulsions, The Journal of chemical physics, 87 (1987) 7229-7241.
[293] S.A. Safran, D. Roux, M.E. Cates, D. Andelman, Origin of middle-phase microemulsions, Physical review letters, 57 (1986) 491.
[294] R.M. Hochmuth, R.E. Waugh, Erythrocyte membrane elasticity and viscosity, Annual review of physiology, 49 (1987) 209-219.
[295] G. Tomaiuolo, M. Simeone, V. Martinelli, B. Rotoli, S. Guido, Red blood cell deformation in microconfined flow, Soft Matter, 5 (2009) 3736-3740.
[296] G. Tomaiuolo, M. Barra, V. Preziosi, A. Cassinese, B. Rotoli, S. Guido, Microfluidics analysis of red blood cell membrane viscoelasticity, Lab on a Chip, 11 (2011) 449-454.
[297] H.J. Deuling, W. Helfrich, Red blood cell shapes as explained on the basis of curvature elasticity, Biophysical Journal, 16 (1976) 861-868.
[298] E.A. Evans, Bending Resistance and Chemically Induced Moments in Membrane Bilayers, Biophysical Journal, 14 (1974) 923-931.
[299] U. Seifert, Configurations of fluid membranes and vesicles, Advances in physics, 46 (1997) 13-137.
[300] M. Staykova, D.P. Holmes, C. Read, H.A. Stone, Mechanics of surface area regulation in cells examined with confined lipid membranes, Proceedings of the National Academy of Sciences, 108 (2011) 9084-9088.
[301] M. Staykova, M. Arroyo, M. Rahimi, H.A. Stone, Confined bilayers passively regulate shape and stress, Physical review letters, 110 (2013) 028101.
[302] M. Deserno, Fluid lipid membranes: From differential geometry to curvature stresses, Chemistry and physics of lipids, (2014).
[303] G.R. Lázaro, I. Pagonabarraga, A. Hernández-Machado, Phase-field theories for mathematical modeling of biological membranes, Chemistry and physics of lipids, (2014).
[304] R. Dimova, Recent developments in the field of bending rigidity measurements on membranes, Advances in colloid and interface science, 208 (2014) 225-234.
[305] R. Lipowsky, Coupling of bending and stretching deformations in vesicle membranes, Advances in colloid and interface science, 208 (2014) 14-24.
[306] A. Kabalnov, H. Wennerström, Macroemulsion Stability: The Oriented Wedge Theory Revisited, Langmuir, 12 (1996) 276-292.
[307] W.D. Harkins, E.B. Keith, THE ORIENTED WEDGE THEORY OF EMULSIONS AND THE INVERSION OF EMULSIONS, Science, 59 (1924) 463-467.
[308] N. Brauner, A. Ullmann, Modeling of phase inversion phenomenon in two-phase pipe flows, International Journal of Multiphase Flow, 28 (2002) 1177-1204.
[309] P. Poesio, G. Beretta, Minimal dissipation rate approach to correlate phase inversion data, International Journal of Multiphase Flow, 34 (2008) 684-689.
[310] L. Y. Yeo, O. K. Matar, E. Susana Perez de Ortiz, G. F. Hewitt, A description of phase inversion behaviour in agitated liquid–liquid dispersions under the influence of the Marangoni effect, Chemical Engineering Science, 57 (2002) 3505-3520.
[311] K. Piela, G. Ooms, J.V. Sengers, Phenomenological description of phase inversion, Physical Review E, 79 (2009) 021403.
[312] B. Hu, L. Liu, O.K. Matar, P. Anqeli, G.F. Hewitt, E.S.P. de Ortiz, Investigation of phase inversion of liquid-liquid dispersions in agitated vessels, Tsinghua Science and Technology, 11 (2006) 202-206.
[313] V. Starov, Wetting, in: T. Tadros (Ed.) Encyclopedia of Colloid and Interface Science, Springer Berlin Heidelberg, 2013, pp. 1399-1422.
[314] G. Kumar, K.N. Prabhu, Review of non-reactive and reactive wetting of liquids on surfaces, Advances in Colloid and Interface Science, 133 (2007) 61-89.
[315] H.A. Stone, Dynamics of drop deformation and breakup in viscous fluids, Annual Review of Fluid Mechanics, 26 (1994) 65-102.
[316] S. Guido, V. Preziosi, Droplet deformation under confined Poiseuille flow, Advances in Colloid and Interface Science, 161 (2010) 89-101.
[317] Y.T. Hu, D.J. Pine, L.G. Leal, Drop deformation, breakup, and coalescence with compatibilizer, Physics of Fluids (1994-present), 12 (2000) 484-489.
[318] B. Dai, L.G. Leal, The mechanism of surfactant effects on drop coalescence, Physics of Fluids (1994-present), 20 (2008) 040802.
[319] J.A. Quinn, D.B. Sigloh, Phase inversion in the mixing of immiscible liquids, The Canadian Journal of Chemical Engineering, 41 (1963) 15-18.
[320] L.Y. Yeo, O.K. Matar, E.S. Perez de Ortiz, G.F. Hewitt, Simulation studies of phase inversion in agitated vessels using a Monte Carlo technique, Journal of colloid and interface science, 248 (2002) 443-454.
[321] L.Y. Yeo, O.K. Matar, E.S. Perez de Ortiz, G.F. Hewitt, A simple predictive tool for modelling phase inversion in liquid–liquid dispersions, Chemical engineering science, 57 (2002) 1069-1072.
[322] A.H. Selker, C.A. Sleicher, Factors affecting which phase will disperse when immiscible liquids are stirred together, The Canadian Journal of Chemical Engineering, 43 (1965) 298-301.
[323] B. Hu, L. Liu, O.K. Matar, P. Angeli, G.F. Hewitt, E.S. Pérez de Ortiz, Investigation of phase inversion of liquid-liquid dispersions in agitated vessels, Tsinghua Science & Technology, 11 (2006) 202-206.
[324] B.J. Azzopardi, G.F. Hewitt, Maximum drop sizes in gas-liquid flows, Multiphase Science Technology, 9 (1997) 109-204.
[325] N. Brauner, The prediction of dispersed flows boundaries in liquid–liquid and gas–liquid systems, International Journal of Multiphase Flow, 27 (2001) 885-910.
[326] M. Tidhar, J.C. Merchuk, A.N. Sembira, D. Wolf, Characteristics of a motionless mixer for dispersion of immiscible fluids—II. Phase inversion of liquid-liquid systems, Chemical Engineering Science, 41 (1986) 457-462.

[327] K.H. Ngan, K. Ioannou, L.D. Rhyne, W. Wang, P. Angeli, A methodology for predicting phase inversion during liquid–liquid dispersed pipeline flow, Chemical Engineering Research and Design, 87 (2009) 318-324.
[328] K. Piela, R. Delfos, G. Ooms, J. Westerweel, R.V.A. Oliemans, R.F. Mudde, Experimental investigation of phase inversion in an oil–water flow through a horizontal pipe loop, International Journal of Multiphase Flow, 32 (2006) 1087-1099.
[329] R.C. Ball, P. Richmond, Dynamics of colloidal dispersions, Physics and Chemistry of Liquids, 9 (1980) 99-116.
[330] S. Arirachakaran, K.D. Oglesby, M.S. Malinowsky, O. Shoham, J.P. Brill, An analysis of oil/water flow phenomena in horizontal pipes, in, Society of Petroleum Engineers.
[331] M. Nädler, D. Mewes, Flow induced emulsification in the flow of two immiscible liquids in horizontal pipes, International journal of multiphase flow, 23 (1997) 55-68.
[332] K. Ioannou, O.J. Nydal, P. Angeli, Phase inversion in dispersed liquid–liquid flows, Experimental thermal and fluid science, 29 (2005) 331-339.
[333] B. Hu, O.K. Matar, G.F. Hewitt, P. Angeli, Population balance modelling of phase inversion in liquid–liquid pipeline flows, Chemical Engineering Science, 61 (2006) 4994-4997.
[334] D. Ramkrishna, M.R. Singh, Population Balance Modeling: Current Status and Future Prospects, Annual Review of Chemical and Biomolecular Engineering, 5 (2014) 123-146.
[335] A. Zaccone, A. Gäbler, S. Maaß, D. Marchisio, M. Kraume, Drop breakage in liquid–liquid stirred dispersions: modelling of single drop breakage, Chemical Engineering Science, 62 (2007) 6297-6307.
[336] D.L. Marchisio, R.O. Fox, Solution of population balance equations using the direct quadrature method of moments, Journal of Aerosol Science, 36 (2005) 43-73.
[337] K. Piela, R. Delfos, G. Ooms, J. Westerweel, R. Oliemans, On the phase inversion process in an oil–water pipe flow, International Journal of Multiphase Flow, 34 (2008) 665-677.
[338] K. Piela, R. Delfos, G. Ooms, J. Westerweel, R.V.A. Oliemans, Phase inversion in the mixing zone between a water flow and an oil flow through a pipe, International Journal of Multiphase Flow, 35 (2009) 91-95.
[339] K. Piela, E. Djojorahardjo, G.J.M. Koper, G. Ooms, Influence of a surfactant or salt on phase inversion in a water–oil pipe flow, Chemical Engineering Research and Design, 87 (2009) 1466-1470.
[340] N. Bremond, H. Doméjean, J. Bibette, Propagation of Drop Coalescence in a Two-Dimensional Emulsion: A Route towards Phase Inversion, Physical Review Letters, 106 (2011) 214502.
[341] J.M. Rallison, A. Acrivos, A numerical study of the deformation and burst of a viscous drop in an extensional flow, Journal of Fluid Mechanics, 89 (1978) 191-200.
[342] J.M. Rallison, The deformation of small viscous drops and bubbles in shear flows, Annual Review of Fluid Mechanics, 16 (1984) 45-66.
[343] J.M. Rallison, Note on the time-dependent deformation of a viscous drop which is almost spherical, Journal of Fluid Mechanics, 98 (1980) 625-633.
[344] S.D. Hudson, J.T. Cabral, J.W.J. Goodrum, K.L. Beers, E.J. Amis, Microfluidic interfacial tensiometry, Applied Physics Letters, 87 (2005) 081905-081903.
[345] J.T. Cabral, S.D. Hudson, Microfluidic approach for rapid multicomponent interfacial tensiometry, Lab on a Chip, 6 (2006) 427-436.
[346] M.K. Mulligan, J.P. Rothstein, The effect of confinement-induced shear on drop deformation and breakup in microfluidic extensional flows, Physics of Fluids (1994-present), 23 (2011) 022004.
[347] M. Ferrari, L. Liggieri, F. Ravera, C. Amodio, R. Miller, Adsorption kinetics of alkylphosphine oxides at water/hexane interface: 1. Pendant drop experiments, Journal of colloid and interface science, 186 (1997) 40-45.
[348] P. Szumała, H. Szeląg, Water solubilization using nonionic surfactants from renewable sources in microemulsion systems, Journal of surfactants and detergents, 15 (2012) 485-494.
[349] S. Tcholakova, N.D. Denkov, T. Danner, Role of surfactant type and concentration for the mean drop size during emulsification in turbulent flow, Langmuir, 20 (2004) 7444-7458.
[350] S. Tcholakova, N.D. Denkov, A. Lips, Comparison of solid particles, globular proteins and surfactants as emulsifiers, Physical Chemistry Chemical Physics, 10 (2008) 1608-1627.
[351] V.B. Fainerman, S.A. Zholob, J.T. Petkov, R. Miller, C14EO8 adsorption characteristics studied by drop and bubble profile tensiometry, Colloids and Surfaces A: Physicochemical and Engineering Aspects, 323 (2008) 56-62.
[352] A. Chartoire, M. Lesieur, L. Falivene, A.M.Z. Slawin, L. Cavallo, C.S.J. Cazin, S.P. Nolan, [Pd(IPr*)(cinnamyl)Cl]: An Efficient Pre-catalyst for the Preparation of Tetra-ortho-substituted Biaryls by Suzuki–Miyaura Cross-Coupling, Chemistry – A European Journal, 18 (2012) 4517-4521.
[353] A. Montesi, A.A. Peña, M. Pasquali, Vorticity alignment and negative normal stresses in sheared attractive emulsions, Physical review letters, 92 (2004) 058303.
[354] A. Javadi, J. Krägel, A.V. Makievski, V.I. Kovalchuk, N.M. Kovalchuk, N. Mucic, G. Loglio, P. Pandolfini, M. Karbaschi, R. Miller, Fast dynamic interfacial tension measurements and dilational rheology of interfacial layers by using the capillary pressure technique, Colloids and Surfaces A: Physicochemical and Engineering Aspects, 407 (2012) 159-168.
[355] F. Ravera, G. Loglio, P. Pandolfini, E. Santini, L. Liggieri, Determination of the dilational viscoelasticity by the oscillating drop/bubble method in a capillary pressure tensiometer, Colloids and Surfaces A: Physicochemical and Engineering Aspects, 365 (2010) 2-13.
[356] H.-J. Federsel, M. Hedberg, F.R. Qvarnström, M.P.T. Sjögren, W. Tian, Construction of a chiral central nervous system (CNS)-active aminotetralin drug compound based on a synthesis strategy using multitasking properties of (S)-1-phenylethylamine, Accounts of chemical research, 40 (2007) 1377-1384.
[357] H.-J. Federsel, M. Hedberg, W. Tian, Optimization and Scale-up of a Pd-Catalyzed Aromatic C− N Bond Formation: A Key Step in the Synthesis of a Novel 5-HT1B Receptor Antagonist, Organic Process Research & Development, 12 (2008) 512-521.
[358] O. Levenspiel, Chemical Reaction Engineering, 3rd ed., John Wiley & Sons, 1999.
[359] R.L. Hartman, J.R. Naber, N. Zaborenko, S.L. Buchwald, K.F. Jensen, Overcoming the challenges of solid bridging and constriction during Pd-Catalyzed C− N bond formation in microreactors, Organic Process Research & Development, 14 (2010) 1347-1357.
[360] H.M. Wyss, D.L. Blair, J.F. Morris, H.A. Stone, D.A. Weitz, Mechanism for clogging of microchannels, PHYSICAL REVIEW-SERIES E-, 74 (2006) 061402.

[361] C. Henry, J.-P. Minier, G. Lefèvre, Towards a description of particulate fouling: from single particle deposition to clogging, Advances in colloid and interface science, 185 (2012) 34-76.

Appendix

Publications

A. Perazzo, V. Preziosi, S. Guido, Phase inversion emulsification: Current understanding and applications. Advances in Colloid and Interface Science, (2015).

V. Preziosi, **A. Perazzo**, S. Caserta, G. Tomaiuolo, S. Guido, Phase Inversion Emulsification, Chemical Engineering Transactions, 32, (2013).

Conferences

1) **A.Perazzo**, V. Preziosi, S. Guido, "86th Society of Rheology Meeting", Philadelphia (U.S.A.), October 2014, Morphology evolution of mesoporous bicontinuous emulsion

2) A.Pommella, D. Donnarumma, **A. Perazzo**, S. Caserta, S. Guido, "86th Society of Rheology Meeting", Philadelphia (U.S.A.), October 2014, Morphology and flow behavior of multilamellar vesicles in surfactant solution

3) S. Caserta, **A. Perazzo**, S. Guido, "86th Society of Rheology Meeting", Philadelphia (U.S.A.), October 2014, Multiphase waxy crude oils rheo-optical characterization

4) V. Preziosi, **A. Perazzo**, R. D'Apolito, G. Tomaiuolo, S. Caserta, S. Guido, "86th Society of Rheology Meeting", Philadelphia (U.S.A.), October 2014, Microfluidics: a Rheo-optical tool to study micro-structured emulsion and their flow instabilities

5) V. Preziosi, **A. Perazzo**, S. Guido, "AERC 2014 – 9th Annual European Rheology Conference", Karlsruhe (Germany), April 2014, Emulsion morphology evolution by phase inversion method

6) R. D'apolito, **A. Perazzo**, V. Preziosi, G. Tomaiuolo, A. Cassinese, S. Guido, "AERC 2014 – 9th Annual Europena Rheology Conference", Karlsruhe (Germany), April 2014, Microfluidic interfacial tensiometry of confined droplets in elongational flow

7) V. Preziosi, **A. Perazzo**, S. Caserta, G. Tomaiuolo, S. Guido, "ECIS - European Colloid and Interface Society Conference", Sofia (Bulgaria), September 2013, "From unstable water-in-oil emulsion to stable oil-in-water emulsion via phase inversion"

8) D. Donnarumma, **A. Perazzo**, G. Tomaiuolo, S. Caserta, S. Guido, "ECIS - European Colloid and Interface Society Conference", Sofia (Bulgaria), Settembre 2013. "Multiphase flow through porous media"

9) V. Preziosi, R. D'Apolito, **A. Perazzo**, G. Tomaiuolo, S. Caserta, S. Guido "ECIS - European Colloid and Interface Society Conference", Sofia (Bulgaria), September 2013, "Microscale extensional flow to determine emulsion interfacial properties"

10) V. Preziosi, R. D'Apolito, **A. Perazzo**, G. Tomaiuolo, S. Caserta, S. Guido, "ECIS - European Colloid and Interface Society Conference", Sofia (Bulgaria), September 2013, "Newtonian and non-Newtonian flow in capillaries and microchannels"

11) V. Preziosi, R. D'Apolito, **A. Perazzo**, G. Tomaiuolo, S. Guido "COST CM1101 workshop - dynamics of liquid interfaces", Potsdam (Germany), July 2013, "Microfluidic interfacial tensiometry of confined droplets"

12) **A. Perazzo**, S. Caserta, S. Guido, "Petrophase 2013 - 14th International Conference on Petroleum phase behaviour and Fouling", Rueil Malmaison (France), June 2013. "Multiphase fluids in Upstream Operations"

13) V. Preziosi, **A. Perazzo**, S. Caserta, G. Tomaiuolo, S. Guido, "Petrophase 2013 - 14th International Conference on Petroleum phase behaviour and Fouling", Rueil Malmaison (France), June 2013. " Experimental investigation of phase inversion for stable emulsion formation "

14) V. Preziosi, **A. Perazzo**, S. Caserta, G. Tomaiuolo, S. Guido. "Icheap 11 - 11th International Conference on Chemical and Process Engineering", Milan, June 2013, "Phase Inversion Emulsification"

15) S. Caserta, **A.Perazzo**, V.Preziosi, R.D'Apolito, G.Tomaiuolo, A.Pommella, S.Guido, "COST MP 1106 - Smart and Green Interfaces workshop", Prague (Czech Republic), March 2013. "Multiphase fluids in confined flow"

16) V. Preziosi, **A.Perazzo**, S.Caserta, G.Tomaiuolo, S.Guido , "COST MP 1106 - Smart and Green Interfaces workshop", Prague (Czech Republic), March 2013, " Experimental investigation of phase inversion for stable emulsion formation "

17) V. Preziosi, **A. Perazzo**, G. Tomaiuolo, S. Guido, "Emulsification", Lyon (France), November 2012,"Morphology evolution of phase inversion emulsification"

18) V. Preziosi, **A. Perazzo**, S. Caserta, G. Tomaiuolo, S. Guido, "Convegno GRICU 2012", September 2012. "Experimental investigation of phase inversion for stable emulsion formation"

19) V. Preziosi, **A. Perazzo**, S. Caserta, G. Tomaiuolo, S. Guido, "The XVIth International Congress on Rheology", August 2012, Lisbon (Portugal), "Rheo-Optical characterization of model emulsion around the phase inversion point"

20) V. Preziosi, S. Caserta, **A. Perazzo**, G. Tomaiuolo, S. Guido, "Società italiana di reologia, 12° convegno nazionale", Ustica (Italy), July 2012, "Caratterizzazione di emulsioni stabili ottenute tramite inversione di fase"

21) V. Preziosi, **A. Perazzo**, S.Caserta, G. Tomaiuolo, S.Guido. "5th International workshop Bubble & Drop Interfaces", Krakow (Poland), May 2012, "Experimental investigation of phase inversion for stable emulsion formation"